



**HAL**  
open science

# Apprentissage des formes de scoliose à l'aide de modèles anatomiques et de la capture de mouvement

Nicolas Comte

► **To cite this version:**

Nicolas Comte. Apprentissage des formes de scoliose à l'aide de modèles anatomiques et de la capture de mouvement. Apprentissage [cs.LG]. Université Grenoble Alpes [2020-..], 2023. Français. NNT : 2023GRALM068 . tel-04594309

**HAL Id: tel-04594309**

**<https://theses.hal.science/tel-04594309>**

Submitted on 30 May 2024

**HAL** is a multi-disciplinary open access archive for the deposit and dissemination of scientific research documents, whether they are published or not. The documents may come from teaching and research institutions in France or abroad, or from public or private research centers.

L'archive ouverte pluridisciplinaire **HAL**, est destinée au dépôt et à la diffusion de documents scientifiques de niveau recherche, publiés ou non, émanant des établissements d'enseignement et de recherche français ou étrangers, des laboratoires publics ou privés.

THÈSE

Pour obtenir le grade de

**DOCTEUR DE L'UNIVERSITÉ GRENOBLE ALPES**

École doctorale : MSTII - Mathématiques, Sciences et technologies de l'information, Informatique

Spécialité : Informatique

Unité de recherche : Laboratoire Jean Kuntzmann

**Apprentissage des formes de scoliose à l'aide de modèles anatomiques et de la capture de mouvement**

**Learning Scoliosis Patterns using Anatomical Models and Motion Capture**

Présentée par :

**Nicolas COMTE**

Direction de thèse :

**Jean-Sébastien FRANCO**

MAITRE DE CONFERENCES HDR, GRENOBLE INP

Directeur de thèse

**Sergi PUJADES-ROCAMORA**

Maitre de Conférences, Université Grenoble Alpes

Co-encadrant de thèse

**François FAURE**

Chief Executive Officer, Anatoscope

Co-encadrant de thèse

**Aurélien COURVOISIER**

PROFESSEUR DES UNIVERSITES - PRATICIEN HOSPITALIER,  
UNIVERSITE GRENOBLE ALPES

Co-encadrant de thèse

Rapporteurs :

**LENNART SCHEYS**

ASSOCIATE PROFESSOR, KATHOLIEKE UNIVERSITEIT LEUVEN

**CLAUDIO VERGARI**

MAITRE DE CONFERENCES HDR, ARTS ET METIERS PARIS TECH

Thèse soutenue publiquement le **29 novembre 2023**, devant le jury composé de :

**LENNART SCHEYS**

ASSOCIATE PROFESSOR, KATHOLIEKE UNIVERSITEIT LEUVEN

Rapporteur

**CLAUDIO VERGARI**

MAITRE DE CONFERENCES HDR, ARTS ET METIERS PARIS TECH

Rapporteur

**JOCELYNE TROCCAZ**

DIRECTRICE DE RECHERCHE, CNRS DELEGATION ALPES

Présidente

**GREGORY CHAGNON**

PROFESSEUR DES UNIVERSITES, UNIVERSITE GRENOBLE  
ALPES

Examineur





# Acknowledgments - remerciements

Je tiens avant tout à remercier toutes les personnes ayant contribué de près ou de loin à ce projet.

Un grand merci à l'ANRT (Association Nationale de la Recherche et de la Technologie) et à Anatoscope pour avoir financé ce projet de thèse CIFRE.

Merci également aux rapporteurs et examinateurs, Lennart Scheys, Claudio Vergari, Jocelyne Troccaz et Grégory Chagnon pour avoir évalué mon travail.

Je tiens à exprimer ma gratitude envers mes superviseurs Sergi Pujades, François Faure, Aurélien Courvoisier, Edmond Boyer et Jean-Sébastien Franco. Merci de m'avoir fait confiance, partagé vos connaissances et conseillé sur ces différentes thématiques complexes telles que la vision par ordinateur, la scoliose idiopathique et la construction de modèles personnalisés. Un grand merci à Sergi tout particulièrement qui m'aura grandement accompagné dans ces projets.

Je n'oublie pas bien-sûr Olivier Daniel, qui a collecté une grande partie des données exploitées dans mes travaux et avec qui nos conversations ont contribué à l'élaboration de ce manuscrit.

Au cours de ce doctorat, j'ai eu la chance de naviguer entre l'hôpital, l'entreprise Anatoscope et l'équipe Morpheo au centre Inria de l'Université Grenoble-Alpes. Je souhaite remercier mes collègues et co-bureaux (G113, H101, 36, ...) avec qui j'ai pu échanger sur les diverses thématiques abordées dans ce manuscrit, sur les aspects techniques, et qui m'ont apporté de précieux conseils. Vous êtes bien trop nombreux pour être cités, et je risque d'oublier des personnes.

Un grand merci à Nathalie à Inria et à Catherine à Anatoscope pour leur support au-delà des aspects scientifiques.

À mes amis de longue date, Pierre-André, Anaïs, Drystan, Virginie, Benjamin, Caroline, Audrey, ... Et ceux rencontrés en chemin dans le Grésivaudan : Sébastien, Gaëlle, Jocelyne, ...

À ma famille, mes parents, mes sœurs, ma cousine Juju... Mais surtout, un grand merci à ma femme, Claire, pour son soutien et son appui tout au long de ces presque 4 années de travaux remplis d'incertitudes.

Je n'oublie bien sûr pas ma petite Victoire qui arrive "à bien grandir".



# Notations

In this manuscript an effort is made to provide a uniform notation with other computer vision references [136]. Thus, scalars  $s$  are in mixed case italic font, vectors  $\mathbf{v}$  are given in lower case bold while matrices  $\mathbf{M}$  are upper case bold. To access vectors or matrices elements, we will use accolades notations by specifying their indices  $\mathbf{M}[i, j]$  with  $i, j \in \mathbb{Z}_0^+$ . Inferred elements will be denoted with "", thus, predicted values  $\hat{\mathbf{a}}$  will be compared with their ground-truth measurements  $\mathbf{a}$ .

$\mathbb{Z}$	Integers numbers
$\mathbb{Z}_0^+$	Positive integers in $0, 1, 2, \dots$
$\mathbb{R}$	Real numbers
$\mathbf{v} \in \mathbb{R}^n$	Vector of size $n$
$\mathbf{M} \in \mathbb{R}^{n \times m}$	Matrix of size $n \times m$
$ a  = \sqrt{a^2}$	Absolute value of $a \in \mathbb{R}$
$\ \mathbf{a}\ $	Norm of $\mathbf{a}$
$\mathbf{t}$	3D translation vector
$\mathbf{R}$	3D rotation matrix
$\mathbf{s}$	3D scale vector $\in \mathbb{R}^3$
$\mathbf{x} = (\mathbf{t}, \mathbf{R})$	3D rigid body



# Contents

Acknowledgments - Remerciements . . . . .	i
Notations . . . . .	iii
Summary . . . . .	v
<b>Introduction</b>	<b>1</b>
1 Motivations and research problems . . . . .	1
2 Challenges . . . . .	2
3 Contributions . . . . .	3
4 Scientific context . . . . .	3
5 Manuscript structure . . . . .	4
<b>1 Anatomy of the trunk and the Adolescent Idiopathic Scoliosis</b>	<b>5</b>
Introduction . . . . .	6
1.1 Descriptive anatomy of the spine and its associated structures . . . . .	7
1.1.1 Reference planes for anatomical description . . . . .	7
1.1.2 General anatomy of the spine . . . . .	7
1.1.3 The rib cage . . . . .	10
1.1.4 The pelvis . . . . .	11
1.2 Functional anatomy of the spine . . . . .	12
1.2.1 General description . . . . .	12
1.2.2 Description at the Functional Spine Unit (FSU) . . . . .	12
1.3 Adolescent Idiopathic Scoliosis . . . . .	14
1.3.1 Generalities . . . . .	14
1.3.2 Pathogenesis . . . . .	14
1.3.3 Clinical analysis . . . . .	16
1.4 Summary . . . . .	18
<b>2 Static characterization of scoliosis</b>	<b>19</b>
Introduction . . . . .	20
2.1 Characterization from X-ray acquisitions . . . . .	21



2.1.1	2D radiographic methods . . . . .	21
2.1.1.1	Anatomical landmarks and descriptors . . . . .	21
2.1.1.2	Scoliosis classification systems . . . . .	22
2.1.1.3	Discussion . . . . .	24
2.1.2	3D radiographic methods . . . . .	24
2.1.2.1	The EOS imaging system . . . . .	24
2.1.2.2	Coordinate systems . . . . .	26
2.1.2.3	Description of the spine curvatures . . . . .	26
2.1.2.4	3D classifications . . . . .	28
2.1.2.5	Discussion . . . . .	28
2.2	Detection and monitoring from superficial analysis of the torso . . . . .	30
2.2.1	Screening strategies from back surface measurements . . . . .	30
2.2.2	Quantification of spine deformities from the surface . . . . .	31
2.2.3	Discussion . . . . .	32
2.3	Contribution: 3D inference of the scoliotic spine from depth maps . . . . .	34
2.3.1	Introduction . . . . .	34
2.3.2	Data collection and processing . . . . .	34
2.3.2.1	The New Mexico Decedent Image Database . . . . .	34
2.3.2.2	The GH dataset . . . . .	37
2.3.2.3	Depth map generation . . . . .	37
2.3.2.4	Spine 3D characteristics . . . . .	37
2.3.2.5	Final dataset . . . . .	38
2.3.3	Method . . . . .	38
2.3.3.1	Data Processing . . . . .	40
2.3.3.2	PCA spine representation . . . . .	41
2.3.3.3	CNN architecture . . . . .	43
2.3.3.4	Evaluation . . . . .	44
2.3.4	Results and Discussions . . . . .	45
2.3.4.1	3D spine prediction accuracy . . . . .	45
2.3.4.2	Ablation studies . . . . .	45
2.3.5	Conclusion . . . . .	47
2.4	Summary . . . . .	49
<b>3</b>	<b>Dynamic characterization of scoliosis</b>	<b>51</b>
	Introduction . . . . .	52
3.1	Approaches in the analysis of the torso in motion with scoliosis . . . . .	53
3.1.1	Methods of tracking the <i>in vivo</i> motion of the vertebrae . . . . .	53
3.1.2	Analysis based on superficial features . . . . .	53
3.2	The biomechanical modeling of the spine . . . . .	55
3.2.1	Types of models . . . . .	55
3.2.1.1	FEM models . . . . .	55

3.2.1.2	Multi-body/Rigid-body models . . . . .	55
3.2.2	Specificity to patient anatomy . . . . .	56
3.2.3	Application to motion analysis . . . . .	56
3.3	Discussion . . . . .	56
3.4	Contribution: Multi-Modal Data Correspondence for the 4D Analysis of the Spine with Adolescent Idiopathic Scoliosis . . . . .	58
3.4.1	Method . . . . .	58
3.4.1.1	Collected data . . . . .	58
3.4.1.2	Data processing . . . . .	59
3.4.1.3	The subject-specific kinematic model . . . . .	60
3.4.1.3.1	Model overview . . . . .	60
3.4.1.3.2	Model registration . . . . .	60
3.4.1.4	Accuracy of the anatomical model . . . . .	62
3.4.1.5	Validation of the kinematic predictions . . . . .	62
3.4.2	Results . . . . .	63
3.4.2.1	Accuracy of the subject-specific model in standing . . . . .	63
3.4.2.2	Accuracy of the subject-specific model in bending . . . . .	64
3.4.3	Discussion . . . . .	66
3.4.4	Conclusion . . . . .	69
3.5	Summary . . . . .	70
<b>Conclusion and perspectives</b>		<b>71</b>
1	Summary . . . . .	71
1.1	3D static characterization of scoliosis with non-ionizing methods . . . . .	71
1.2	Towards a 4D analysis of the spine with AIS . . . . .	71
2	Discussions and near future research directions . . . . .	73
2.1	Contribution 1: 3D inference of the scoliotic spine from depth maps . . . . .	73
2.2	Contribution 2: Multi-Modal Data Correspondence for the 4D Analysis of the Spine with Adolescent Idiopathic Scoliosis . . . . .	74
2.2.1	The localization of the radio-opaque markers in biplanar X-rays . . . . .	74
2.2.1.1	Facilitate marker identification . . . . .	74
2.2.1.2	Quantify precision noise . . . . .	74
2.2.2	Increase the classification of the numerical twins to the patients characteristics . . . . .	74
2.2.3	Limitations with dynamic validations . . . . .	75
2.3	On both contributions . . . . .	75
2.3.1	Need of additional acquisition of patients with scoliosis . . . . .	75
2.3.2	Facilitate validation and comparisons between studies . . . . .	75
3	Long term directions . . . . .	77
3.1	3D inference of the spine alignments from depth maps . . . . .	77

3.1.1	Creation of an accessible mobile screening tool . . . . .	77
3.1.2	Additional features . . . . .	78
3.2	Towards a facilitated comprehensive 4D analysis of the spine . . . . .	78
3.2.1	The use of marker-less motion capture methods . . . . .	78
3.2.2	Towards a comprehensive analysis of the spine to investigate new biomarkers . . . . .	79
3.3	Incorporation of our models into longitudinal studies . . . . .	79
<b>Bibliography</b>		<b>81</b>
<b>Acronyms</b>		<b>95</b>
<b>Glossary</b>		<b>96</b>
<b>List of figures</b>		<b>99</b>
<b>List of tables</b>		<b>101</b>
<b>A Appendix A: Anatomical model registration workflow for creation of patients digital twins including their internal and external anatomy</b>		<b>103</b>
1	Overview of the anatomical models . . . . .	104
2	Model registration workflow . . . . .	104
<b>B Appendix B: Detection and quantification of scoliosis from splines</b>		<b>109</b>
3	The Choi - Watanabe method . . . . .	110
3.1	Introduction . . . . .	110
3.2	Methods . . . . .	111
3.2.1	Our dataset . . . . .	111
3.2.2	Metrics . . . . .	111
3.3	Results and discussion . . . . .	111
3.4	Conclusion . . . . .	112
4	Our proposal . . . . .	113
4.1	Algorithm . . . . .	113
4.2	Results and discussion . . . . .	113
4.3	Conclusion . . . . .	116

# Introduction

## 1 Motivations and research problems

Adolescent Idiopathic Scoliosis (AIS) is a progressive disease, with multiple forms, mostly affecting young women and evolving throughout the period of growth. 1% to 3% of the population is concerned [147]. It causes lateral deformations of the spine resulting in changes in the global shape of the trunk and its posture. For the most severe cases, this condition impacts the respiratory functions, causes back pain, discomfort, posture asymmetry and other disorders in locomotion. Currently, diagnosis and analysis are based on clinical examinations and the analysis of X-rays showing spinal deformities [75].

The current recommendation is the use of an orthopaedic brace [114, 147] to stop the progression of the sideways curvatures. In the most severe cases of scoliosis, or in the event of orthopedic brace failure, surgery is indicated to correct vertebral rotation anomalies. These treatments are subject-specific and rely primarily on a precise description of the patient's anatomy obtained through clinical analysis and X-rays. In addition, due to the progressive nature of scoliosis, a regular follow-up is required. However, radiography raises several concerns, mainly due to the recurrent radiation exposure, thereby increasing the likelihood of cancer development [78].

However, scientific literature show promising results in the detection and monitoring of scoliosis from non-ionizing acquisition methods [135]. These methods are based on superficial measurements of the torso that can be correlated with spinal deformities. Yet, they cannot enable the evaluation of the progression of scoliotic curvatures. However, recent methods, combining outer images and deep-learning algorithms, have been developed to correlate internal and external back characteristics [80, 146]. These methods have focused so far on a 2D and partial characterization of the spinal deformations, while scoliosis is inherently a three-dimensional condition [130].

Beside the static analysis of the torso, motion capture (mocap) analysis is also investigated as a non-ionizing approach highlighting dynamic patterns in AIS patients [134]. Motion capture provides a superficial analysis of the patient's motion and does not directly capture the actual dynamics of the spine inside the body. Several works have investigated how to describe the spinal alignments in motion by acquiring 3D trajectories of mocap markers positioned on the palpable spinous process of the vertebrae [101, 122, 125]. However, these methods are validated towards Adult Spinal Deformity (ASD), without back surface representation, and cannot be easily implemented on young patients with AIS.

The promising results provided by the recent literature demonstrate a strong correlation between internal characteristics of the spine and external static and dynamic measurements of the back.

The objective of this thesis is to quantify the correlation between these superficial measurements and the 3D shape of the scoliotic spine in individuals with AIS. This research aims to contribute to the development of safe, non-invasive and non-ionizing methods for the early detection and monitoring of idiopathic scoliosis through static and dynamic assessments.

## 2 Challenges

The various aspects of this thesis require detailed and precise acquisitions of both the internal (spine) and external anatomy (skin) of the patient. While the main part of the state-of-the-art relies on 2D acquisitions, addressing these issues in three dimensions demands specific techniques and methods.

For the spine, the recent advancements in biplanar X-ray imaging, notably through technologies like EOS systems (EOS Imaging, Paris, France), now enable a detailed 3D reconstruction of the vertebrae alignments and geometries [62]. These methods are also adapted to address scoliosis in the young population with a lower radiation emission compared to conventional 3D acquisition methods such as computed tomography [52].

However, for the skin, the reconstruction from X-rays remains challenging [100], especially for scoliotic patients whose trunk can be significantly deformed. Low-cost 3D scanning tools have become essential as they allow for fine acquisition of the body's surface [56, 104]. Nevertheless, the capture of the spine and skin are usually performed in different conditions (acquisition tool, time, environment, etc.) leading to difficulties in their registration, especially concerning posture aspects [18].

In addition, this thesis aims to investigate the dynamic aspects of idiopathic scoliosis, made feasible through the collection of marker-based motion capture data. In addition, to the difficulties in aligning such data with the surface and radiographic modalities mentioned earlier, the existing state-of-the-art in this field is currently sparse, without consensus, when it comes to the dynamic characteristics of adolescent scoliosis.

Another challenge involves the recruitment of a sufficient number of patients, encompassing a diverse range of phenotypes (sex, age, scoliosis condition), to create a database for the development and validation of our methods. This is particularly complicated since the required data are themselves challenging to obtain for a single patient. It should be noted that our data collection has been impacted by the global health crisis caused by the Covid-19 pandemic. In addition, there is currently no public database offering such data, making it difficult for the research community to properly compare the different approaches and obtained results.

### 3 Contributions

Different contributions will be presented in this manuscript.

A first contribution is a novel method of reconstruction of the spinal alignments from a single depth map of the back. This method is designed to provide a detailed analysis of the spine alignments in 3D allowing the detection and characterization of scoliosis using accessible and non-ionizing 3D sensors. To develop our approach, we built a database consisting of digital twins of hospital patients completed with CT-scan segmentations derived from a public database, the New Mexico Decedent Image Database (NMDID). Our inference algorithm is trained to predict a latent PCA representation of the spine from depth images. This dimensional reduction allows us to preserve most of its information and variability while reducing the complexity of the 3D spine positions. Our Convolutional Neural Network predicts 3D vertebrae positions with an average error of below the *cm*. From the predicted 3D positions, scoliosis can be located and estimated like the sagittal alignments, namely kyphosis and lordosis. In addition, our non-ionizing approach can detect scoliosis with an accuracy of 89%. This project has been presented as abstracts in national [4] and international [2] conferences and received the Best Poster award at IABM 2023 (national symposium in artificial intelligence applied in biomedical imaging) [5]. We make our inference code publicly available for research purpose<sup>1</sup>.

The second contribution is named "Multi-modal data correspondence for the 4D analysis of the spine with Adolescent Idiopathic Scoliosis". In this work, we propose a novel approach allowing the creation of subject-specific kinematic models of patients with AIS that includes a 3D representation of their spine and their back surface. To address the issue of the correspondence between different data modalities (skin, scan, mocap), we leverage radio-opaque markers to register the model into the inner and outer observations. With respect to the previous work, our method does not rely on a precise palpation for the placement of the markers. Once created, the resulting numerical twin can be driven by solely external measurements to reconstruct spinal motion. As a preliminary result, we validated our approach with X-rays of two patients in lateral bending and show an accuracy of the vertebra positions below 1 cm on each orientation axis and near 5 degrees in orientations. This project has been presented in an international conference [2] and published in a peer-reviewed journal, Bioengineering 2023 (MDPI) [22].

### 4 Scientific context

The PhD project started the 1st of April 2020 with the support of the ANRT within the CIFRE agreement (Industrial Convention of Formation by Research), no.2019/1197, with Anatoscope, Inria and Grenoble Alpes University Hospital. A part of the presented work was established at Anatoscope, under the supervision of François Faure (CEO) and Inria (French national research

---

<sup>1</sup>Link to the source code repository: [https://gitlab.inria.fr/spine/skin\\_to\\_spine](https://gitlab.inria.fr/spine/skin_to_spine)

institute of computer science and automation), in the Morpheo project team, under the supervision of Sergi Pujades, Edmond Boyer and Jean-Sébastien Franco.

Data were collected at Grenoble Alpes University Hospital under the direction of Aurélien Courvoisier and Olivier Daniel. The studies were approved by two Ethical Committees: CECIC Rhône-Alpes-Auvergne, Clermont-Ferrand, IRB 5891 and CPP Ile de France 2 on the 07/20/2020, no ID RCB: 2020-A01071-38. All parents and patients received an information letter and signed a consent form for publication.

## 5 Manuscript structure

Scoliosis is a complex medical condition affecting different parts of the human body. Thus, this manuscript will start with anatomical definitions of the spine and an introduction of Adolescent Idiopathic Scoliosis in a dedicated chapter. Next, we will outline the existing methodologies and state-of-the-art approaches that allow for a comprehensive characterization of this condition and its early detection. Then, we will present our contributions and how they address the current challenges. By covering different kind of examination approaches of the spinal disorders in this thesis, we facilitate the dissertation by categorizing them into two distinct types: static and dynamic.

The first is the *static* method of examination from medical images. We will point out the current limitations and challenges in the characterization of the spinal alignments using X-ray radiographs. A particular emphasis will be placed on the quantification of the 3D deformities from non-ionizing methods by the external analysis of the torso using machine-learning methods. We will make a review of the literature before a presentation of our contribution that allows a 3D characterization of the full thoracolumbar spine alignments while proposing an accessible, non-ionising examination method.

The second type of approach is *dynamic*, based on motion capture analysis. We will present the different biomarkers that are usually tracked during the acquisitions, methods presented in the literature with their limitations. Then, we will present our approach to address the current challenges in the dynamic characterization of scoliosis with motion capture analysis. In this work, we use a kinematic subject-specific model of the patients leveraging multi-modal data: X-rays in several positions, surface scans and motion capture. Once created, the model can be driven by solely external measurements.

# 1

## Anatomy of the trunk and the Adolescent Idiopathic Scoliosis



## **Introduction**

Idiopathic scoliosis is a progressive disorder that affects the entire spine and its connected structures. Before delving into the description of this condition, we need first to introduce the foundational anatomical concepts required for describing all anatomical components. We will then provide a detailed overview of the asymptomatic spinal anatomy and its associated anatomical structures namely the rib cage and the pelvis. Interested by the dynamic behaviour of the spine, we will also explore these aspects in a dedicated section. Then, we will introduce the focal syndrome of this manuscript: Adolescent Idiopathic Scoliosis. We will provide an overview of the condition, its impacts, its causes and describe its evolutionary aspect.

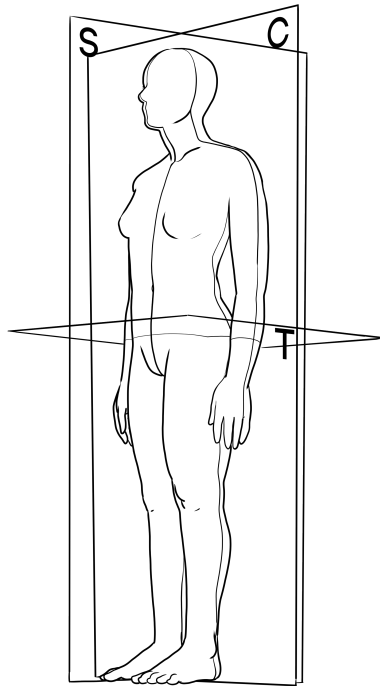


*Figure 1.1: The three anatomical planes of reference. S: sagittal ; C: coronal; T: transverse. Created by Nicolas Comte.*

## **1.1 Descriptive anatomy of the spine and its associated structures**

### **1.1.1 Reference planes for anatomical description**

Before a description of the anatomy of the spine, we need to address some anatomical concepts that provide reference points regarding the position and orientation of anatomical structures in space.

The human body and its anatomical components are usually described from three planes of reference (fig. 1.1). These planes are defined by three orientation axis: antero-posterior, medio-lateral and infero-superior. They can be described as follow:

**The coronal (or frontal) plane** : divides the body into front (anterior) and back (posterior) sides.

**The sagittal (or profile) plane** : divides the body into the left and right. It gives a view from the profile (left or right).

**The transverse (or axial) plane** : is an orthogonal plane from the two others. It gives view from the top (cranial, superior) or the bottom (caudal, inferior) of the anatomical structures.

### **1.1.2 General anatomy of the spine**

The spine is a complex structure that can be summarized by stacked articulated vertebrae, housing the spinal cord, part of the central nervous system [98]. The vertebral column is generally

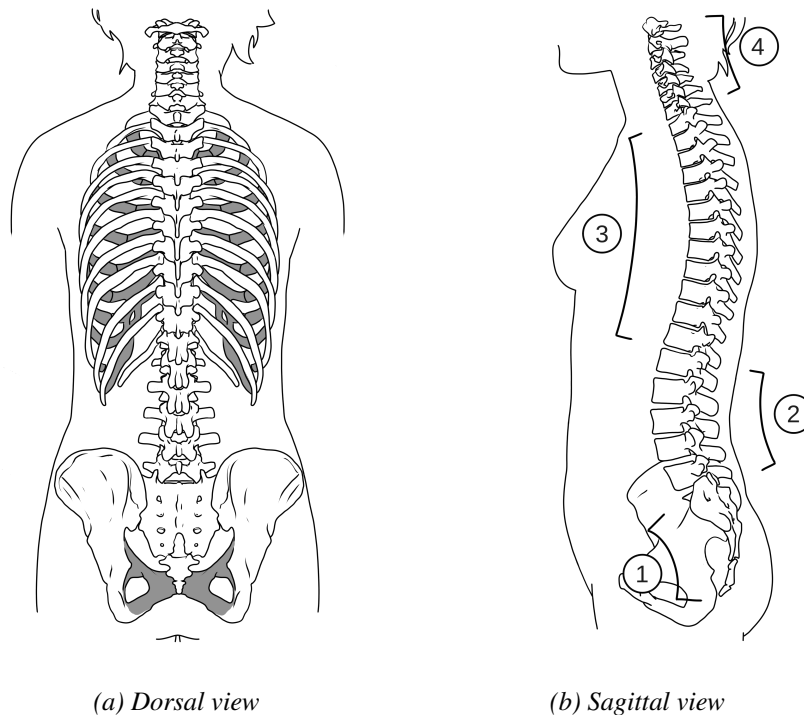


Figure 1.2: Anatomy and curvatures along the spine. 1. sacral-coccyx kyphosis ; 2. lumbar lordosis ; 3. thoracic kyphosis ; 4. cervical lordosis. Created by Nicolas Comte, based on models provided by the company Anatoscope [1].

composed by 33 vertebrae, in average, named and classified according to their region:

- 7 cervical vertebrae ;
- 12 thoracics, parts of the rib-cage ;
- 5 lumbar ;
- Sacrum: composed of 5 fused vertebrae, part of the pelvis ;
- Coccyx, also composed of fused vertebrae (part of the pelvis too).

The asymptomatic spine can be seen almost straight frontally (fig. 1.2a), it's not the case on the profile. The column follows 4 successive natural curvatures of two different types [71] (fig. 1.2b):

**kyphotic** : convex curvature at the thoracic and sacral-coccyx regions ;

**lordotic** : concave curvature at the cervical and lumbar regions.

The shape of the vertebrae varies according to their region (fig. 1.3). However they share a similar structure (fig. 1.4): a vertebral body on the anterior part and the posterior part formed by eleven elements: two pedicles, two laminae and seven processes (one spinous, two transverses and four articulares).

Vertebrae are connected each other by three joints:

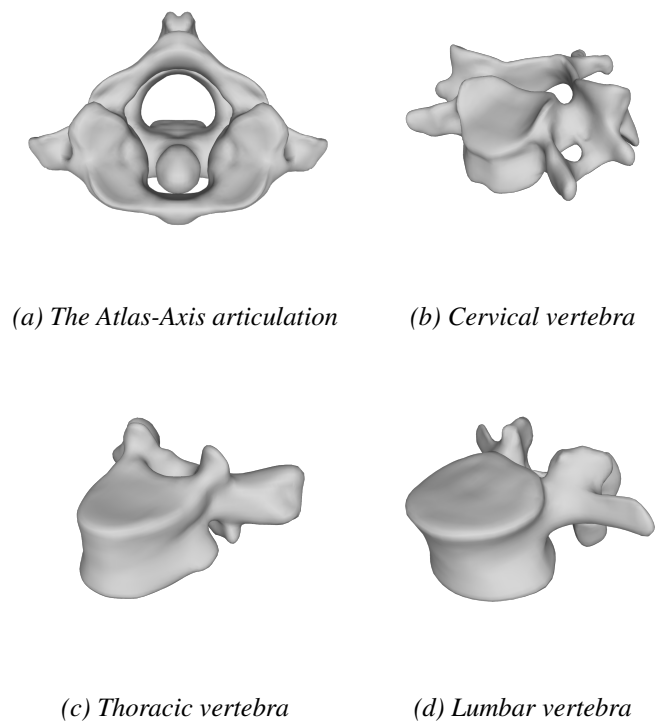


Figure 1.3: Differences in shape of the vertebrae along the spine. Geometries obtained from anatomical models provided by the company Anatoscope [1].

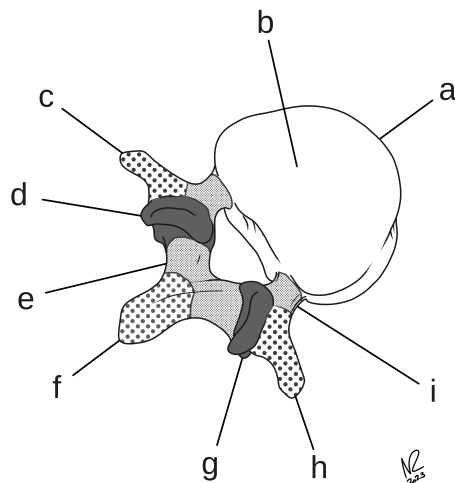


Figure 1.4: Structure of a vertebra. a: vertebral body ; b: superior endplate ; c: left transverse process ; d: upper-left articular process ; e: lamina ; f: spinous process ; g: lower-right articular process ; h: left transverse process ; i: pedicle. The vertebral body with the pedicles and lamina form the spinal canal. Created by Nicolas Comte.

- the Intervertebral disc (IVD) joint;
- two facet-joints (or zygapophyseal joints) on the articular processes.

Furthermore, there are several ligaments that connect the vertebrae, ensuring the stability of the joints. They also provide a high mechanical protection to the spine [71].

It should be noted that vertebrae can have anatomical particularities according to their region:

- the axial articulation (pivot-joint) between the Atlas (C01) and the Axis (C02) in the cervical region (fig. 1.3a) allowing a large rotation of the head in the transverse plane;
- the articular facets of the thoracic vertebrae connecting the ribs on the body and the articular processes.

### 1.1.3 The rib cage

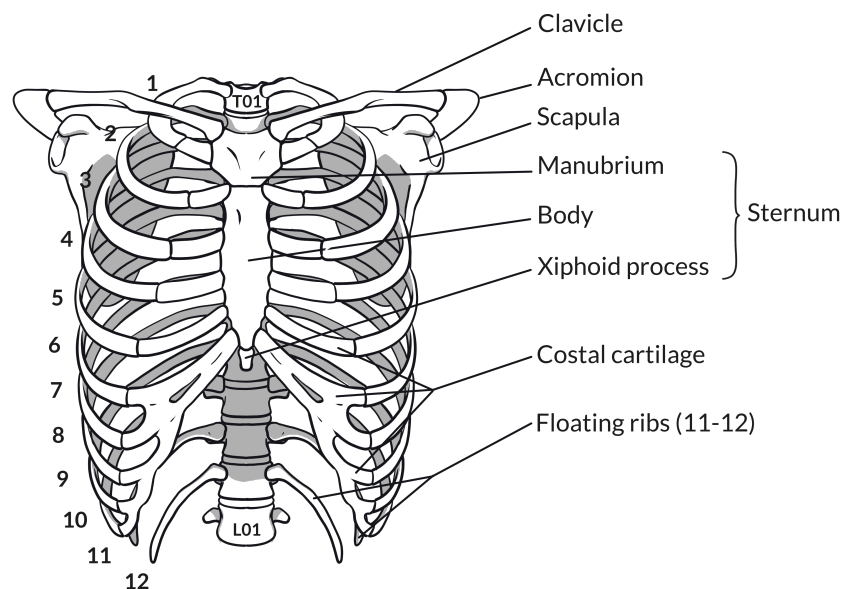


Figure 1.5: Anatomy of the thoracic skeleton. 1-7 true ribs ; 8-12 false ribs. Created by Nicolas Comte with elements from Netter 2018 [98].

The rib cage is formed by the thoracic column, the ribs, and the sternum (fig. 1.5). This structure plays a major role on the protection of vital organs (great vessels, lungs, heart) and mechanics of the respiratory system (ventilation).

Ribs are long and curved bones that can be described in five successive parts (from the back to the front) [98]: the head connected to the vertebral body (form the costo-vertebral joint), the neck, the tubercle connected to the transverse process (form the costo-transverse joint), the angle, the body joined to the sternum with costal cartilage on the front.

We can distinguish two kind of ribs depending on the attachment to the sternum. The first seven pairs, called *true* ribs, are directly connected to the sternum with the costal cartilage. The others are

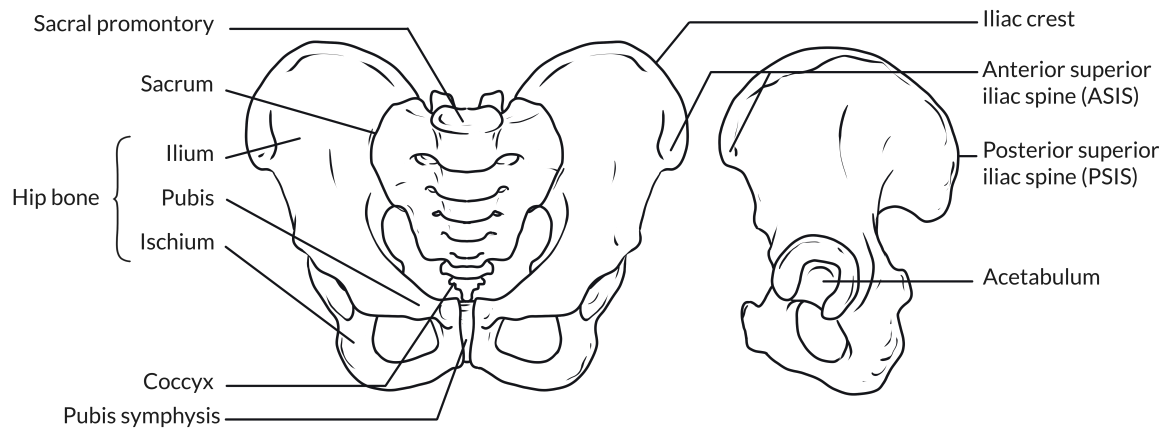


Figure 1.6: Anatomy of the pelvis. Left: face view of the pelvis ; Right: lateral view of the left hip bone. Created by Nicolas Comte.

considered as *false ribs*. They can be connected indirectly to the sternum by the costal cartilage above them or, like the two lowermost ribs, simply not connected. These ones are also called *floating ribs*.

The sternum is located in the middle of the front of the chest (fig. 1.5). It's structured in three parts (from the top to the bottom): the manubrium connected to the two clavicles on its top and the first pair of ribs on its bottom, the body connected to the other costal cartilages and the xiphoid process.

#### 1.1.4 The pelvis

The pelvis is the lower part of the trunk and plays a vital role in supporting the upper body, providing stability and transmitting forces between the spine and the lower limbs. It also houses and protects various organs, including the reproductive organs, urinary bladder, and part of the digestive system.

The pelvis is composed of several bony structures (fig. 1.6): the right and left hip bones (or os coxae) connected to the sacrum.

The hip bone is composed of different regions: the ilium, the ischium and the pubic bone. Several parts are palpable from the skin and are usually used as anatomical landmarks: the anterior superior iliac spine (ASIS) and the posterior superior iliac spine (PSIS).

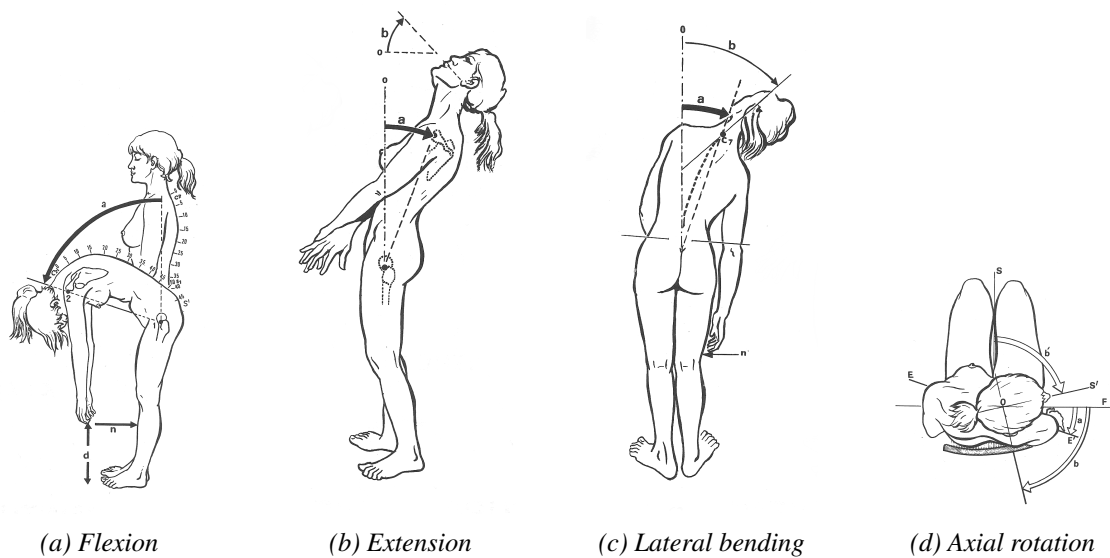


Figure 1.7: Global movements of the spine. Figure from Kapandji 2004 [71].

## 1.2 Functional anatomy of the spine

### 1.2.1 General description

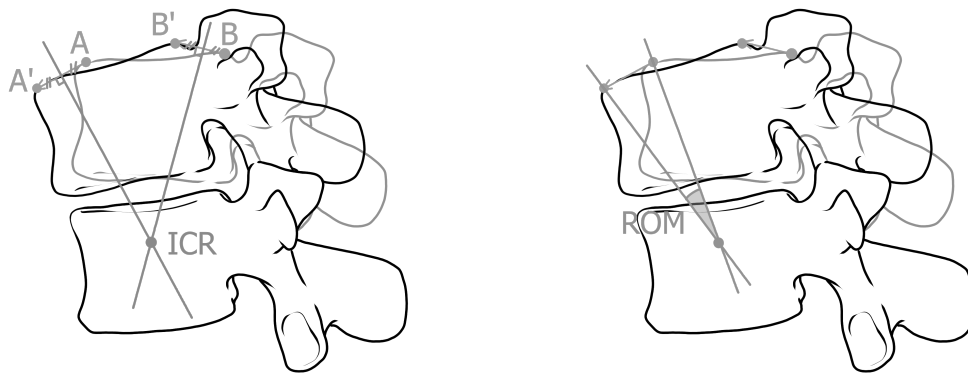
The general motion of the trunk, and the spine, can be described in the three anatomical planes [71, 103] (fig. 1.7):

- sagittal (or profile) plane on which they are moving in flexion/extension ;
- coronal (or frontal, dorsal) plane, in lateral bending ;
- transverse (or axial) plane, in axial rotation.

### 1.2.2 Description at the Functional Spine Unit (FSU)

The movements of vertebrae are often defined at the Functional Spine Unit (FSU) itself. The FSU is a unit of two connected vertebrae describing the motion of the upper vertebra according to the lower one on the three anatomical planes. The rotation is usually described by the Instantaneous Center of Rotation (ICR) and the Range of Motion (ROM) [103]. These elements can be measured with two landmarks defined on the upper vertebral body, that are moving with the vertebra (fig.1.8). Then, a line is drawn according to the displacement of the landmarks and perpendicular bisectors are erected on these segments. The resulting 2D intersection point is called ICR. The angle measured by the rotation around this point is the ROM.

ROM and ICR change according to the vertebra region. For example the axial rotation at the cervical level is high at about 45-50 degrees while the lumbar spine is at about 5 degrees. It can be explained by the local characteristics of each vertebrae: the Atlas (C01) and the Axis (C02) are moving with a pivot-joint while the lumbar part is constrained laterally by its zygapophyseal



(a) Instantaneous Center of Rotation (ICR)

(b) Range of Motion (ROM)

Figure 1.8: Example of measurements for a flexion at the FSU. A and B are two landmarks taken at the beginning of the movement moving both to A' and B'. The perpendicular bisector is drawn at each segment (A-A', B-B') and the intersection gives the ICR location, here on the sagittal plane. The ROM is the angle given by this rotation. Created by Nicolas Comte.

joints [71].

It should be noted that the spine is also affected by natural and non-voluntary movements. Specifically, when the spine bends laterally, the vertebral bodies exhibit an inherent automatic response in the transverse plane, where they rotate naturally towards the convexity of the curvature. This can be seen in X-ray radiographs on the coronal plane when the patients bends and also in scoliotic spines inducing lateral curvatures of the spine [71, 75]. On the image, the vertebral bodies loose their symmetry aspect and the spinous processes move towards the concavity with the two pedicles.

However, there is a lack of consensus on the movements between the vertebrae, even for asymptomatic cases. *In-vivo* experiments are rare and non-invasive measurements are made from X-rays before and after the movement and can be subject to a lack of reliability [107, 123]. More direct insights can be made *in-vitro* on cadaveric pieces [102, 150] although they may be susceptible to tissue degradation and the absence of active muscle functions. *In silico* simulations using biomechanical spine models are considered as promising approaches [37]. However, their limitations arise from the incomplete description and validation of the loadings experienced along the spine [35, 36, 102].



## **1.3 Adolescent Idiopathic Scoliosis**

After introducing the anatomical foundations of the spine, we can observe that the vertebral column is a complex structure that plays a central role in the human body structure. Thus, deformities in this structure can have significant health impacts. This thesis focuses more specifically on the analysis of these deformities in Adolescent Idiopathic Scoliosis (AIS). Therefore, in this section, we will describe this condition, its underlying causes and the consequences in time for the patient.

### **1.3.1 Generalities**

Adolescent Idiopathic Scoliosis is a complex medical condition that primarily affects young individuals between the ages of 10 and 16 [147]. It is characterized by the development of three-dimensional deformities in the spine during the growth period. The term "idiopathic" is used because the exact cause of the condition is unknown. Anomalous vertebral rotations take place throughout the spine, exhibiting themselves in three dimensions [24,64,83]. These rotations particularly impact the frontal plane, leading to the appearance of lateral curvatures known as scoliosis.

The severity of the deformations in AIS is commonly assessed using the Cobb angle from 2D radiographs in the frontal plane. The Cobb angle is determined by measuring the absolute angle between the most tilted vertebrae located at the top and bottom of the abnormal curvature [75] (fig. 1.9). This measurement quantifies the magnitude of the abnormal lateral deviation, with a higher Cobb angle suggesting a more pronounced deformity. Approximately 1-3% of adolescents are affected by this condition, characterized by a major curvature with a Cobb angle greater than 10 degrees [147].

The spine has a central role in the structural support of the body. Thus, scoliosis impacts also the connected structures (pelvis and ribcage) and can lead to various consequences as pulmonary disorders, cardiac issues, physical restrictions in terms of mobility, muscle strength, and back pain, as well as cosmetic concerns in severe cases.

Bracing has been regarded as the standard of care for patients at a high risk of progression, particularly those with curves greater than  $25^{\circ}$  (Cobb) in skeletally immature individuals, and for patient with progression exceeding  $5^{\circ}$  per year. For greater angles ( $> 45^{\circ}$ ) surgery can be planned [75, 147]. The main objective of these therapeutic interventions is to effectively rectify the abnormal spinal rotations present in patients. Therefore, the design of the orthopedic brace and the surgical treatment rely on a detailed understanding of the patient's anatomy provided by clinical analysis and X-ray images.

### **1.3.2 Pathogenesis**

Causes of scoliosis are not clear and still being investigated. Several conditions are studied, because of their relation with the disease. The erect posture of humans is a notable focus in research. As humans are the only animals that can stand, they are also the only animals affected by scolio-

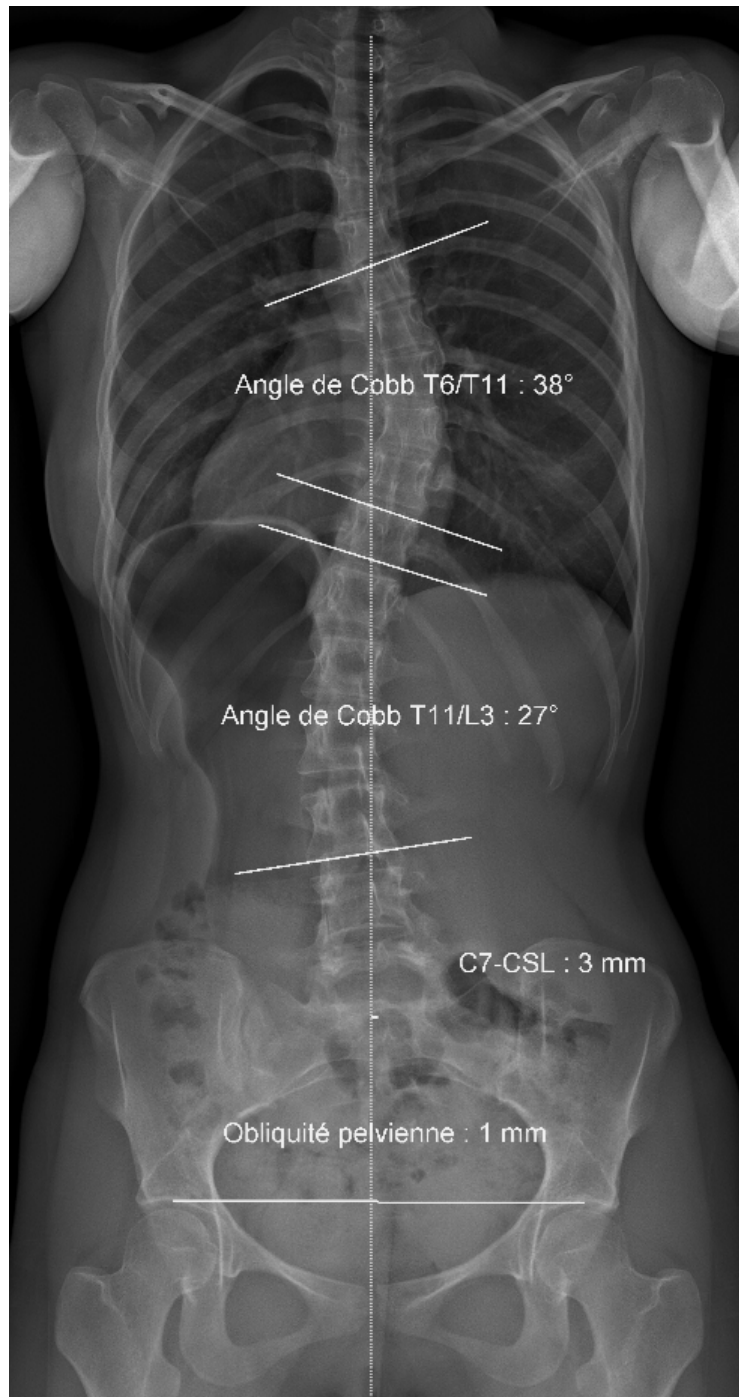


*Figure 1.9: X-ray on scoliotic patient showing its thoracic and thoracolumbar scoliotic curvatures on the frontal plane. The Cobb angle is measured between the superior endplate of the upper end-vertebra of the curvature and the inferior endplate of the lower end-vertebra. The coronal balance is also measured (3 mm).*

sis [30, 83]. An assumption is that upright bipedal posture may induce a rotator instability from which scoliosis found its origin [41].

Genetic patterns are also investigated, as there are instances of scoliosis running in families. However, a reliable profile directly correlated with the disease has yet to be identified [83].

Anatomical asymmetries, growth and deformities of the spine are pointed out at the musculoskeletal level. The role of the nervous system in scoliosis is also under investigation. Researchers are exploring potential connections between nervous system abnormalities and the development of the condition [30, 70, 83]. Even a correlation with abnormal platelets is also considered [83].

Despite all these research efforts scoliosis continues to be considered as an idiopathic disorder, i.e., a disease for which the cause is unknown.

### 1.3.3 Clinical analysis

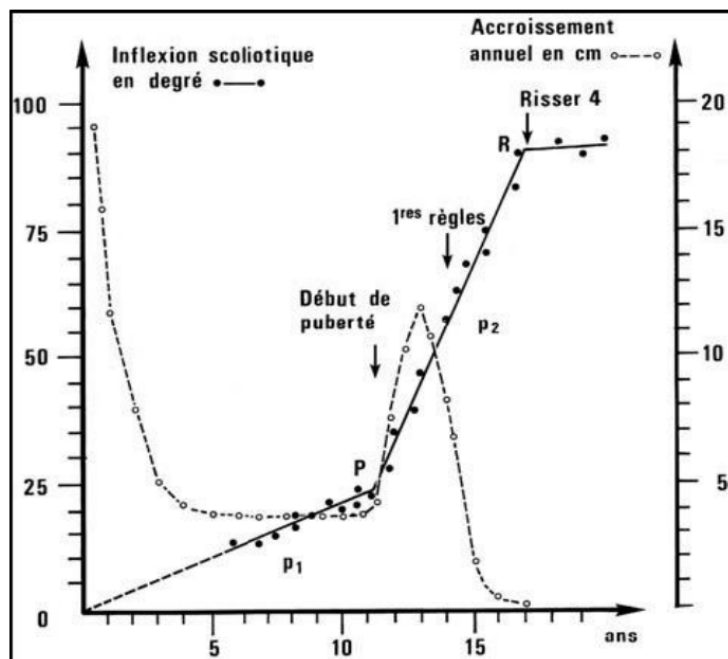
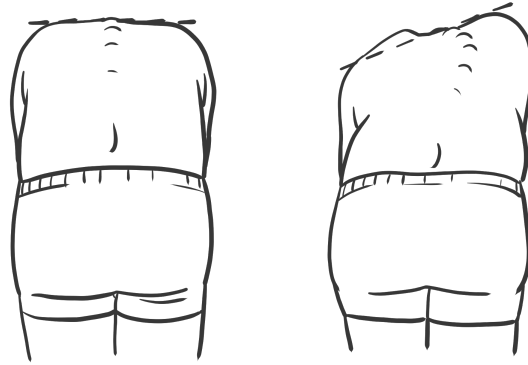


Figure 1.10: Scoliosis evolution law of Duval-Beaupere (1988) showing curvature evolution (degrees, in bold line according to the age in years). Dashed line represents the annual growth increment of the patient in cm. Arrows along the line are showing three events of the adolescent growth peak: starting of puberty at about 10 y., first menstruations and then the Risser sign (bone age) at stage 4 corresponding to the end of the growth peak.

During the peak growth period, there is a notable progression of the sideways curves in scoliosis (see fig. 1.10). As a result, there is a strong motivation to detect and stop the advancement of the disease as early as possible. To achieve this, regular clinical analyses are planned, including interviews, clinical physical examinations and radiograph acquisitions. The clinical examination aims to evaluate the general condition of the patient such as stage of puberty, trunk asymmetries, posture anomalies or muscular rigidity. The Adam's Forward Bend test can be used to assess



*Figure 1.11: The Adam's forward bend test. Left: asymptomatic case; Right: case with scoliosis. Created by Nicolas Comte.*

scoliosis [147] (fig. 1.11). The test highlights the rib-hump caused by rotational anomalies of the spine, breaking the symmetry of the back.

Finally, the radiographic examination is planned to confirm the presence or absence, of spinal deformities, usually from a coronal view. The Cobb angle is measured, from the images, to evaluate the magnitude of the lateral deviations. In case of mild scoliotic curvature, the progression of the deformity can be assessed with an additional X-ray in the next months. Other factors are also taken into consideration when assessing the risk of curve progression, including age at diagnosis, menarchal status (onset of menstruation) and Risser score (an indicator of skeletal maturity) [43]. Thus, follow-up intervals are adapted according to these elements [78].

However, the dynamics of scoliosis evolution are specific to each patient making the estimation of deformity progression challenging. More recent studies have demonstrated promising results with machine learning approaches to estimate the risk of progression [25, 129] by integrating the three-dimensional profile of the spine. In addition, these methods are exhibiting potential in predicting the shapes of scoliosis curvatures as in [8, 51].

## 1.4 Summary

In this chapter, we introduced the essential anatomic concepts that allow the description the spine shape and its motion. The spine is a complex structure composed of vertebrae, of different shapes and properties, associated with various bony elements. It plays several roles in the human body in terms of structural support and mobility.

Then, we presented Adolescent Idiopathic Scoliosis (AIS), which is a multifaceted medical condition that evolves over time and impacts the entire three-dimensional structure of the spine. Given its progressive nature, early detection and comprehensive characterization of the curvatures are crucial for prompt and effective treatment. However, as the term "idiopathic" suggests, the underlying causes are unknown, making AIS prediction challenging. As a result, scoliosis needs to be screened to detect the first signs of the deformity. For an early detection, a detailed characterization of the trunk is implemented, describing both external and internal patient's anatomy.

Consequently, in this thesis work, it is essential to understand the current methodology that enables a comprehensive overview of the spine and its deformities. In addition, this thesis also focuses on exploring the early stages of AIS. Therefore, in the next chapter, we will focus on the existing AIS descriptors measured for the detection and monitoring of scoliosis.

# 2

## Static characterization of scoliosis

## Introduction

Adolescent Idiopathic Scoliosis (AIS) is a progressive disease of the spine with causes that remain unknown. Consequently, patient healthcare rely on a regular follow-up evaluating deformities magnitude over years. A main interest is to detect scoliosis as early as possible in order to plan a prompt treatment, usually with an orthopaedic brace that stops progression. Moreover, the implementation of treatment requires patient-specific approaches to these deformations through a comprehensive characterization of the patient's anatomy.

Historically, this characterization is done in 2D through the analysis of radiographic images in the frontal plane highlighting lateral deviations of the spine [75]. From this view, the Cobb angle can be measured, which is the standard measurement quantifying magnitude of deformations. Usually, angles exceeding 10 degrees are regarded as curvatures with a risk of progression [147]. The recent advances in three-dimensional imaging have allowed access to the 3D shape of the spine and improved the understanding of scoliosis. However, these radiographic approaches have been shown to increase the risk of cancer development, particularly in the case of repeated exposure required for medical follow-up in diagnosed patients [60,91,115].

Scoliosis also manifest itself on the surface of the body, for instance by breaking the symmetry of the trunk. Given the prevalence of AIS in the population, these external signs allows the implementation of screening strategies. The methods are based on an analysis of the back but do not allow an examination of the internal deformations required to assess scoliosis progression.

Studies comparing these external measurements with internal ones show the possibility to estimate the magnitude of scoliosis deformity. More recent studies, using deep-learning approaches were also able to predict the Cobb angle from external back images. Yet, these methods provide an estimation of the Cobb angle, which is a partial and 2D measurement of the deformity while scoliosis is better characterized in 3D in its full length.

In a contribution, we propose a new non-ionizing approach that address the current challenges into the analysis of scoliosis. We trained a Deep Learning algorithm to predict the 3D thoracolumbar vertebra positions, encoded in a PCA representation, from depth images of the back. We evaluated our method against X-ray observations and showed that our approach presents promising results into the analysis of the spinal alignments, in different anatomical planes, and the detection of scoliotic curvatures.

In this chapter, we will present for the first time, the various radiographic measurements used to describe spinal deformations. Secondly, we will introduce non-ionizing analysis methods for monitoring scoliotic patients through the superficial examination of the back. We will highlight their limitations before the presentation of our contribution.

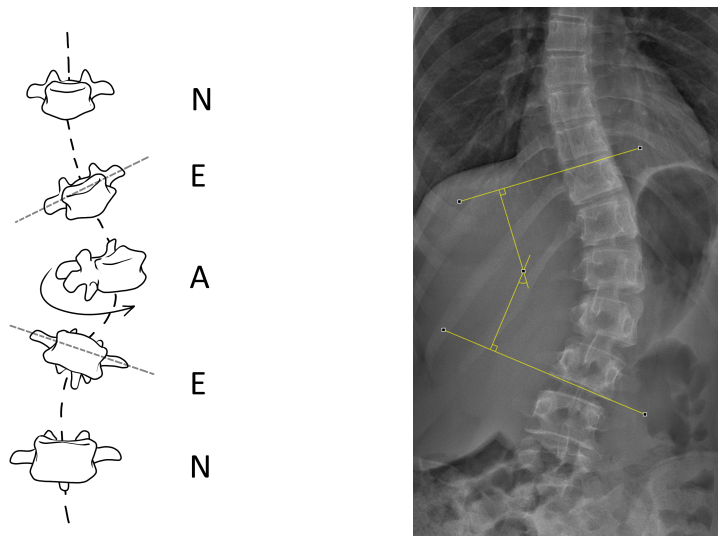


Figure 2.1: Structure of a scoliotic curvature and measurement of the Cobb angle from X-rays (left). N: neutral vertebra; E: end vertebra; A: apical vertebra

## 2.1 Characterization from X-ray acquisitions

Traditional characterization techniques rely on individual 2D X-ray images, thus providing 2D descriptors of the spine alignments like the Cobb angle. More recent approaches use bi-planar X-ray imaging techniques which allow to extract 3D characteristics of the spine. In a first time, we will describe the different descriptors that are measured from the 2D X-ray images and the classifications built from these elements. In a second time we will introduce the different 3D measurements provided by the recent imaging systems.

### 2.1.1 2D radiographic methods

#### 2.1.1.1 Anatomical landmarks and descriptors

The measurements of the spinal alignments are usually gathered on a coronal view of the spine exhibiting the scoliotic deformities. From these images, several landmarks are located and descriptors computed following Scoliosis Research Society (SRS) recommendations.

**The end and apical vertebrae.** Scoliosis can be described from X-rays in the coronal plane showing lateral deviations. The curvature is delimited by two end (or limit, junctional) vertebrae which are the two most rotated elements in the plane (fig. 2.1). The most deviated vertebra along this segment is called "Apical"

**The Cobb angle.** As described in section 1.3.1 page 14, the Cobb angle is a descriptor employed to assess the magnitude of a spinal curvature. On the coronal plane, an angle superior than  $10^\circ$  spine is defined as a true scoliotic curvature with risk of progression [147]. A measurement between  $10^\circ$ - $20^\circ$  is considered as mild scoliosis, from  $20^\circ$  to  $45^\circ$  moderate and severe for curvature



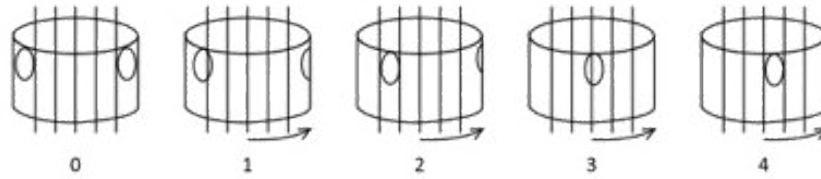


Figure 2.2: Grading of vertebral axial rotation with the Nash-Moe method [95], from [99]: grade 0 (neutral position) to 4. The rotation is quantified on the basis of the pedicle's position on the frontal view (seen in X-ray as ovals) in one of these imaginary lines.

over  $45^\circ$  [75].

**The Kyphosis and Lordosis angles.** These angles give the magnitude of the corresponding curvature on the sagittal plane. They are measured according to the Cobb angle method between two vertebra references. From T01 (or T04) and T12 to compute thoracic kyphosis and L01 and L05 for lumbar lordosis.

**The Vertebral Axial Rotation (VAR).** VAR (or AVR) is quantifying the rotation of a vertebra on the transverse (axial) plane. It's historically evaluated with the Nash-Moe method [95] from coronal views of the spine. Its measurement is usually made from the pedicle location according to the vertebral body. In the Nash-Moe method, the body is divided into three imaginary segments and the rotation is quantified on the basis of the pedicle location in regard to them (fig. 2.2). It should be noted that other methods of measurements, based on the pedicle or spinous process locations, are presented in the literature [142].

### 2.1.1.2 Scoliosis classification systems

The analysis of scoliosis and its inherent complexity in shape has led to the creation of different classifications. First mentions in the literature are showing the Schulthess classification system since 1905 [94] dividing scoliosis according to the curve location. Ponseti and Friedman published in 1950 a new classification [112] that distinguishes spines according to the global shape of the spine and their evolution. Other works extend or introduced new curvatures to classify shapes of scoliosis as Moe and Kettle's (1970). In 1983, King et al. [76] published a new system to give guidelines for surgical treatment, mainly for Harrington rod instrumentation. This classification has been widely used but gives a poor inter- and intra-observer reliability [27]. Within the evolution of spine surgery, Lenke et al. published in 2001 a new classification system [86], with better reliability scores. It mainly distinguish spines according to the frontal plane, according to trunk imbalance, the number of curvatures and their shape. It's currently recognized as a gold-standard classification in scoliosis surgery. This system splits spines into 6 classes with 3 additional "modifiers" given from the sagittal profile, for a total of 14 classes (fig. 2.3).

However this classification, coming from surgery, may not be suitable for designing braces intended to prevent and correct scoliosis curves through external forces. For instance, the Rigo et al.

<b>Lumbar Spine Modifier</b>	<b>Curve Type (1 - 6)</b>					
	Type 1 (Main Thoracic)	Type 2 (Double Thoracic)	Type 3 (Double Major)	Type 4 (Triple Major)	Type 5 (TL/L)	Type 6 (TL/L - MT)
<b>A (No to Minimal Curve)</b>	 1A*	 2A*	 3A*	 4A*		
<b>B (Moderate Curve)</b>	 1B*	 2B*	 3B*	 4B*		
<b>C (Large Curve)</b>	 1C*	 2C*	 3C*	 4C*	 5C*	 6C*
<b>Possible Sagittal structural criteria (To determine specific curve type)</b>	 Normal	 PT Kyphosis	 TL Kyphosis	 PT + TL Kyphosis		

- : <10°  
 \* T5-12 sagittal alignment modifier: -, N, or + N : 10-40°  
 + : >40°

Figure 2.3: Lenke et al. 2001 classification, figure from the original paper [86]

2010 classification [114] or the De Mauroy et al. 2008 classification [29], which are used to formulate brace design guidelines, rely on radiographic measurements, like the Lenke classification, with additional external descriptors like trunk asymmetry, rib hump, balance and pelvis position.

### **2.1.1.3 Discussion**

The main interest of these classifications is to label spinal deformity in order to give guidelines for brace conception and surgery planning and instrumentation. These systems are mainly based on a static descriptive analysis from the frontal plane that can be subject to errors and ambiguity. For instance, the Cobb angle, used for the assessment of scoliosis, is subject to intra- and inter-reliability scores decreasing for smaller curvatures and that vary with 95% confidence interval ranging from  $3^\circ$  to  $10^\circ$  [11, 141]. The source of error has been found in the practitioner's ability in interpreting the X-ray images, specifically in locating the end-vertebrae and estimating the slopes from the vertebral endplates to define the angle [57]. The exact identification of the anatomical landmarks can be difficult due to variations in vertebrae appearances, patient positioning, orientation, overlap between bony structures or the quality of the X-ray images. In addition, successive studies have shown the constraints of the Cobb angle, as it solely characterizes the deviation in the coronal plane, missing important features of the curvature, especially in the transverse plane involving vertebral axial rotations [25, 64, 108, 129].

## **2.1.2 3D radiographic methods**

As scoliosis is acknowledged as a three-dimensional deformity of the spine, the existing clinical approach of analyzing the spine in two dimensions provides only a limited overview of the deformities. Thus, there is a clear need to establish new coordinate systems and descriptors that allow for a thorough and comprehensive assessment of the three-dimensional spinal alignment.

### **2.1.2.1 The EOS imaging system**

The 3D analysis of the spine was usually made from radiograph techniques like Computed Tomography (CT). However, numerous studies have documented the risk of cancer, increased in repeated ionizing exposure as implemented in AIS monitoring [78]. In addition, CT-Scans and Magnetic Resonance Imaging (MRI) are performed with the patient lying down and do not allow a weight-bearing analysis, in upright physiological position, as required to analyse spinal alignments. This change in position is also affecting the analysis, for instance scoliosis shape changes by  $11^\circ$  (Cobb angle) in average (std:  $5^\circ$ ) [138].

The EOS imaging system has been designed to address these issues by leveraging less-ionizing radiograph techniques [52]. Two X-ray emitters and detectors are placed orthogonally (fig. 2.4). During the acquisition, the sources move vertically and simultaneously producing two images (coronal and sagittal) of the patient in standing pose. Then, the 3D reconstruction can be done using the SterEOS software (EOS Imaging, France). This software allows the semi-automated reconstruction of the skeleton geometries from anatomical stereo-landmarks manually located onto



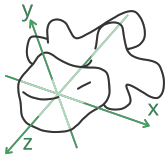
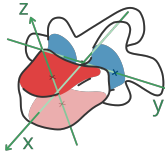
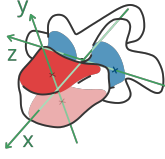
the biplanar images [62]. An additional manual step allows the refinement of the resulting model on the radiographs. This method allow a fine reconstruction of the patient anatomy with an accuracy in shape of 1.1 mm with 95% CI less than 1.7 mm compared to CT reconstructions [54].

Due to its less ionizing nature, this technique is also investigated in the analysis of the spinal alignments in different poses [101]. This system will be used in our following contributions.

### 2.1.2.2 Coordinate systems

Recommendations of 3D coordinate systems have been proposed to describe spine and individual vertebra positions and orientations. Usually two systems are described: a local axis system (at each individual vertebra) and a spinal axis system (describing the entire trunk position and orientation). Three definitions are often used in the literature: from Panjabi (1978) [103], from the Scoliosis Research Society (SRS) [130] and the International Society of Biomechanics (ISB) [149], tables 2.1.

*Tableau 2.1: Definitions of the local axis system orientations in the literature. The SRS and ISB systems are based on the location of anatomical landmarks: the middle of the endplates (red) and the pedicles (blue). Figures by Nicolas Comte.*

Axis system	x	y	z	Figure
Panjabi system [103]	Left	Up	Forward	
SRS system [130]	Forward	Left	Up	
ISB system [149]	Forward	Up	Right	

These systems differ in their orientations definitions (see table 2.1) and in their construction. Both the SRS and ISB systems use the same landmarks on the vertebrae (center of the endplates, pedicle locations, ...) that allow for definition of a 3D position and orientation of the vertebra.

### 2.1.2.3 Description of the spine curvatures

In the goal to better characterize scoliosis in 3D, the SRS Working Group on 3D Terminology of Spinal Deformity has been constituted. The group was tasked with the development of descriptors to ultimately elaborate a 3D characterization of scoliosis [130]. The resulting report provides

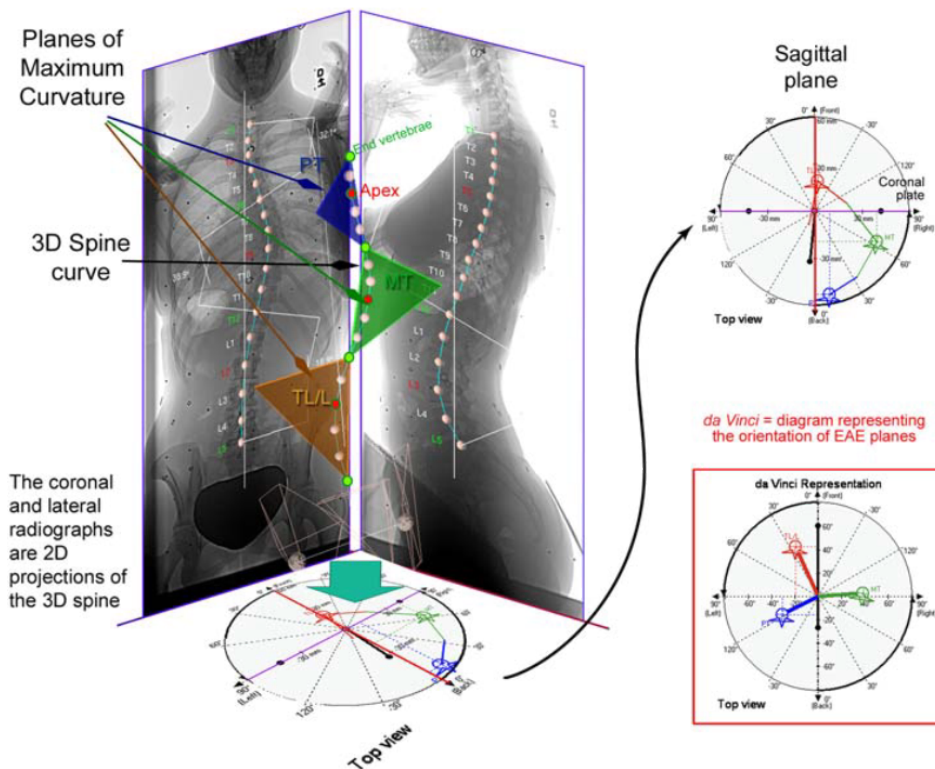


Figure 2.5: The da Vinci view, figure from Labelle et al. 2011 [84].

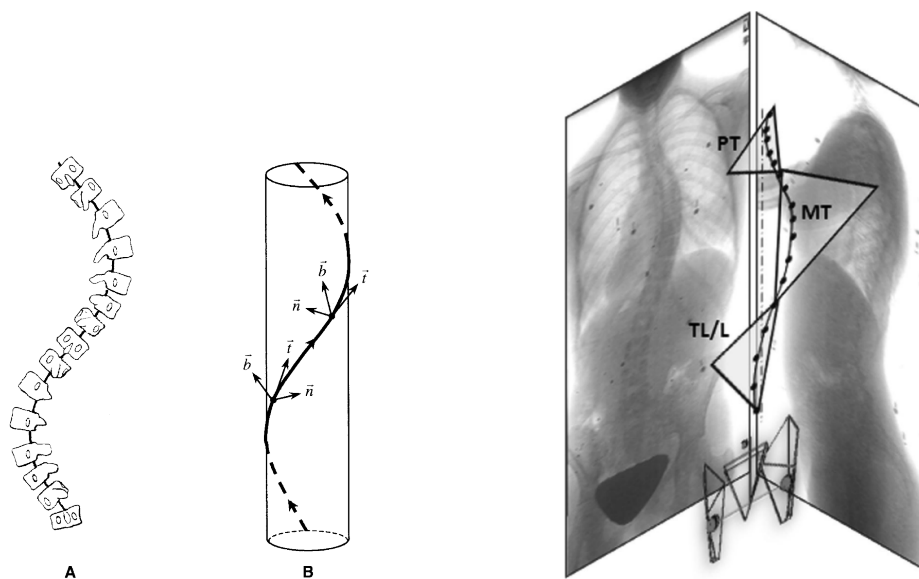
references to describe the spine in 3D, with vertebra orientations and the global 3D shape of scoliosis within planes:

**The Best fit plane (BFP)** This element is defined as the plane which best fits the curve defined by the centroid of each vertebral body of a specified region of the spine. It's mostly useful to define Plane of maximum curvature (PMC) [130] at the scoliosis level defined by the end and apical vertebrae.

**The Cobb angle on the Plane of maximum curvature** Measured between the end-vertebra following the Cobb angle method on this plane.

**The Torsion Index** Described in Drevelle [39], this index is the mean of the sum of the Inter-vertebral Axial Rotations of the upper hemicurve (upper limit to the apical vertebra) and of the lower hemicurve (apical to lower limit vertebra) inside the scoliotic curvature. The descriptor is usually computed from 3D reconstructions.

In addition, the SRS recommend a new visualization tool summarizing and locating in one picture the 3D properties of the spine: the da Vinci view [117]. This figure is a top-view projection of the planes of maximum curvature showing scoliosis locations and orientations (fig. 2.5).



(a) Poncet et al. 2001 classification [111] is based on the geometrical torsion index. Figure from [110].

(b) Sangole et al. 2009 classification [117] use planes of maximum curvatures and angles. Figure from [117].

Figure 2.6: Different approaches of the 3D nature of the spine for 3D classification

#### 2.1.2.4 3D classifications

There are several 3D classifications systems in the literature. Their main differences are coming from their approach to describe the spine mathematically. The first one is coming from Poncet et al. 2001 [111] considering the spine as an helicoidal structure and computing at each level a geometrical torsion index from Frenet's formula. Duong et al. 2006 [42] classified scoliosis shapes using wavelets transformations of the vertebra centroids. The other classifications tend to use the angles in the three anatomical planes (cobb angles, kyphosis, lordosis, vertebral axial rotations...), the Plane of maximum curvature and its orientation like Sangole et al. 2009 [117] for example. Similar classifications [64, 69, 117, 126] are showing subgroups inside the Lenke classification. These profiles can be distinguished from the transverse plane suggesting a lack of personalization of the scoliotic treatment. Thus, it highlights the limitations of this classification and the importance of a full 3D representation of the skeleton.

#### 2.1.2.5 Discussion

The three-dimensional capture of the spine provides a more detailed understanding of the patient characteristics. In particular, it allows the measurements of descriptors that are still poorly described by traditional methods, such as axial rotations in the transverse plane. These descriptors enable a more specific description of scoliosis, and thus improve the characterization process essential for the implementation of a specific treatment as required for the design of an orthopedic brace or surgery. These studies show that 2D characterization of the scoliotic curve reveals inherent structural differences that are not apparent in a single view and illustrate the influence of the

measure on curve classification [69]. Even the Lenke 2001 classification is affected: 3D analysis is highlighting sub-classes that can be distinguished from the transverse plane [42, 69, 117, 126].

Beside shape classification, descriptors of the transverse plane have also been correlated with scoliosis progression [25]. Thus, Skalli et al. 2017 [129] investigated the use axial rotations (apical and inter-vertebral) and torsion index to estimate a risk of progression of scoliotic curvatures and were able to obtain in their validation process an accuracy of 89% in classification.

Let us note that these 3D classifications have not been adopted in clinical usage and remain used in research studies only. Donzelli et al. [34] points several reasons: the inherent complexity of 3D analysis, not intuitive for clinicians for an everyday activity and the significant resources and equipments to capture the 3D shape of the spine that are currently not common in hospitals.





*Figure 2.7: The Adam's forward bend test with a scoliometer. Created by Nicolas Comte.*

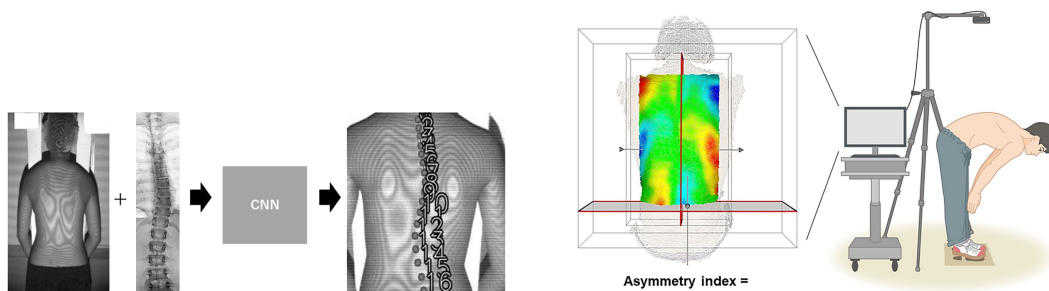
## **2.2 Detection and monitoring from superficial analysis of the torso**

Despite the reliability of X-ray imaging methods for detecting scoliosis, they have limitations that make them unsuitable for screening. They are complex techniques requiring considerable resources to use, in terms of cost, maintenance, acquisition time and qualified personnel. Furthermore, these techniques involve ionizing radiation, which increase the potential risk of cancer development [60, 91, 115], especially with repeated exposure, as necessary for diagnosed patients with regular monitoring.

### **2.2.1 Screening strategies from back surface measurements**

By affecting the entire spine and its connected structures, scoliosis alters the overall symmetry of the torso. Therefore, screening methods focus on the evaluation of external features. The primary approach, the Adam's forward bend test, visually identifies rib humps, which serve as indicators of scoliosis. This method can be combined with a scoliometer, a goniometer, designed to quantify the degree of asymmetry of the trunk (fig. 2.7). Another method, developed in the literature, is Moiré topography [148]. This is a photostereometric imaging method where the examiner identifies irregularities of contour lines representing depth levels of the back surface (called Moiré) [72].

In addition to their high potential in the detection of scoliosis, these examination approaches provide a quantitative analysis of the trunk deformations. Recent methods leveraging three-dimensional capture and digitization of the back surface [15, 61, 79, 81, 113] allow the automation of these measurements. These techniques, using depth sensors or rasterstereography [38], facilitate three-dimensional analysis of the body surface in relation to spinal deformations, with good reliability and validity scores [135].



(a) In Choi et al. 2017 [20], authors were able to predict the positions of the vertebrae from moiré images using CNN. They presented an other method to give the axial rotations in a second study [19, 146]. Figure from [146].

(b) Kokabu et al. 2019 [81] and 2021 [80] proposed methods to predict the Cobb angle from a 3D image of the back in Adam's forward bend test. They measured asymmetries of the captured point-cloud related to spine deformities. Figure from [81]

Figure 2.8: Different works allowing scoliosis monitoring from outer images of the back and CNN approaches.

## 2.2.2 Quantification of spine deformities from the surface

These free-radiation methods are promising in the assessment of scoliosis but are not allowing measurements of the spinal deformities as provided by X-ray imaging tools.

This is due to the lack of understanding regarding the connection between the internal and external deformations. Given the complexity of this relationship, machine learning tools have been investigated to learn this relationship from the available data. Jaremko et al. 2001 [66] present a first artificial neural network regressor of the Cobb angle from different features obtained from torso surface cross-sections. In 2002 [67], authors proposed an other model, coupled with a genetic algorithm to identify the relevant torso asymmetry descriptors improving the regression task. Adankon et al. 2012 [7] uses least-squares support vector machines to determine scoliosis curve type from torso surface beyond thoracic major, lumbar major, thoracolumbar major and double major curves.

Since 2019, the recent advances in Deep Learning, coming from Convolutional Neural Network (CNN) models, facilitate the inference of the Cobb angle from images of back. CNNs are particularly used due to their ability to interpret visual informations from diverse kind of images (depth maps, RGB, etc.). In these models, each image is processed through different convolutional layers in charge of the extraction of the visual features. Then, additional components like activation functions, pooling or fully connected layers can be associated to process the relevant features for regression or classification.

For instance, Yang et al. [151] proposed a method of screening scoliosis automatically from RGB images of unclothed back. A first CNN model delimits the region of interest (the back) on the photo and an other model classifies the region according to the Cobb angle among four classes (asymptomatic, mild, moderate, severe). In their study, Watanabe et al. 2019 [146] estimate 2D spinal alignments [20] and axial rotations [19] from Moiré images cropped around the spine

(fig. 2.8a). Kokabu et al. 2021 [80] extend the Adam’s forward bend test, using a depth sensor by predicting the main Cobb angle. Their method has also been evaluated from depth maps in different poses and garment conditions [65].

### 2.2.3 Discussion

As a summary, surface analysis techniques are designed to characterize external 3D deformities of the back in order to detect scoliosis and estimate the magnitude of its severity. Recent studies, based on deep-learning [80, 146, 151], present methods that facilitate the modeling of the complex relation between external and internal deformations, enabling the inference of radiographic measurements, like the Cobb angle, from images of the back. These works opens the possibility of non-ionizing detection of scoliosis and the follow-up of the internal spinal deformities to monitor their progression. For instance, Choi et al. 2017 [20] reported an average error in the evaluation of the Cobb angle from Moiré images of  $3.13^\circ$  (std:  $2.22^\circ$ ) for early-onset scoliosis (Cobb angle between  $10$ - $20^\circ$ ). It should be noted that the Cobb angle measured from X-ray images, is reported with 95% CI ranging from  $3$  to  $10^\circ$  [11]. Making these results promising in the assessment of scoliosis progression evaluation.

In case of monitoring and characterization for treatment decision and planning, a full 3D characterization is preferred as discussed section 2.1.2. Unfortunately, these methods are usually providing a limited 2D characterization of the deformities. To the best of our knowledge, some studies investigate regression methods to retrieve 3D spine informations from torso surfaces. Nérot et al. 2016 [96] trained Principal Component Analysis (PCA) models to regress the 3D positions of the spinal joint centers from reconstructed skin point-clouds of healthy spines. In 2018, Nérot et al. 2018 [97] employed regression equations to deduce sagittal alignments from external landmarks. However, these investigations did not specifically address scoliosis and were applied and validated on asymptomatic subjects. In contrast, Caturano et al. introduced a similar approach in 2022 [18] on scoliosis subjects, with a regression model inferring the 3D spine alignments from keypoints of a 3D back surface scan.

However, the inference process of internal positions from external scans remains challenging. Beyond the difficulty of collecting 3D patient data, the different modalities must be consistent with each other. In their study, Choi et al. 2017 [20] projected the X-ray view on the back image to obtain the 2D vertebra positions inside. Caturano et al. 2022 [18] fused the biplanar X-ray images and 3D optical scans with 3D rigid transformations. However, as highlighted in their publication, these acquisitions were not performed simultaneously, and patients may change their posture, leading to a lack of correspondence. Addressing the discrepancy in these data should be considered, in the future, to improve model inferences.

An other solution is to reconstruct the body surface directly from X-rays. However, this task is also challenging: only the silhouette can be easily distinguished in the images, and the use of anatomical stereo-landmarks, as employed in 3D reconstruction of the spine in the SterEOS software [62], is limited. Nérot et al. 2015 [100] employed an anatomical model based on a set of control points

identified in the images, with refinement performed on the silhouettes contours. This method is based on an asymptomatic deformable model and is challenging to implement in scoliotic subjects characterized by a deformed and asymmetrical back. Gajny et al. 2019 [49] addressed this issue by using a statistical model of the torso comprising skeleton characteristics (spine, rib cage, and pelvis), which can be refined using a set of 10 radio-opaque markers. Yet, this method has not been evaluated against true surface scans. Another strategy is the use of calibrated depth cameras during radiograph acquisitions from which a skin surface can be reconstructed [56]. In practice, the available size of the radiography cabin should be taken into account when positioning cameras to obtain comprehensive views of the patient's back. For instance, the dimensions of the available place inside the EOS cabin is 76 cm width  $\times$  76 cm length [74].

## 2.3 Contribution: 3D inference of the scoliotic spine from depth maps

### 2.3.1 Introduction

Detection and monitoring of scoliosis rely on a comprehensive characterization of spine deformities. Recent studies [80, 146, 151] showed a strong correlation between 2D spinal alignments and back surface. Their results are promising, thus paving the way for a non-ionizing detection and monitoring of Adolescent Idiopathic Scoliosis from external back images. As recommended in the literature, scoliosis is better described in 3D [130]. The aim of the following contribution is to quantify the correlation of the back with the 3D spinal alignments. Our hypothesis is that the information present in a depth map of the back of a person has a very strong correlation with the underlying 3D shape of the spine, i.e. the 3D location of each vertebra. Thus, a model taking as input a depth map could predict the 3D shape of the spine. The goal of this study is to evaluate such a strategy and its accuracy by comparing the predictions made by a CNN model with real-life measurements of spine positions and curvatures.

### 2.3.2 Data collection and processing

There is currently no database to our knowledge that provide both a 3D image of the torso and its skeleton of a large amount of patients. We need to create our own database from available resources where these data can be retrieved. We identified two among them:

- The New Mexico Decedent Image Database (NMDID) ;
- Data collected in our institution Grenoble Hospitals (GH).

In the following sections we will describe how we constituted our database from these two data sources.

#### 2.3.2.1 The New Mexico Decedent Image Database

**Database overview.** The NMDID, *New Mexico Decedent Image Database* [44], is a collection of *post mortem* CT-Scans, full-body, from the New-Mexico University. These volumetric images are associated within metadata about the medical history of the body like informations about the presence of scoliosis. Yet, about 5% of these corpses present scoliosis with a high variability of conservation and preservation. This is due to different conditions as the state of the decomposition or the causes of death that can affect partially or completely the body integrity. Still, this database is an important source of data providing volumetric internal and external information of human bodies. For our project, we selected the full-torso scans which are captures in the axial planes with 0.5mm thickness between each slice (1 mm ×1 mm pixel spacing in average). By segmenting the volumetric images, we can extract the 3D geometries of the relevant structures (skin and spine).

**Inclusion and exclusion criteria.** For our analysis we selected cases with torso scans according to different criteria listed below and based on the available metadata as well as on visual inspec-

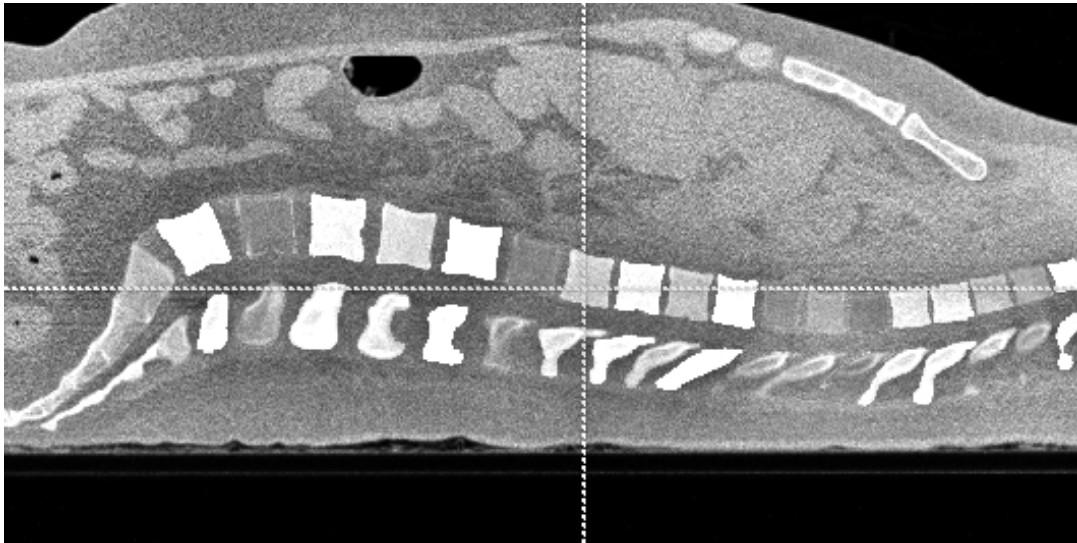


Figure 2.9: Example of the issue of back flattening. Ventral part on the top, back is below. This issue appears particularly with individuals with obesity condition.

tions of the images:

- Annotation with presence or not of scoliosis disorder.
- Age between 0-30 y.
- 17 thoracolumbar vertebrae (12 thoracic, 5 lumbar, without transitional vertebra).
- On the Body Mass Index (BMI): a selection on BMI was needed since the corpses are in supine position, and the back is flattened during the CT-acquisition. High BMI bodies had completely flat backs with no shape information (fig. 2.9). So we compute the BMI according to metadata and exclude cases up to  $30 \text{ kg/m}^2$ , threshold of obesity.
- On the body integrity: the torso needs to be preserved without modification or alteration of its shape by external factors (condition of death, decomposition score, materials, etc.). Therefore we excluded cases in a decomposition condition and according to the causes of death that can affect the quality of the body. Several cases with surgery history of the torso are also excluded.

**Trunk segmentation.** From the selected cases, we automatically segmented the thoracolumbar spine vertebrae using Meng et al. 2023 method [92] and the skin with a binary segmentation approach on each slice of the volumetric image.

Meng et al. 2023 [92] algorithm performs well on the majority of the patients but failed when facing some conditions like:

- Damaged body, broken bones ;
- Voxel noise due to materials inside or near the body (implants, surgical instruments, bullets,

handscoffs, ...)

- Severe scoliosis.

For the skin, the segmentation can be performed with classical segmentation methods based on thresholding. Volumetric images are 3D matrices where each voxel contains one value at the Hounsfield unit describing the local radiodensity. With this element, we have informations about the material nature at the voxel level.

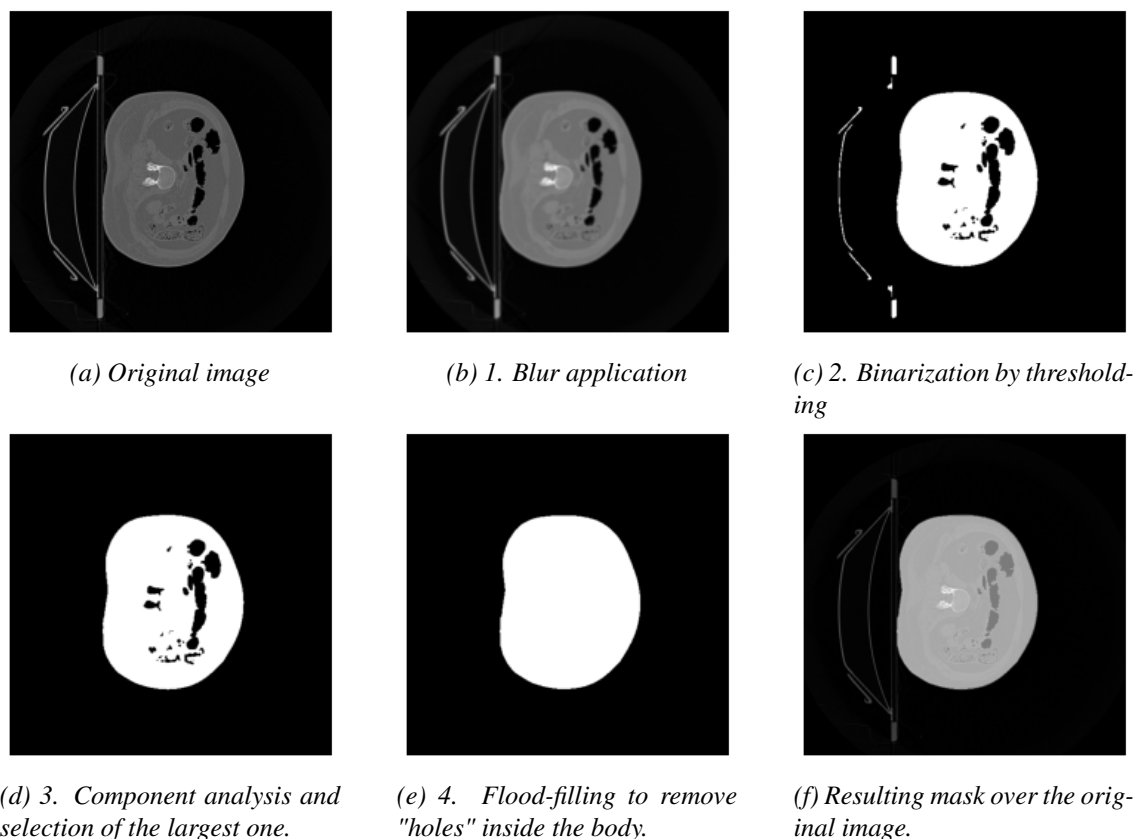


Figure 2.10: Segmentation on a trunc slice, step by step.

Thus, we created a 4-steps method segmenting each slice of the volumetric image (fig. 2.10):

1. Blur to limit ambient noise ;
2. Segment soft-issues to eliminate the void and instruments (metallic pieces, bed, etc.). The result is a binary image ;
3. Remove small elements (noise, clothes, instruments, etc.) using connected components analysis ;
4. Removing internal "holes" like lungs or intestinal lumen using flood filling.

The results are then turned into meshes using the marching-cubes algorithm [89]. Then, we create 2D renderings of the resulting back surfaces in depth maps that facilitate the body inspection in order to select manually well-preserved bodies.

### 2.3.2.2 The GH dataset

**Collected data.** Patient recruitment and data collection were approved by two Ethical Committees. The dataset was collected and published in Courvoisier et al. 2019 [26]: CECIC Rhône-Alpes-Auvergne, Clermont-Ferrand, IRB 5891. The IRB for recent cases is CPP Ile de France 2 on the 07/20/2020, n° ID RCB: 2020-A01071-38. All parents and patients received an information letter.

Two types of data were collected from 32 patients with AIS (7-16 y. old, 81% females) with no treatment:

- a 3D surface scan of the back or the torso with an optical scan (ScanGogh II Vorum Research Corporation or the Occipital Structure Sensor Mark II)
- the 3D spine reconstruction obtained from biplanar X-rays with the EOS Imaging systems [62].

**Skin and spine correspondence.** As discussed in 2.3.4, body surface reconstruction from X-rays is challenging. In our case, we have 3D surface acquisitions obtained outside the EOS radiography cabin. As the surface scan and the EOS images were not performed simultaneously, the patient pose can vary between both acquisitions as encountered by Caturano et al. 2022 [18]. We therefore added an additional step to adjust the skin surface pose to match the EOS pose. We use a 3D kinematic anatomic model in Sofa [33], which we personalize to the spine and the back surface. We then deform the pose of the avatar to match the visual envelope extracted from the biplanar EOS radiographs after binarization (fig. 2.11a and fig. 2.12). To facilitate the registration the visual envelope has been manually edited by removing parts that are not included in the surface scans (head, upper and lower limbs).

The obtained avatar has thus the skin surface in the same pose as the one observed during the radiographs. The registration steps are detailed in Appendix A page 103.

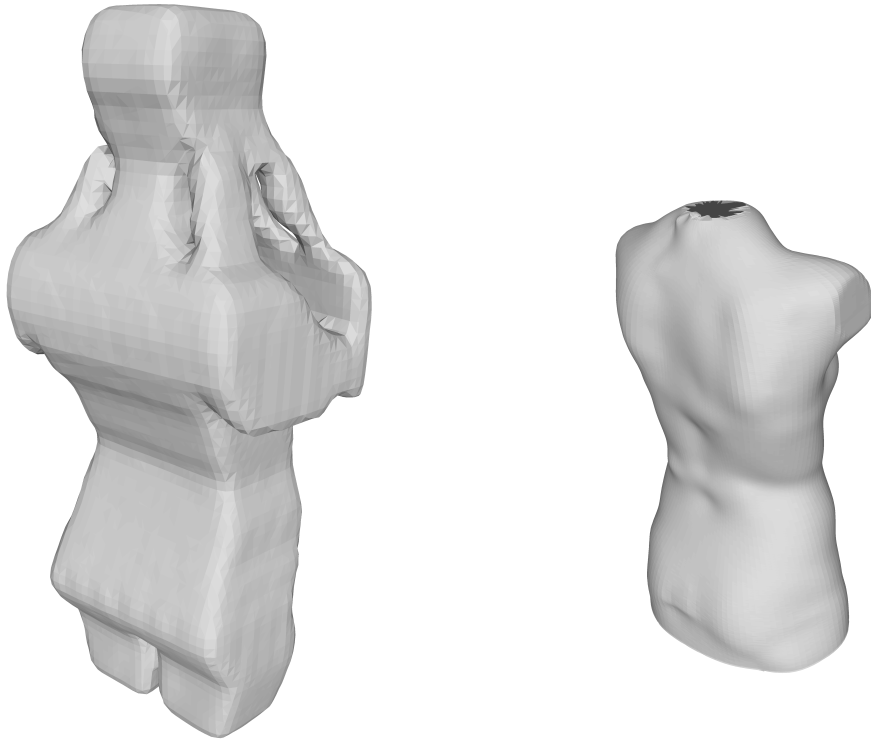
### 2.3.2.3 Depth map generation

From the meshes of the backs of the patients we rendered depth maps using an orthographic camera model. Depth maps are greyscale images where all pixels represent the distance of the object from the camera. For the NMDID subjects, we directly used the segmented skin, whereas for the GH subjects, we used the skin of the repositioned avatar matching the 3D spine shape in the radiographs.

### 2.3.2.4 Spine 3D characteristics

The 3D vertebra model geometries obtained from the EOS Imaging system [62] and the automatic CT segmentation [92] are translated into centers of gravity from which we computed the 3D spine characteristics. Using the method by Choi et al. [20] based on cubic B-Splines, we computed the scoliosis severity by selecting the maximum absolute Cobb angle value. Kyphosis and lordosis





(a) Visual hull constructed from the biplanar images

(b) Surface scan of the patient obtained with an optical scan

Figure 2.11: The use of the visual hull

were obtained with splines fitted in the sagittal plane between T04-T12 and L01-L05 respectively. As we do not model S01, we computed the lordosis Cobb angle using the L05 centroid.

### 2.3.2.5 Final dataset

From the NMDID and GH datasets we reconstructed 121 pairs of 3D spines and surfaces of the back: 89 from the NMDID and 32 from GH. The input dataset we consider is therefore composed of 45% females aged between 7 and 30 years old. 38 cases with scoliosis are included in our analysis with different type of curvatures (simple, double curvatures). Fig. 2.14 illustrates one case of each dataset with the depth map and the 3D characterization of the associated spine. Fig. 2.15 shows the distribution of the scoliosis severity measured in our dataset in using [20].

### 2.3.3 Method

Our method takes as input a depth map of the back of a patient and outputs the 3D location of the thoracolumbar vertebrae. To ease the spine prediction we use a low dimensional representation of the spine based on Principal Component Analysis (PCA). Fig. 2.20 presents the overview of the inference method.



*Figure 2.12: Superimposition of the skin according to the silhouettes. In green are the silhouettes on the radiographs and blue the rendered silhouettes of the surf. scan. Intersection of the shapes is in yellow. Usually, to make a rigid registration, the Iterative Closest Point algorithm can be applied [13]. But it needs the source mesh to be correctly initialized spatially. To do that we find the best position of the surf. scan inside the visual hull by overlapping their silhouettes and by maximizing the Intersection over Union score.*



*Figure 2.13: Resulting avatar of the patient with the spine coming from 3D reconstruction of the SterEOS software and the skin from our anatomical registration workflow.*

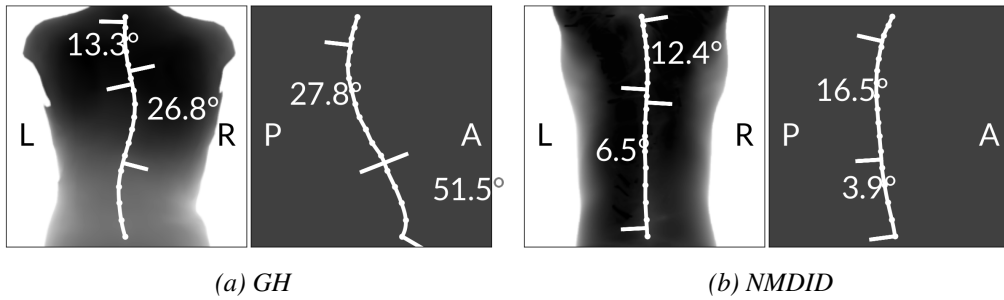


Figure 2.14: Dataset examples. For each subject we have a depth map, the 3D vertebrae locations and the measured angles. Coronal (left) and sagittal (right) views.

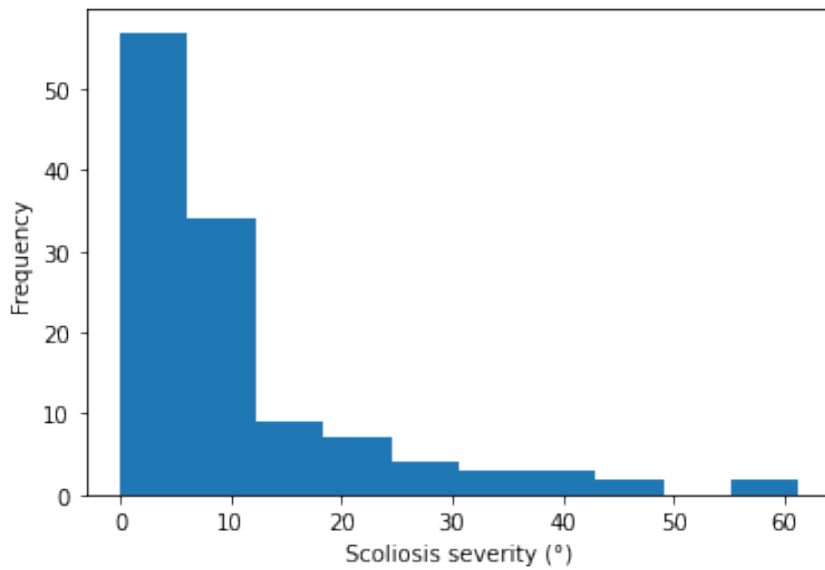


Figure 2.15: Distribution of the main Cobb angle (scoliosis severity in  $^{\circ}$ ) in our dataset.

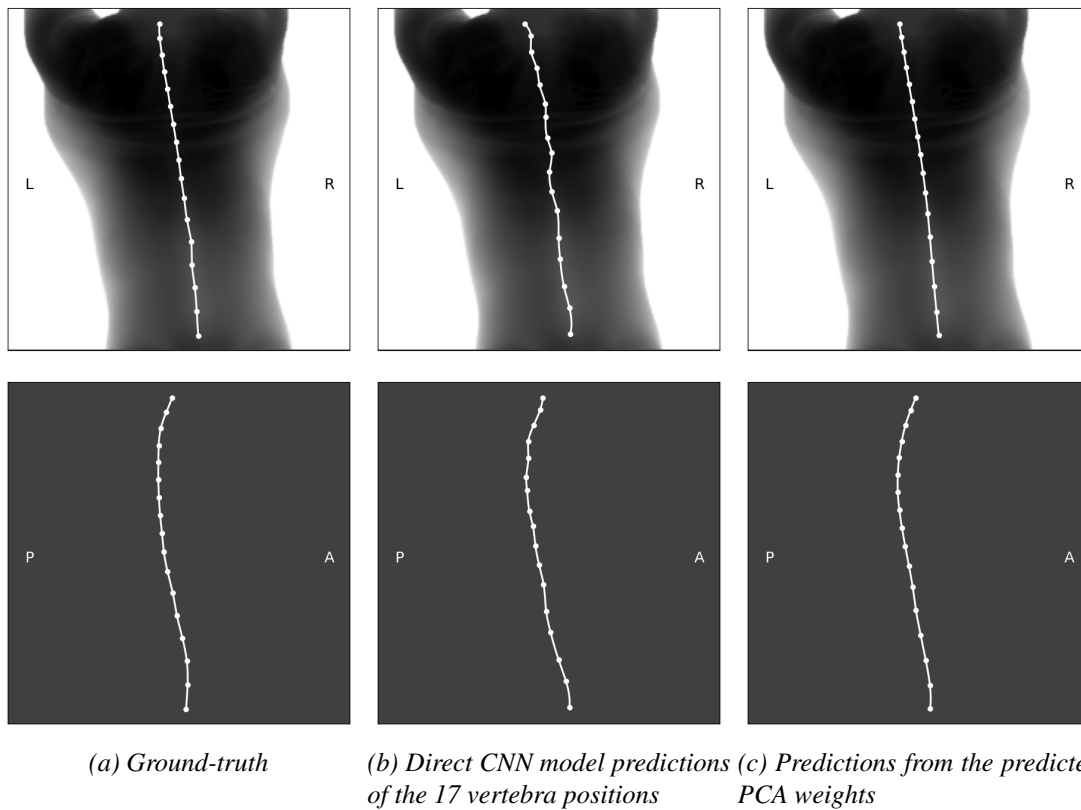
### 2.3.3.1 Data Processing

To structure the dataset and ease the learning task we process the data. Following Choi et al. [20], the depth maps on the spine are centered and cropped according to its length, then resized to a  $224 \times 224$  resolution. Depth pixel observations are further normalized between  $[-1, 1]$ , and the antero-posterior positions of the vertebrae are defined with respect to a median vertebra (T08). This 3D transformation allows a simpler representation of the spine while keeping the vertebrae alignment information. It differs from [97] and [18] which are regressing absolute positions.

We augment the dataset applying a random set of different transformations, such as mirroring and rotating the torso in 3D. From the 121 rendered depth maps, the data augmentation raises the amount of images to 10,890.

### 2.3.3.2 PCA spine representation

To ensure that the predicted individual vertebrae create a consistent spine shape, we use a low dimensional representation based on PCA [47]. The learned PCA space can produce a compressed latent representation of the spine data, while preserving most of its information and variability. Two main advantages follow. The prediction of PCA coefficients is less complex than the prediction of each of the 17 individual vertebrae 3D locations ( $17 \times 3 = 51$ ). In addition, the compressed latent representation enforces regularization over the estimated spine locations. In fig. 2.16, we show the main difference of the direct prediction (without PCA) of the vertebra positions by our CNN model against their indirect inference with a PCA.



(a) Ground-truth (b) Direct CNN model predictions (c) Predictions from the predicted of the 17 vertebra positions PCA weights

Figure 2.16: Effects of the PCA in the prediction of the vertebra positions with our CNN model. Example on an asymptomatic case from the NMDID. First row shows predictions on the input depth map (coronal plane) and second row predictions projected in the sagittal plane.

In a detailed analysis, we can see that a PCA model trained with our data can explain 95% of the variability with only 9 dimensions (from  $17 \times 3$  with the raw coordinates), see fig. 2.17.

From the fig. 2.18, we can interpret the first components of the the PCA. The first highlights differences in poses in our datasets between supine (NMDID) and upright standing (GH) conducting in changes of kyphotic and lordotic curvatures. The second and the third components change the global rotation of the spine in the coronal and sagittal planes. The fourth component modifies the kyphosis and lordosis curvatures. Finally, the fifth component is the first one that controls scoliosis.

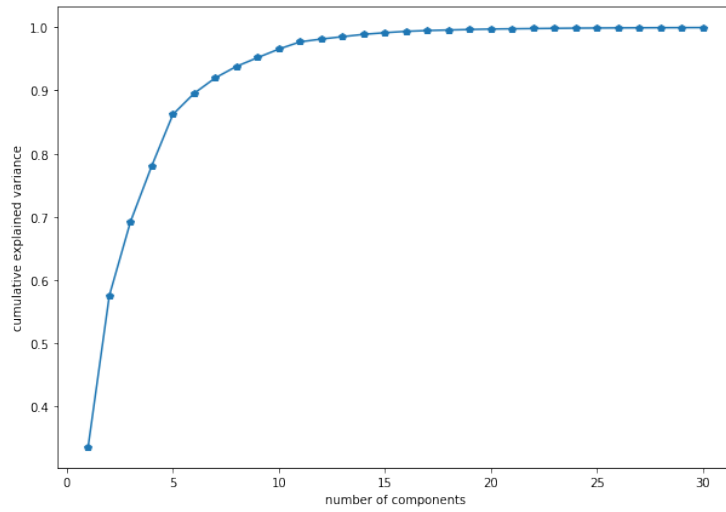


Figure 2.17: Cumulative explained variance by the PCA according to the number of components.

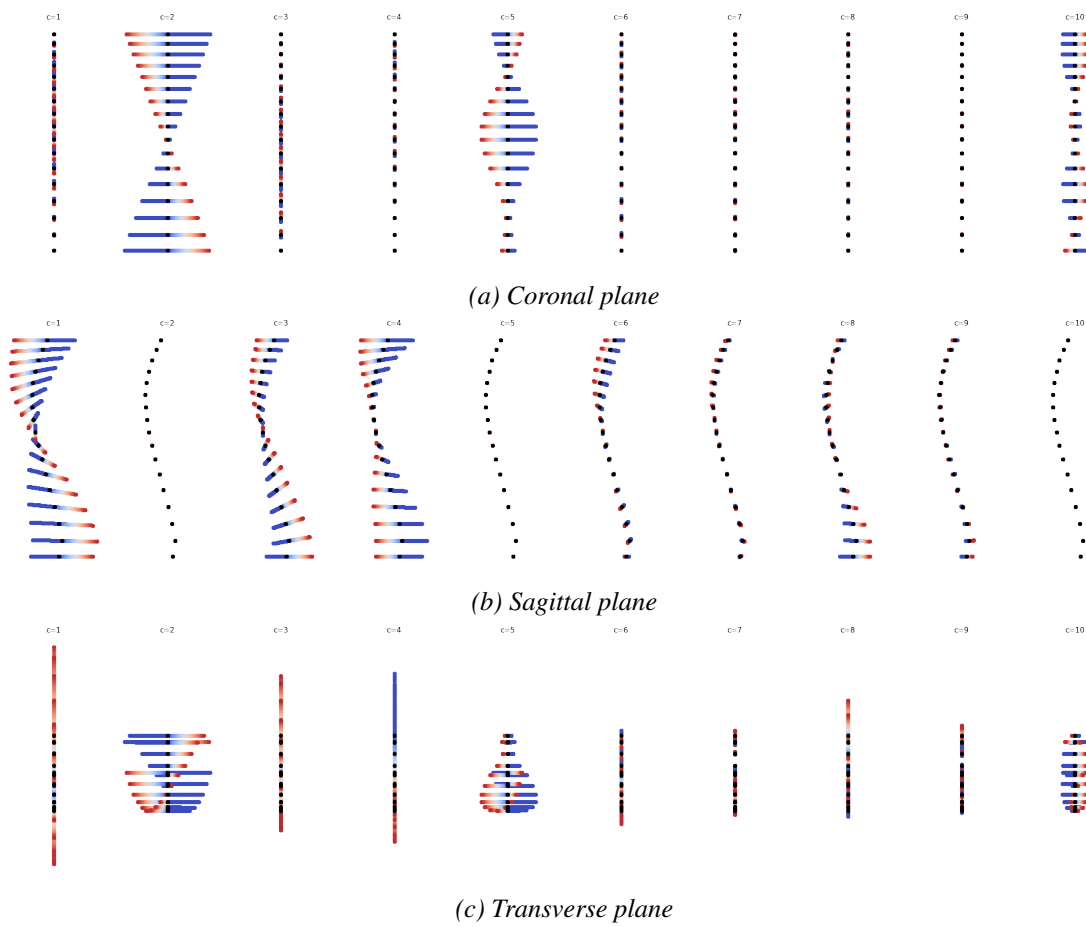


Figure 2.18: Effects of the first components on the PCA average of the spine positions.

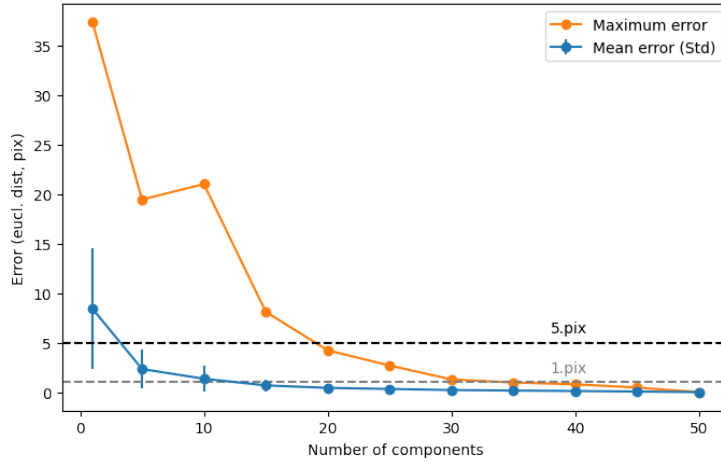


Figure 2.19: Reconstruction error by the PCA on the training dataset according to the number of components.

In fig. 2.19, we plot the average reconstruction error according to the number of components of the PCA. The maximum error of the reconstruction becomes lower than 5 pix ( $\sim 1$  cm) passed 20 components (fig. 2.19) with an average error below 1 pix ( $\sim 2$ mm).

We also test the PCA model on an unseen dataset. Using a stratified 20-fold cross validation, we obtained reconstruction errors, scaled to the mm, of 0.92 mm (std: 0.75 mm) in average with a maximum distance error of 7.94 mm. The scoliosis curvatures (below and up to  $10^\circ$ ) are also preserved with a mean absolute error of 2.71 degrees (std: 2.49 deg.).

In conclusion, the use of a PCA model provides a detailed representation of the spine with fewer dimensions, from 51 to 20 (60% reduction). This type of model enables the entire thoraco-lumbar spine to be reconstructed with reasonable accuracy, less than one mm in average.

### 2.3.3.3 CNN architecture

Our model aims to predict a vector of  $17 \times 3$  values representing the 3D coordinates of the thoracolumbar vertebrae from a single grayscale image. Our problem is similar to 3D connected keypoints coordinates estimation found in Human Pose Estimation. These field are interested to estimate the articulated 3D joint locations of the body from images or videos. That was also this approach that has been investigated by Choi et al. 2017 [20] using an adapted AlexNet’s architecture made for 2D Human Pose Estimation purpose.

We use ResNet-18 [58] model as our backbone CNN architecture, which has been shown to be efficient for regression tasks. It encodes the depth image ( $224 \times 224$ , 1 channel) into the aforementioned latent PCA representation of the spine, which is in turn easily decoded into the 3D vertebra positions (fig. 2.20). We train the network to minimize Mean Squared Errors ( $MSE$ ) between the vertebrae coordinates  $\Theta_i \in \mathbb{R}^{17 \times 3}$  and PCA coefficients  $\theta_i \in \mathbb{R}^{20}$  predicted by the neural model

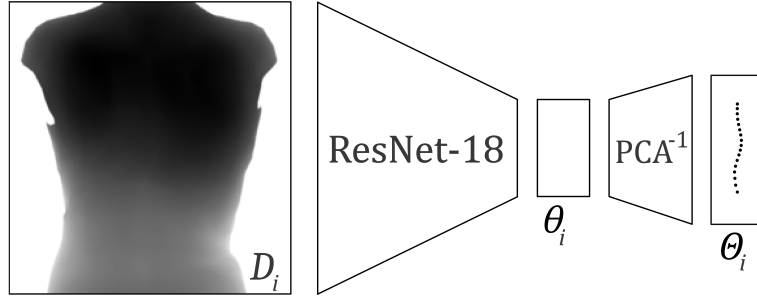


Figure 2.20: Global architecture of our network: Resnet18 is making a regression on the depth image in order to find a reduced representation of the coordinates. A PCA inversion module is added to transform this representation to the actual coordinates.

and their corresponding elements  $i$  of the training dataset:

$$Loss = \omega_{\theta}MSE(\hat{\theta}, \theta) + \omega_{\Theta}MSE(PCA^{-1}(\hat{\theta}), \Theta) \quad (2.1)$$

Each loss component is associated with a constant weight  $\omega_{\theta}$  and  $\omega_{\Theta} \in \mathbb{R}$ .

The model is trained using an Adam optimizer with PyTorch [106] with 2500 epochs and a learning rate of 1e-4.

### 2.3.3.4 Evaluation

**Stratified K-Fold Cross Validation.** To evaluate our approach we chose a k-fold cross-validation strategy which splits our dataset into three subsets. The first is the *train* dataset which will be used by the network for the training process. The second, *validation* dataset is used to estimate the model skill during the training and, usually, check if the model overfits. In this case, the model is not able to make accurate predictions from unseen data and became too specialized on the training images. Thus, we stop the training process. Since the validation dataset is also conditioning the training process, we need a last un-seen sample of data that can be used to evaluate the final state of the model.

Because of the diversity in data origin (NMDID or CHUGA) and medical condition (scoliosis or not) we need to maintain their ratio in the samples. Thus, we are stratified.

**Evaluation metrics.** We evaluate the vertebrae location accuracy by computing the 3D distances between the ground-truth and the predictions as well as 2D distances in the coronal and sagittal planes. We evaluate the spine curvature accuracy by computing the Mean Absolute Error (MAE) in three angles: the main coronal Cobb angle [20], kyphosis (T04-T12) and lordosis (L01-L05). As the 3D predicted spine of our method can also be used for spine classification. We chose the main Cobb angle threshold of 10° related to early-stage progressive scoliotic curvatures [147]. We compute binary classification metrics: sensitivity, specificity, positive predictive value, accuracy and Area Under the Curve (AUC) of the Receiver Operating Characteristic. All of our quantita-

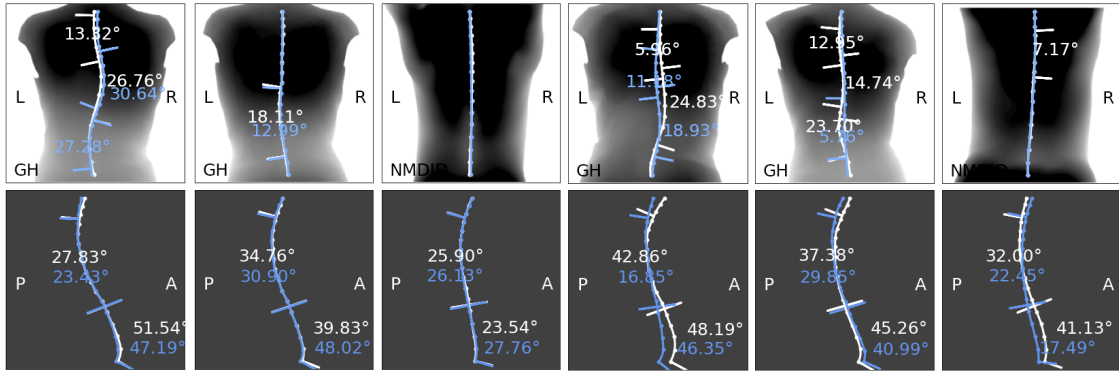


Figure 2.21: Selection of results. White: ground-truth; blue: predictions. Top row: coronal view for each case, bottom row: sagittal view. GH: institution; NMDID: New Mexico Decedent Image Database; L: Left; R: Right; P: Posterior; A: Anterior.

tive results are computed using the stratified 20-fold cross-validation (CV) on the full dataset as described in 2.3.3.4. All metrics are computed by averaging over all test sets.

## 2.3.4 Results and Discussions

### 2.3.4.1 3D spine prediction accuracy

**Vertebra locations.** MAE of the vertebrae location predictions are reported in table 2.2. Our model is able to predict the 3D vertebra positions with an average 3D error below the cm. These predictions allows the characterization of the spinal alignments (scoliosis, kyphosis, lordosis) with automated measurements [20]. Visuals of the predictions are presented in fig. 2.21.

**Spine 3D characteristics.** Table 2.2 reports the angle errors between the predicted spine shapes and the ground truth ones. The last three lines of the table 2.4) are provided for the comparison with the literature. Note how our approach is the only one predicting kyphosis and lordosis. Numerical results are provided for informative comparison on the range of values, as the considered datasets are different, both in size and population.

**Classification.** Classification results are reported in table 2.2. Our method is able to discriminate cases with scoliosis with a sensitivity of 64% and a specificity of 99%. We report a positive predictive value of 95%, an accuracy of 89% and an AUC of 90%. Fig. 2.22 shows the predicted severity against the ground truth one with the  $10^\circ$  classification thresholds. Let us note how several miss-classifications arise near the  $10^\circ$  threshold and the underestimation of moderate and severe scoliosis cases. In conclusions we provide leads to improve these predictions.

### 2.3.4.2 Ablation studies

To further understand the proposed approach we performed two complementary experiments.

Recent work by Klarqvist et al. 2022 [77] has shown that it is possible to estimate body compo-



Tableau 2.2: Spine prediction accuracy. Vertebrae errors in mm of the 3D locations (3D) and 2D coronal (Cor.) and sagittal (Sag.) projections. Angle errors in degrees in the scoliosis severity (Sco. sev.), kyphosis (Kyph.) and lordosis (Lord.). Scoliosis classification ( $\geq 10^\circ$ ) sensitivity (Sens.) and specificity (Spec.).

Study	Locations (mm)			Characteristics ( $^\circ$ )			Classification	
	3D	Cor.	Sag.	Sco. sev.	Kyph.	Lord.	Sens.	Spec.
Ours	7.07 (4.69)	4.51 (2.99)	5.60 (4.62)	5.46 (6.19)	6.44 (5.49)	8.26 (6.85)	0.64	0.99
[20]	×	5.4 (3.5)	×	3.42 (2.64)	×	×	NA	NA
[151]	×	×	×	×	×	×	0.88	0.84
[80]	×	×	×	[4.4 - 4.7]	×	×	0.99	0.42

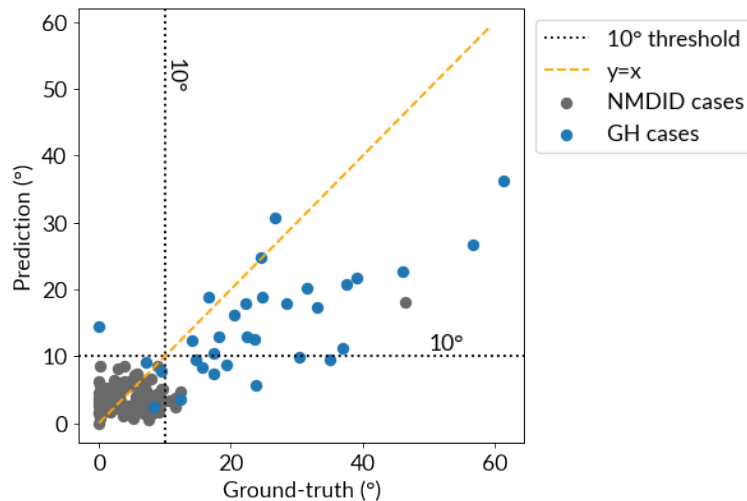


Figure 2.22: Comparison between predicted scoliosis severity and ground-truth measurements.

sition from solely body silhouettes. We consider the analogous case for the prediction of the 3D spine: instead to use a depth map as input we consider the case where only the binary silhouette of the back surface is observed.

In addition, we also experiment by training and testing on the two different datasets (GH and NMDID) to see if the imbalance of scoliotic patients in the datasets has an effect on the predictions.

**Predictions from binary images.** We tested the impact of depth information by training our model to reconstruct the 3D positions on binary images that show only the silhouette of the torso. The results in table 2.3 illustrate that model using depth maps achieves overall better performance. Depth is informative for the network. It is interesting to note the capability of the silhouette network to reconstruct scoliosis curvatures with a severity error of  $6.34^\circ$ . The biggest difference is obtained in the sagittal plane alignments, which is coherent with the lack of depth information in the binary

Tableau 2.3: Comparison with binarized depth information, i.e. silhouette (silh). MAE (with std.) on locations in 3D, coronal (Cor.) and sagittal (Sag.) plane and the estimated scoliosis severity. Detection is evaluated sensitivity (Sens). and specificity (Spec.).

Type	3D (mm)	Cor. (mm)	Sag. (mm)	Severity (°)	Sens.	Spec.
silh	10.02 (6.96)	4.91 (3.34)	8.55 (7.22)	6.34 (7.86)	0.52	0.98
depth	7.07 (4.69)	4.51 (2.99)	5.60 (4.62)	5.46 (6.19)	0.64	0.99

silhouette image.

**Datasets difference.** The inclusion of NMDID allows us to validate the approach on asymptomatic cases. However, it could have a negative impact on the prediction of the scoliotic cases by adding bias. We thus evaluate the impact of the NMDID dataset on the network regression performance. We train solely on GH (scoliotic data) and on both GH and NMDID (scoliotic + asymptomatic) data and report the results on table 2.4. Including the NMDID cases in the training set does not introduce any bias in the prediction performances (first two lines) on GH subjects and confirms that the inclusion of spines without scoliosis from deceased subjects in supine position does not deteriorate the predictions over living patients acquired with the regular protocol.

Tableau 2.4: MAE in locations in mm and standard deviations comparing results according to subjects included in training and testing processes.

Study	Train	Test	3D	Coronal	Sagittal
Ours	GH	GH	8.81 (5.19)	5.87 (3.73)	6.76 (4.97)
Ours	GH+NMDID	GH	8.80 (5.46)	5.90 (3.73)	6.74 (5.26)
Ours	GH+NMDID	NMDID	6.45 (4.21)	4.01 (2.49)	5.19 (4.30)
Ours	GH+NMDID	GH+NMDID	7.07 (4.69)	4.51 (2.99)	5.60 (4.62)

### 2.3.5 Conclusion

In this work, we presented an approach to predict the 3D spine shape of a patient from a depth map of the back. This depth map can be obtained with depth sensors, which are usually inexpensive, portable, making them a promising cost-effective, non-ionizing approach to quantify scoliotic deformities. Our approach provides 3D predictions of the vertebrae locations and allows to compute relevant anatomic curvatures along the spine as well as a fast scoliosis diagnosis.

To address the challenge of 3D reconstruction, we leveraged personalized kinematic models that allow a full representation of GH patients with their spine and skin in the pose of the X-rays acquisition. Thus, a part of our study is constrained by the use of a simulated skin in training and testing times. The incorporation of the actual scans, for these patients, has the potential to improve outcomes and validate the models under genuine conditions. This issue can be solved with a ground-truth representation of the spine in the pose of the scan acquisition that is currently

not possible to obtain.

Another venue of improvement of the presented work would be to add more subjects with moderate and severe scoliosis in the training pipeline. As shown in fig. 2.22, our model tends to underestimate severe deviations due to the low number of such cases in our dataset. To make this possible, as well as to foster future research in this direction, we make our trained model and training code available for research purposes<sup>1</sup>.

In addition, our work does not consider their individual vertebrae 3D orientation. It has been studied that the axial vertebra rotation contains information related to the early detection of scoliosis [25] and its evolution [129]. Our approach could be adapted in the future to also predict the orientations of the individual vertebrae. To that end, the PCA representation should be reconsidered, as a linear approach might not be well suited to capture the 3D rotations.

---

<sup>1</sup>[https://gitlab.inria.fr/spine/skin\\_to\\_spine](https://gitlab.inria.fr/spine/skin_to_spine)

## 2.4 Summary

In this chapter, we described the different examination methods of the patient spine and surface. First, we presented the approaches of evaluation from X-ray observations of the body. 2D radiograph analysis of the torso is the main technique to describe spinal alignments and deformities. We described the different measurements that can be made from the images like the Cobb angle. Several classification systems, based on these measurements, like the Lenke classification, have been created to guide treatment planning.

These methods provide a partial analysis of the spine, usually limited to the frontal plane, whereas scoliosis is by nature a three-dimensional deformity. Recent advances in 3D imaging, like the EOS imaging system, show the importance of the analysis of the transverse plane highlighting the rotational anomalies of the vertebrae. This comprehensive approach provides a more accurate assessment of the deformities and aids in tailoring effective treatment strategies for each patient, ultimately leading to improved clinical outcomes. Therefore, emphasizing the importance of adopting three-dimensional imaging techniques for a thorough evaluation of the spine is crucial in advancing our understanding and management of spinal deformities.

However, it is crucial to take into account the potential risks of cancer associated with repeated exposure to radiation from X-rays. We presented several studies that have paved the way for scoliosis monitoring with radiation-free imaging techniques like rasterstereography. Some of these works, using artificial intelligence, are able to predict internal radiographic measurements, from external views, and detect scoliosis with an high sensitivity. Despite the great advances coming from these methods, the resulting characterization is partial or limited in 2D.

In section 2.3, we proposed, in a contribution, a novel approach of inference that takes as input a depth map of the back of a person and outputs the 3D shape estimation of the thoracolumbar spine. Combining a CNN model to extract the relevant features in the input images, our model predicts an efficient PCA latent representation of the spine in 3D. With this approach, our method predicts 3D vertebrae positions with an average 3D error of 7.1mm (std: 4.7mm). From the predicted 3D positions, coronal (scoliosis) and sagittal (kyphosis and lordosis) spine alignments can be located and evaluated. By measuring scoliosis, we showed that we are also able to detect scoliosis disorders from the input depth map. For future research investigations, we make our code publicly available with the trained models.



# 3

## Dynamic characterization of scoliosis

## Introduction

The spine has a central role in the structure and mobility of the trunk. Deformations of the spine, in the case of idiopathic scoliosis, have significant impacts on the entire body. Despite the recent advances in the acquisition and description of the torso anatomy in 3D, the causes and factors contributing to scoliosis progression remain poorly understood. Thus, it is necessary to identify early clinical and radiographic markers associated with progressive scoliosis. A notable observation is that current analysis methods primarily rely on a static characterization of the torso (surface and spine), neglecting its dynamic aspects.

The dynamic analysis of the spine is currently challenging because it requires observing and measuring vertebral movements either invasively by inserting markers [116] or by using ionizing imaging systems [16]. According to these limitations, current methods primarily rely on superficial body measurements through motion capture, highlighting dynamic patterns in Adolescent Idiopathic Scoliosis patients [134]. Currently, there is no consensus emerging from the literature regarding the impacts of scoliosis on movement.

Recent methods presented in the literature propose to make in correspondence static radiographic data with superficial markers to digitally reconstruct spine movements [101, 125]. These methods demonstrate promising results as they enable, tracking movements of spinal alignments using motion capture. However, these approaches have only been applied and validated in individuals with Adult Spinal Deformity (ASD) without surface representation.

In a new contribution, we present a novel approach aimed to address the current challenges by leveraging a personalized kinematic model registered in multi-modal acquisitions, internal and external, of AIS patients. This digital twin can then be driven by external measurements to predict the 3D trajectories in translation and rotation of the patient's vertebrae. In a preliminary study, we show that these predictions are close to radiographic measurements, i.e. near 1 cm in each orientation axis and  $5^\circ$  in orientation, quantifying that the spine and the back surface motion patterns are highly correlated.

### **3.1 Approaches in the analysis of the torso in motion with scoliosis**

As discussed in part 1.2.1, the spine assumes a pivotal role in orchestrating various aspects of trunk motion. Therefore its study is mandatory to further investigate the patient's condition and improve the characterization of the disorders. In this section, we present the different methods in the literature that allow the measurement of the spine dynamics. Then, we will present the non-ionizing methods allowing the analysis of the motion of patients with Adolescent Idiopathic Scoliosis.

#### **3.1.1 Methods of tracking the *in vivo* motion of the vertebrae**

Motion of the spine is usually described at the vertebra level as described in 1.2. However, the *in vivo* measurements of the vertebra motion are challenging and rely on invasive and ionizing approaches. For instance, MacWilliams et al. 2013 [90] use indwelling bone pins inserted into the vertebrae of interest. Connected to reflective markers they were able to track the motion of the lumbar vertebrae during gait analysis. Less invasive, dynamic radiography imaging techniques like dual-fluoroscopy can be used to study spine motion [16]. However, these methods have a limited field of view, focusing the analysis on a small region like the lumbar part. In addition, fluoroscopy involves the use of continuous ionizing radiation, exposing patients to potentially harmful dose. Less-ionizing, Dynamic Digital Radiography [3] shows promising results in dynamic analysis but, to our knowledge, has not been used for the spine analysis. However, these dynamic and ionizing methods are limited to the analysis of 2D motion. MRI can also be considered as an alternative [48] and can provide three-dimensional images without the risk of ionizing emissions. However, this imaging system is limited to a non-weight bearing analysis with a high cost and longer acquisition times, making this method less practical.

#### **3.1.2 Analysis based on superficial features**

Other non-invasive and non-ionizing techniques are focused on superficial feature measurements of the body with force platforms, goniometers or Electromyography (EMG). In addition, recent methods using motion capture (mocap) facilitated the analysis of the patient motion by recording 3D trajectories of a set of markers placed on the back. We can report several biomechanical descriptors investigated in gait or flexion analysis:

- Ground Reaction Force (GRF) using force platforms [119] mainly used to describe asymmetry on patient's pose or motion (gait for instance).
- Range of Motion (ROM) at spine levels, pelvic, hip or knee with motion capture [50, 122, 133, 134] or in some papers with the rachimetre [14, 109].
- Gait descriptors like speed of walking, cadence, stride/step length, width and gait asymmetry [28].
- Physiological descriptors are also investigated in relation to motion as Electromyography



(EMG) measuring muscle activity [105] and more indirectly, heart, respiratory activity or oxygen consumption during motion [9].

As highlighted in a review by Daryabor et al. in 2017 [28] regarding gait analysis, there is a lack of agreement concerning the impact of AIS on temporal-spatial parameters. The literature presents varying viewpoints on the influence of AIS on gait asymmetry descriptors and the ROM in the frontal and transverse planes at the hip and pelvis. In particular, gait kinematics asymmetry have been observed, particularly as postural instability increased in individuals with scoliosis, leading to alterations in lateral bending movement [133, 134].

A main drawback present in the current analysis methods is the fact that motion capture offers a surface-level examination of a patient's motion dynamics through generalized measurements of spinal alignments. However, this approach lacks the granularity required for describing motion at the level of individual vertebrae. A detailed analysis of the spinal alignments can be obtained by acquiring 3D trajectories of markers positioned on the palpable spinous process of the vertebrae. These approaches, however, are sensitive to the palpation task and underestimate the coronal curvatures measurements [59, 121]. This issue can be fixed with numerical correction regarding the true anatomy [101, 124, 125].

## 3.2 The biomechanical modeling of the spine

As we show, the invasive nature of the *in-vivo* measurements of spinal loads or dynamic makes these methods unsuitable for clinical analysis. Even, the trajectories of the spinous processes are not representing the internal spine behaviour. Thus, biomechanical models can be presented as alternative tools to reconstruct, *in silico*, the musculo-skeletal system mechanics.

### 3.2.1 Types of models

From the recent literature, we can differentiate two types of models that differ by their mathematical representation of the anatomic structures and interactions: Finite Element Model and Multi-body model (fig. 3.1).

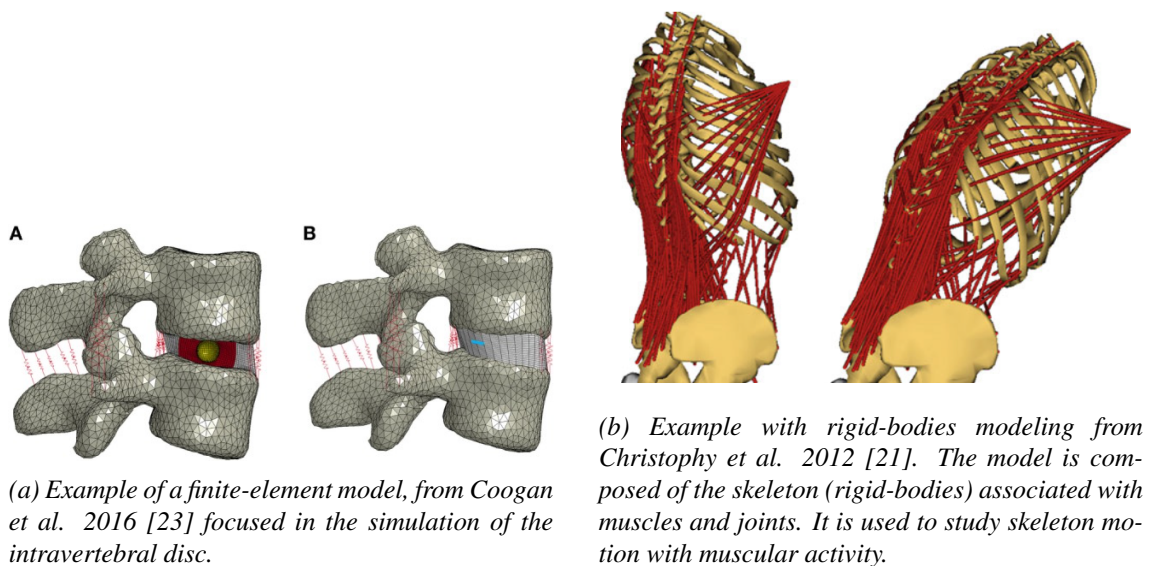


Figure 3.1: Different types of models of the spine and purposes

#### 3.2.1.1 FEM models

Finite-Element modeling (FEM) is a common approach to study spine behaviour [143]. It approximates the system as a multitude of functions within complex geometrical and material properties. All elements are usually considered as deformable volumes. It is used to determine force distribution, loadings and motion properties [36, 37] along the spine with injuries [145], surgical instrumentation [127, 145] or brace treatment [10, 118, 139, 140]. There are also several models that investigate the effect of aging and bone growth in individuals with AIS [70, 131].

#### 3.2.1.2 Multi-body/Rigid-body models

With fewer parameters than FEM, less consuming in computation time, these models are composed of non-deformable elements like bones, connected with elastic structures (joints, ligaments and other flexible tissues) [17, 21, 63, 120]. These models are used to determine loadings, me-

chanical properties, muscular activity [17, 31, 63, 120] along the spine. As FEM, they can be involved in studies about spine instrumentation [32] or brace treatment [26]. These models can also be useful for medical imaging registration [40, 53] and can be associated with motion capture analysis [101, 128].

### 3.2.2 Specificity to patient anatomy

Models are often rich, incorporating a detailed representation of the spine with the rib-cage, its disks, ligaments or muscles. Depending on the collected information captured from a single patient, we can categorize the modeling strategies in two main types: scaled models and subject-specific models. Scaled models can be useful in situations where obtaining subject-specific data is challenging: they involve a generic model, which is a standardized anatomical representation, adjusted to match the subject's general body dimensions. While scaled models are computationally efficient and require less time for data collection, they may not accurately represent subject's characteristics and may lead to less accurate results compared to subject-specific models. By including patient anatomy (vertebra geometries and alignments for instance), subject-specific approaches allows for a more precise biomechanical analysis and better understanding of individual movement patterns.

In the analysis of scoliosis condition, these models are mainly focused on the treatment (brace or surgery) simulation. For example, Courvoisier et al. [26] leverage a subject-specific biomechanical models to simulate and predict the effectiveness of the spine response of a brace.

### 3.2.3 Application to motion analysis

We have identified one model that allows the reconstruction of vertebrae motion under scoliosis condition, Overbergh et al. 2020 [101]. In their study the authors proposed and validated a workflow that incorporates a subject-specific kinematic model, created from [17], that can be used towards marker-based motion capture analysis. The model, fig. 3.2, is composed of vertebra geometries, obtained from segmented CT-Scans and aligned with EOS biplanar X-rays images. Each bone is connected to the adjacent structure with a spherical joint (3 DOFs in rotation). Then, they were able to validate their kinematic predictions against low-dose biplanar X-rays of patients in different poses. Their approach demonstrates encouraging outcomes with transnational errors below the 5 mm in average in each orientation axis, and rotational errors around 5°. We should note that their methodology has been assessed within the context of Adult Spinal Deformity (ASD) and rely on a meticulous palpation task which can be tedious to apply to young patient with Adolescent Idiopathic Scoliosis (AIS).

## 3.3 Discussion

Given the challenges associated with *in vivo* spinal motion measurement, analysis predominantly relies on external dynamic body motion capture. While a variety of features are captured, the level

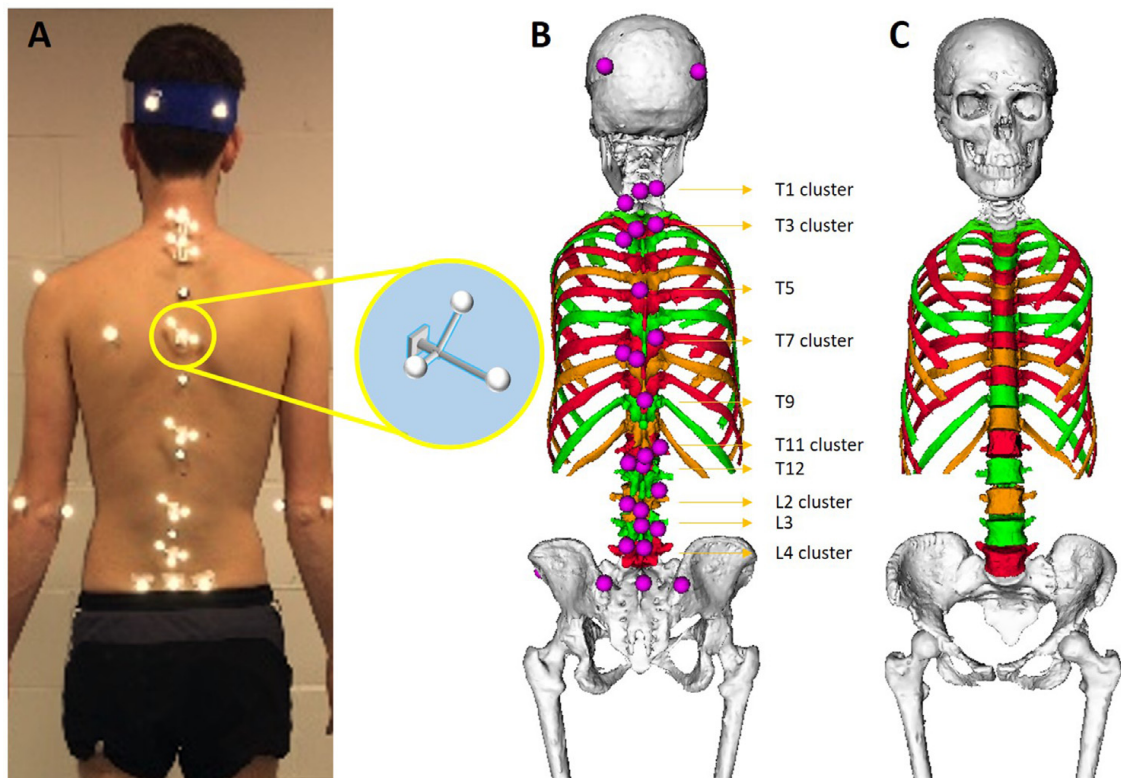


Figure 3.2: Model involved in the study of Overbergh et al. 2020, figure from [101].

of detail in these measurements might contribute to the limited comprehension of scoliosis effects on spinal movement. Novel analysis methods using mathematical representations of the spine and coupled with motion capture [122, 124, 125], facilitate the reconstruction of 3D spinal alignments from superficial markers. These approaches leverage recent advancements in low-dose biplanar radiography, enabling the 3D reconstruction of the spine with the superficial marker positions.

However, these methods do not comprehensively describe individual vertebral movement, particularly in terms of rotation [125]. Subject-specific biomechanical models can address this gap. These models enable the analysis of the motion at the vertebra level using external markers placed on spinous processes as presented in Overbergh et al. 2020 [101].

### 3.4 Contribution: Multi-Modal Data Correspondence for the 4D Analysis of the Spine with Adolescent Idiopathic Scoliosis

The current methods for analyzing trunk motion with scoliosis rely on measurements from the surface and do not allow for a comprehensive analysis of spinal kinematics at the vertebra level as X-ray imaging techniques can provide. In this work, we propose to build a subject specific kinematic model of patients with AIS that captures both their internal and external specificities. The resulting digital twin can then be driven with mocap markers on the back of the patient, which yields the actual kinematics of the spine. In a preliminary study, we present a validation of the predictions against 3D spine reconstructions of two patients who performed lateral bendings.

#### 3.4.1 Method

##### 3.4.1.1 Collected data

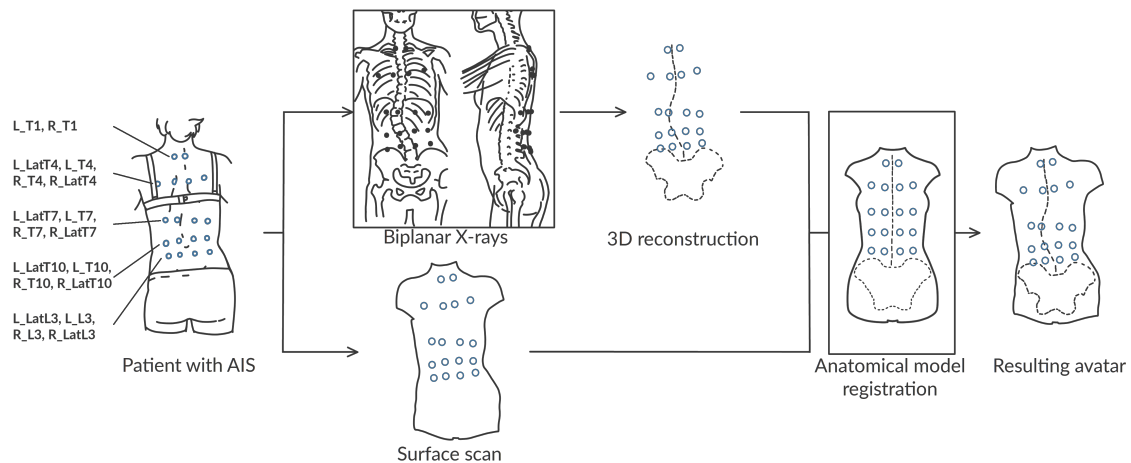


Figure 3.3: Summary of our workflow with the annotated data. A set of radio-opaque markers (blue circles) are placed on the back approximately according to different vertebra levels. No palpation is required. The acquisition of their 3D location in both modalities (surface scan and Biplanar X-Rays) allows the spatial correspondence between the internal and external structures (skin and spine).

Our dataset consists of 8 patients aged between 8 and 16 years, with AIS (Cobb angle range: 14-68°) and without any treatment history. They have been included in our study following the IRB CPP Ile de France 2 on the 07/20/2020: n° ID RCB: 2020-A01071-38. All parents and patients received an information letter. Two data modalities have been collected in our institution for each subject (fig. 3.4):

- A biplanar X-ray of their trunk made with an EOS imaging system
- A surface scan of the back using an Occipital Structure Sensor Mark II (XRPro, LLC, Saratov)

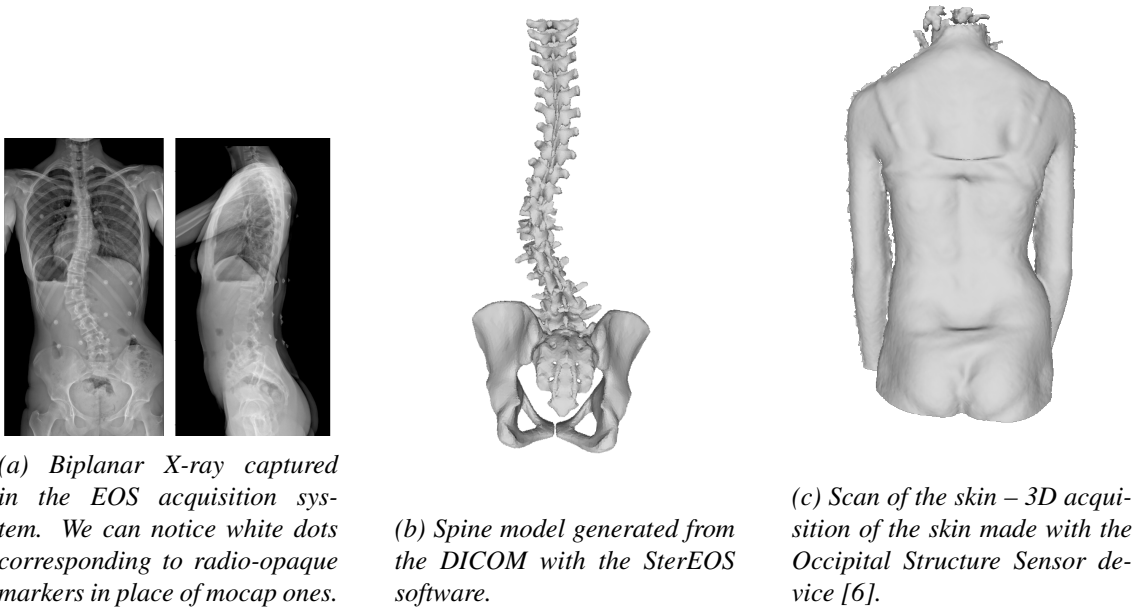


Figure 3.4: Types of data collected for a single patient at Grenoble Hospitals.

During all acquisitions, the patients wear a set of 18 radio-opaque markers positioned on the neighbourhood of 5 vertebra: T1, T4, T7, T10 and L03. The marker placement does not require a precise palpation. The markers can be identified and located in the X-ray images and the surface skin mesh (fig. 3.3 and 3.6).

To evaluate the kinematic predictions of the model, X-rays of two voluntary patients, Cobb angles of  $14^\circ$  and  $29^\circ$ , were captured in left and right lateral bending. These images will be used to quantify the inference of the spine motion inside the body in different poses.

### 3.4.1.2 Data processing

Some manual steps are needed to annotate the images. The first step is to make the semi-automated reconstruction of the 3D geometries of the spine from the biplanar radiographs with the SterEOS software [62] (EOS Imaging, Paris, France). Then, the radio-opaque markers, visible in the images, are located in 2D and their 3D position is computed using the calibration information available in the DICOMs metadata [55].

The transformation into 3D coordinates is facilitated by the conception of the EOS imaging system. Knowing the geometry of the system, we can retrieve the 3D coordinates of the identified landmarks of the biplanar images by drawing lines between the emitters and the identified landmarks.

From the surface skin mesh, the markers locations are identified. As the surface scan and the EOS reconstruction are defined in a different global frame, we use a rigid registration to bring them in the same frame. Namely, we compute the translation and rotation that minimize the distance between the 3D markers identified in both modalities. Let us note, that as the pose might be

slightly different in both acquisitions, we use RANdom SAmple Consensus (RANSAC) [46] to filter out markers, whose positions might have significantly changed with the patients pose. This registration provides a first association between the surface scan and the spine 3D reconstruction.

### 3.4.1.3 The subject-specific kinematic model

To create a 4D numerical twin of the patient, we leverage the Anatoscope technology based on "Anatomy transfer" [26, 33]. This method deforms an initial anatomical model to capture the internal and external shapes of the patient with rigid and elastic registration processes. The resulting avatar can then be used for biomedical simulations, namely, the parameters of the model can be optimized so that the skin of the model matches the mocap markers, while enforcing biomechanical constraints on the spine behaviour.

#### 3.4.1.3.1 Model overview

The kinematic model is composed of  $N_x = 18$  articulated rigid-bodies  $\mathbf{x}_i$  defined in positions  $p_i \in \mathbb{R}^3$  and rotations  $R_i \in \mathbb{R}^{3 \times 3}$ , corresponding to each  $i$  thoracolumbar vertebra and the pelvis. In addition each bone is associated with a set of scale parameters  $\mathbf{s}$  that modify the model geometries (of 5000 vertices in average). The bones are connected by  $K = 17$  joints of 6 degrees-of-freedom (DOFs), in translations and rotations as defined by Ignasiak et al 2016 [63]. We followed the modification applied by Koutras et al 2021 [82] allowing a symmetrical definition of the vertebra motion (table 3.1). The position of the joints is defined in the middle of the segment drawn between the two adjacent endplate centroids (fig. 3.5). Their orientation is defined accordingly to the inferior rigid-body. The model also has a skin surface (mesh of 2173 vertices) which is rigged by the articulated rigid bodies.

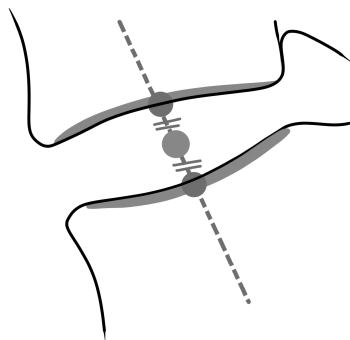


Figure 3.5: Positioning of the joints relatively to the two connected vertebrae.

#### 3.4.1.3.2 Model registration

The following section gives an overview of the registration process. A detailed description of the workflow is provided in Appendix A page 103.

Tableau 3.1: Stiffness values at each joint of the model. Shear and compression are expressed in  $kN/m$ , flexion-extension, axial-rotation and lateral bending in  $N.m/rad$ .

Joint region	shear	compr.	flex.-ext.	ax.-rotation	lat. bending
Thoracic	262	1720	286	177	223
Lumbar	245	1720	143	498	149

The first step of the registration process is to change the pose  $\mathbf{x}$  and the shape  $\mathbf{s}$  parameters of the model so that the models' spine fits the 3D reconstructed spine and the models' skin surface captures the surface scan. As the shape parameters  $\mathbf{s}$  only capture several deformation models, the obtained geometries do not precisely match the patient-specific geometries. Thus, in a second step, we refine the geometries of the model's vertebrae and skin to match the patient's observations (EOS geometries and surface scan). Once the patient surfaces are captured by the model, the shape parameters are fixed.

Let us note that the patients pose during the surface scan is slightly different than the pose in the radiography, thus, the location of the markers  $\mathbf{l}^A$  on the resulting model differs from the marker locations  $\mathbf{l}^X$  on the X-rays.

To fix this issue, we transfer the  $M$  markers positions  $\mathbf{l}^{Ss} \in \mathbb{R}^{3 \times M}$  located on the surface scan onto the model skin mesh. We identify the closest mesh face of the model to a marker and define the marker location on the model mesh using the barycentric coordinates of the face vertices.

Then, we use a temporary set of pose parameters  $\mathbf{x}'$  that are optimized so that the model markers  $\mathbf{l}^A(\mathbf{x}')$  match the ones in the X-rays  $\mathbf{l}^X$ . This effectively changes the model skin surface to match the pose of the patient in the EOS device.

The marker-based optimization is computed as

$$\hat{\mathbf{x}}' = \arg \min_{\mathbf{x}'} \left( \sum_{i=1}^{i=M} \|\mathbf{l}_i^A(\mathbf{x}') - \mathbf{l}_i^X\|^2 + E_A(\mathbf{x}') \right), \quad (3.1)$$

where the energy  $E_A$  is a regularization term enforcing anatomic constraints on joints of the model.

The resulting model skin surface matches the pose of the back surface during the X-ray acquisitions. Thus, we create a synced skin and spine model by disregarding the temporal parameters  $\mathbf{x}'$  and associating the current optimized skin to the original model parameters  $\mathbf{x}$  obtained during the first registration process. As a result, the anatomical model is a numerical twin of the patient, including the skeleton and the skin rigged with common model parameters. The association of the skin and spine is performed on the pose observed during the X-ray acquisitions with the help of the radio-opaque markers. Given a new set of markers, the model parameters can be optimized using Equation (3.1) and obtain the skin model matching the input markers, as well as a prediction



of the spine geometry inside the body.

#### 3.4.1.4 Accuracy of the anatomical model

To evaluate the quality of our model, we compute several metrics related to the accuracy in shape, positions and orientations of the vertebrae. The ground-truth measurements of the vertebrae are based on the 3D annotations provided by the SterEOS software. We compare our model meshes with the reconstructed ones.

The vertebra location is defined with the center of mass of the corresponding mesh. The euclidean distance between the corresponding ground truth and model meshes is then computed with their mean absolute difference on each anatomical axis. Differences in orientations are given by the 2D projection of a vertebra orientation vector, computed according to the recommendations of the ISB (International Society of Biomechanics) [149] on a given anatomical plane. The resulting angle between the SterEOS measurement and our model is then measured for each vertebra on each plane. To assess the quality of the model vertebrae geometry we compute the absolute mean and standard deviation of the point-to-surface distances between the model geometries and the EOS 3D reconstructed spines.

As the body surface of the back during the radiograph acquisitions is not available, we evaluate the model fit to radiographs by computing the 3D euclidean distances between the radio-opaque markers on the model and in the X-ray. We also quantify the contribution of the model skin correction step used to reconstruct the pose of the back during the X-ray acquisition.

#### 3.4.1.5 Validation of the kinematic predictions

We validate the motion of the spine inside the body predicted by our model as follows. Two voluntary subjects with AIS were acquired in different poses in the EOS imaging system. The standard pose, standing with hands on the cheeks, was used to create the digital twin (fig. 3.6 left). Then two other poses, right and left lateral bending, were also acquired (fig. 3.6 right). From the resulting images the marker positions were identified and located and the 3D spine model reconstructed. The markers of these poses are used to drive the model, and the obtained 3D spine is compared to the reconstructed one. Specifically, given a set of 3D markers in the X-rays  $\mathbf{l}^X$ , the model parameters  $\mathbf{x}$  can be optimized, so that the model markers  $\mathbf{l}^A$  best match the input markers  $\mathbf{l}^X$  by optimizing Eq. 3.1.

Let us note that the 3D reconstruction of the vertebrae in lateral bending is not straightforward due to the overlapping of the different bones on the profile X-ray (fig. 3.6b right). Thus, the vertebra details needed for the reconstruction are difficult to extract: the computed geometries of the vertebrae do not accurately match the image and do not match the geometries obtained in the standing pose. To overcome this issue, we rigidly registered the model vertebra geometries obtained in the standing position to the reconstructions in bending position. This step computes the optimal rigid transformation of each vertebra to minimize the projected distances of the model geometries in standing and those obtained in bending.



Figure 3.6: Biplanar X-rays of the same patient in standing and lateral bending. During the acquisitions the patient wears radio-opaque markers. In bending, several stereo-landmarks, needed for the spine reconstructions are hidden, particularly in the thoracic part.

With this procedure we obtain the 3D rigid location and orientation of each vertebra from the bending images. Thus, we compute the orientation errors with respect to the predictions by using the intrinsic Euler angles defined by the ISB XYZ sequence (coronal, axial, sagittal). The accuracy in position is given as described in 3.4.1.4.

### 3.4.2 Results

We evaluate the created digital twin in two settings. We first quantify the capability of the model to capture the data in the standing position, and then we evaluate the precision of the model on the bending position. For each position we assess the external accuracy, i.e. how well does the model fit the 3D markers, as well as the internal accuracy, i.e. how well does the model capture the shape and position of the 3D spine inside the body.

#### 3.4.2.1 Accuracy of the subject-specific model in standing

**External accuracy.** We tested our method to correct the pose of the model skin according to the 3D positions of the markers in the X-rays. In fig. 3.7, it appears that we were able to have a significant gain in accuracy of the surface reconstruction of the model, reflected by the position of the markers, with the correction step. The average distance error decreases from 9.86 mm (std: 8.10 mm) to 4.47 mm (std: 2.70 mm).

**Internal accuracy.** Measurements in positions are made by computing the center of mass of each mesh. Orientations of each thoracic and lumbar vertebra (T01-L05) are produced according to the ISB recommendations. The shape accuracy is given for each vertebra by computing the

mean of the absolute point-to-surface distances. The results are detailed for each vertebra on table 3.2. The error in positioning T01 is due to a model registration error on a unique patient whose vertebra has a particular shape. Despite this result, the model performs well in capturing the morphological specificities of the patient’s spine.

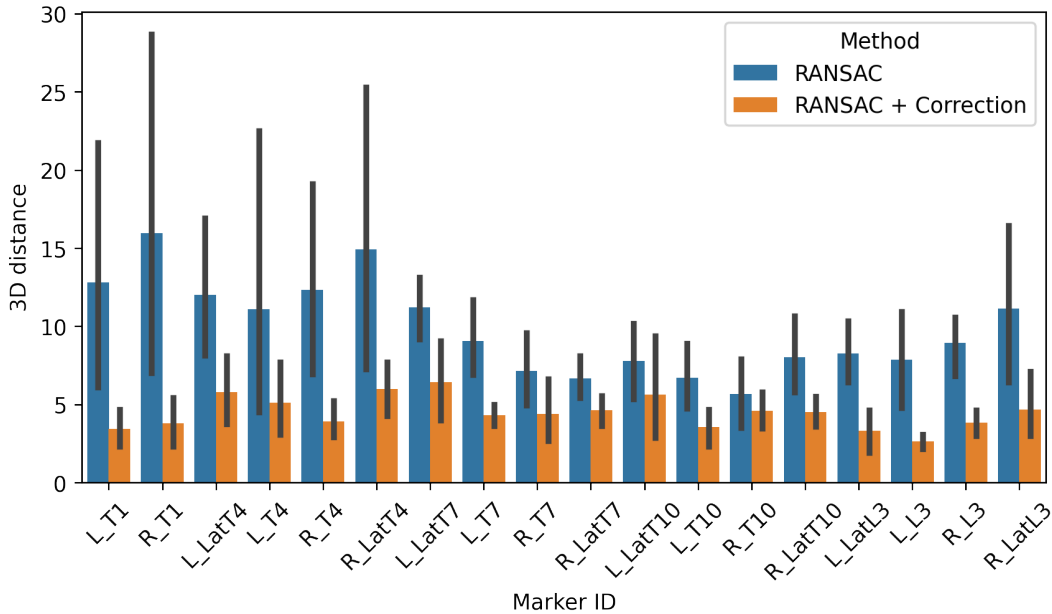


Figure 3.7: Distance error per marker from the resulting model to the radiograph positions. We compare a simple rigid registration of the skin onto the radio-opaque markers using RANSAC (blue) with an additional step of the pose correction using a kinematic model (orange).

### 3.4.2.2 Accuracy of the subject-specific model in bending

From the X-ray images, the radio-opaque marker positions were manually extracted and their 3D location triangulated. Their positions serve as inputs for the inverse-kinematics problem.

For this experiment, we removed the two most lateral markers at the T04 level as these markers are subject to the movement of the scapula, which is not included in our model. We can notice that their positions have not correctly fit their target by the anatomical model for these two subjects with an average 3D error of 6.68 mm (std: 1.25 mm).

Let us note that for one subject, the right bending pose resulted in most markers being out of the X-ray frontal plane view. Thus we do not report metrics on this case.

**External accuracy.** After the marker optimization, the model markers reached their corresponding targets with an average distance error of 4.66 mm (std: 2.14 mm).

**Internal accuracy.** We evaluated the accuracy of our predictions in positions by comparing the center of mass of each vertebra. The errors in rotations are given by comparing the intrinsic Euler

Tableau 3.2: Accuracy (Mean Absolute Error, MAE) of the avatar vertebrae in shape, positions and orientations

ID	Positions (mm)			Orientations (deg)			Shape (mm)	
	3D distance	Anteropos.	Mediolat.	Inferosup.	Coronal	Sagittal	Axial	P.-t.-S. distance
T01	1.32 (3.28)	1.05 (2.78)	0.7 (1.78)	0.11 (0.18)	1.67 (2.92)	1.98 (2.6)	3.58 (5.33)	0.31 (0.33)
T02	0.33 (0.7)	0.15 (0.26)	0.27 (0.66)	0.06 (0.08)	1.25 (1.23)	3.19 (2.34)	1.55 (1.09)	0.28 (0.27)
T03	0.17 (0.18)	0.14 (0.19)	0.06 (0.04)	0.05 (0.06)	1.33 (0.77)	7.22 (4.66)	1.87 (1.38)	0.28 (0.25)
T04	0.27 (0.28)	0.23 (0.26)	0.06 (0.06)	0.1 (0.12)	2.16 (1.44)	3.4 (3.69)	1.28 (0.86)	0.31 (0.28)
T05	0.18 (0.23)	0.14 (0.23)	0.04 (0.02)	0.07 (0.09)	2.77 (2.98)	1.52 (1.0)	1.67 (0.53)	0.29 (0.28)
T06	0.07 (0.06)	0.06 (0.06)	0.03 (0.02)	0.02 (0.01)	1.48 (1.55)	2.14 (1.47)	2.47 (2.23)	0.26 (0.24)
T07	0.24 (0.25)	0.15 (0.2)	0.09 (0.08)	0.15 (0.14)	1.04 (1.52)	2.23 (1.56)	1.17 (1.13)	0.31 (0.28)
T08	0.13 (0.06)	0.1 (0.06)	0.03 (0.02)	0.06 (0.04)	0.92 (0.79)	5.14 (2.36)	3.07 (3.09)	0.29 (0.31)
T09	0.15 (0.07)	0.12 (0.08)	0.06 (0.04)	0.03 (0.04)	1.17 (0.58)	4.35 (2.29)	2.29 (3.84)	0.28 (0.25)
T10	0.14 (0.06)	0.11 (0.08)	0.04 (0.03)	0.04 (0.02)	1.79 (0.96)	7.8 (3.5)	4.21 (3.44)	0.31 (0.3)
T11	0.21 (0.23)	0.16 (0.16)	0.05 (0.06)	0.12 (0.17)	1.4 (0.87)	8.11 (2.24)	2.63 (2.21)	0.3 (0.28)
T12	0.12 (0.15)	0.09 (0.14)	0.05 (0.07)	0.04 (0.04)	1.34 (0.63)	1.63 (1.56)	2.27 (2.02)	0.29 (0.27)
L01	0.19 (0.28)	0.14 (0.28)	0.07 (0.04)	0.06 (0.09)	1.78 (1.83)	3.84 (3.28)	1.79 (1.17)	0.31 (0.3)
L02	0.29 (0.27)	0.24 (0.27)	0.07 (0.06)	0.1 (0.12)	1.57 (1.61)	5.43 (4.81)	4.66 (8.08)	0.28 (0.26)
L03	0.31 (0.27)	0.28 (0.24)	0.05 (0.06)	0.1 (0.14)	2.62 (3.85)	4.74 (1.3)	2.79 (2.64)	0.28 (0.26)
L04	0.44 (0.23)	0.43 (0.22)	0.05 (0.06)	0.06 (0.06)	1.16 (1.22)	5.74 (2.15)	3.04 (5.16)	0.31 (0.29)
L05	0.61 (0.29)	0.58 (0.26)	0.1 (0.1)	0.15 (0.09)	1.65 (1.4)	2.37 (2.25)	3.7 (5.79)	0.3 (0.28)
All	0.31 (0.83)	0.25 (0.70)	0.11 (0.46)	0.08 (0.10)	01.59 (1.73)	4.17 (3.32)	2.59 (3.49)	0.29 (0.28)

angles between the ground-truth and predictions according to the XYZ order given by the ISB recommendations [149]. The results are presented for each vertebra table 3.3.

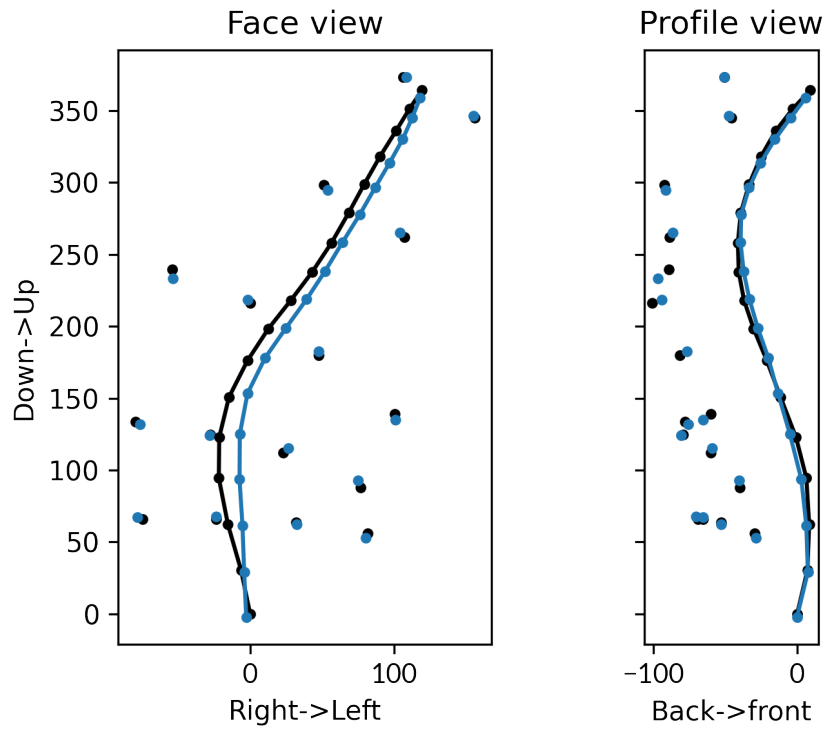
*Tableau 3.3: Accuracy of the predictions (MAE) of the vertebra positions and orientations according to the marker positions in lateral bending.*

ID	Positions (mm)			Orientations (deg)		
	Anteropos.	Mediolat.	Inferosup.	Coronal	Sagittal	Axial
T01	4.53 (1.32)	2.38 (1.21)	3.62 (2.56)	6.17 (6.03)	2.3 (2.47)	2.2 (1.63)
T02	3.84 (1.9)	3.35 (3.84)	3.71 (2.47)	7.73 (6.57)	1.7 (1.36)	5.27 (4.24)
T03	3.47 (2.64)	4.98 (4.97)	2.6 (2.99)	6.39 (4.48)	1.17 (1.05)	3.41 (3.92)
T04	3.78 (3.13)	6.31 (5.98)	2.6 (1.71)	4.56 (4.52)	1.53 (0.98)	2.04 (1.04)
T05	4.21 (3.57)	7.13 (6.23)	1.86 (0.9)	4.87 (2.11)	1.69 (1.2)	2.96 (0.63)
T06	4.94 (4.25)	7.45 (6.25)	1.38 (1.17)	2.53 (1.45)	2.47 (1.99)	4.32 (2.0)
T07	5.55 (3.54)	7.12 (6.92)	0.92 (1.45)	2.03 (1.14)	2.35 (0.8)	4.4 (4.34)
T08	5.24 (2.64)	7.57 (6.86)	1.29 (1.03)	2.14 (2.15)	2.83 (1.35)	2.94 (1.33)
T09	4.39 (2.73)	9.0 (6.03)	1.49 (1.43)	3.65 (3.58)	1.8 (1.77)	2.99 (0.43)
T10	4.22 (3.44)	10.66 (2.45)	1.05 (0.95)	4.59 (6.29)	1.31 (1.07)	5.48 (4.8)
T11	3.32 (4.42)	12.01 (0.78)	1.53 (0.82)	4.19 (4.46)	1.55 (1.81)	7.28 (4.04)
T12	3.26 (2.65)	12.93 (1.76)	2.15 (0.37)	4.39 (4.06)	3.54 (1.08)	7.14 (4.02)
L01	5.42 (5.78)	14.42 (3.96)	1.36 (0.76)	7.69 (11.85)	8.1 (9.25)	8.01 (6.84)
L02	5.19 (5.13)	13.79 (4.57)	1.82 (1.19)	2.98 (2.99)	4.0 (1.19)	9.54 (6.36)
L03	5.39 (5.58)	11.09 (2.7)	0.94 (0.33)	2.9 (3.03)	1.23 (0.92)	7.1 (0.32)
L04	4.04 (3.97)	6.75 (3.64)	1.43 (0.19)	6.05 (7.55)	3.12 (2.57)	6.13 (5.55)
L05	3.78 (3.2)	7.38 (4.52)	1.59 (0.92)	4.76 (3.16)	2.95 (3.06)	13.98 (5.02)
All	4.39 (3.13)	8.49 (5.13)	1.84 (1.45)	4.57 (4.53)	2.57 (2.77)	5.60 (4.38)

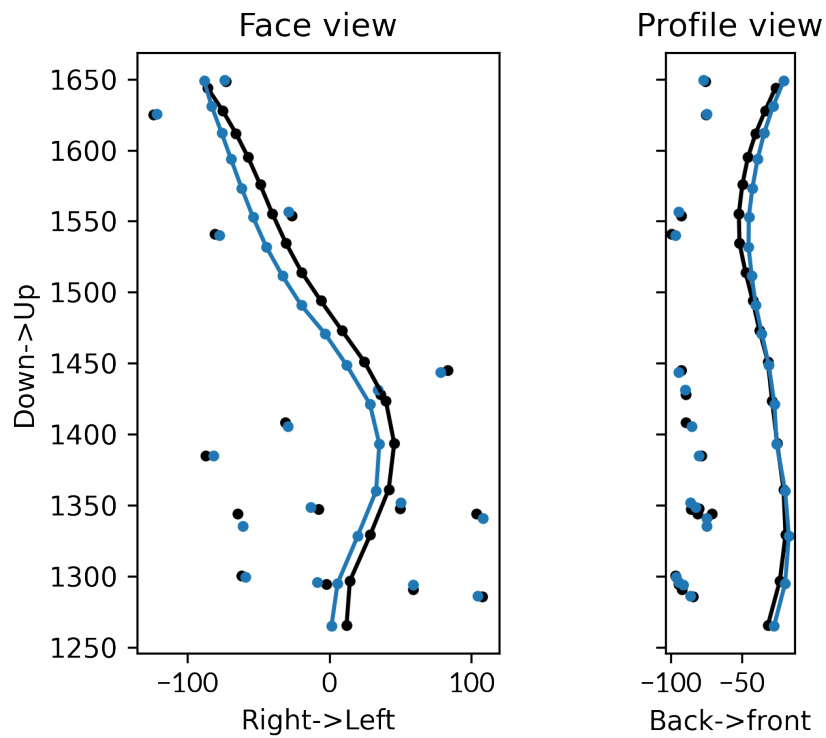
The 3D accuracy of the predicted positions is close to the cm in average with 1.07 cm (std: 0.42 cm). It can be noted that the predictions are affected by a global lateral shift in the side of the movement (fig. 3.8) highlighted on the mediolateral axis (MAE 8.49 mm, std: 5.13 mm). Despite this error, the orientation in the corresponding plane (coronal) is closer to the expectations (4.57°, std: 4.53°, table 3.3). The greater error in the L05 transverse rotation can be due to a lack of superficial constraints (i.e. markers) in this region.

### 3.4.3 Discussion

In this section, we presented a semi-automatic workflow that allows the creation of a 4D numerical avatar of patients with AIS reflecting their inner and external anatomy. The inputs were captured using safe and low-dose imaging methods and do not need a sensitive palpation task that cannot be easily applied on young subjects in a daily clinical usage. An anatomical avatar is deformed in order to capture the internal (spine) and external (skin) specificities of the patient obtained from



(a) Patient A, bending left



(b) Patient B, bending right

Figure 3.8: Predictions (blue) against the ground-truth (black) on the coronal and sagittal planes (scale in mm). The free dots represents the marker positions and the connected ones the vertebrae.

the different modalities. The model was able to capture the vertebra geometries with a mean error below the mm (0.29 mm, std: 0.28 mm) allowing us to compute several descriptors of the vertebra positions and orientations automatically. One major challenge is to recover the external shape of the patient during the X-ray acquisitions, as the patient's pose is necessarily different from the surface scan acquired separately. A solution can be found in the introduction of 3D sensors during the X-ray acquisition [56]. We proposed a method that leverages radio-opaque markers, visible in both X-ray images and surface scan, to correct the pose of the model's back. This additional step in our workflow allows us to capture the change in pose of the patient in standing and to increase the correspondence with the markers in the X-rays from 9.86 mm (8.10 mm) in average to 4.47 mm (std: 2.70 mm). However, we can notice the difficulty of our model to fit the lateral markers particularly on the upper part of the body. This can be explained by the fact that we are not modeling the shoulder girdle and some markers, positioned near T04 for instance, are placed on the scapula.

In a preliminary study, we validate the predictions of the kinematic model with secondary X-rays of two voluntary patients asked to make lateral bending (left and right, fig. 3.6). One capture was rejected due to the low visibility of the markers. The marker positions were used as inputs of the simulator and the predicted positions and orientations of the vertebrae compared to 3D X-ray reconstructions. Beside the low number of subjects in our study, a limitation can be found in our evaluation which is restricted to an analysis of the spine in two different poses which is not allowing a comprehensive analysis of the full motion. It should be noted that kinematic evaluations are currently possible only through semi-static measurements, as a true kinematic analysis is not feasible with the current methods of capture of the vertebral motion.

The creation of a thoracolumbar kinematic model of patients with scoliosis condition was also investigated by Overbergh et al 2020 [101]. They were able to make a subject specific model of their patients comprising bone geometries and a set of superficial markers. Then, they compared their kinematic predictions against secondary X-rays of subjects in different poses. However, this workflow was designed towards Adult Spinal Deformity analysis and was not integrating the external surface of the back. We proposed a method that is leveraging the 3D acquisition of the back avoiding any precise or time-consuming task of palpation. Thus, this protocol can be used by less experienced medical staff.

Today, to our knowledge, we don't have reference values determining whether the accuracy of kinematic predictions is sufficient for daily clinical analysis. Only Overbergh et al. [101] allows us to compare results in the context of spine with scoliosis. Our predictions are in the range of values of those reported in [101] in positions and orientations except for the mediolateral axis measurements. In this case, the predicted spine was affected by a global lateral shift in the side of the bending. The orientations of the vertebrae were in the range of acceptable values with an average accuracy below  $6^\circ$  on the intrinsic Euler rotations. The reconstructions in the lumbar part of the spine showed a more important error particularly on the axial rotations. This is also the most flexible part of the spine where rotations can be underestimated by our kinematic model.

A source of the errors can be identified in the joints of our generic model where stiffness matrices are defined using the Ignasiak et al. 2016 [63] and Koutras et al. 2021 [82] values, obtained from healthy adult observations. Optimization processes can be planned in order to estimate more specific kinematic parameters such as the joints stiffness or the markers constraint [144]. The addition of radio-opaque markers on the hips would allow us to improve the model predictions in the lower part of the spine and to validate predictions with the inclusion of the pelvis. In addition, compared to the literature, our approach relies on markers which are not placed closely to bony structures. Thus, we should also consider potential errors introduced by skin deformation artifacts. Furthermore, the recruitment of more patients, with and without AIS, captured in a wide variety of poses (flexion, extension, lateral bending, etc.), would provide a more comprehensive overview of the model's performances.

#### **3.4.4 Conclusion**

Combined with 3D X-ray imaging, the characterization of the spine in motion provides valuable insights about the scoliosis condition of the patient. The dynamic analysis of AIS presents a significant challenge due to the absence of non-invasive and non-ionizing techniques for capturing vertebra motion. In this study we investigated the use of a subject-specific kinematic model obtained from low-dose biplanar X-rays, a surface scan and a set of radio-opaque markers. In our preliminary result, we evaluated the kinematic behaviour of the model against secondary biplanar X-rays of two patients in lateral bending. We show that our predictions are close to the radiograph observations with an accuracy near 1 cm in 3D position and  $5^\circ$  in orientation.

Future work can be considered such as the addition of markers or the optimization of the physical model constraints. Leveraging bigger cohorts of patients in motion will further allow to better characterize the individual physical properties of the patients. Ultimately, a comprehensive understanding of scoliosis using 4D digital twins will lead to improved scoliosis classification, its diagnosis and the treatment with biomedical simulation.



### 3.5 Summary

Given the challenges associated with *in vivo* spinal motion measurement, the analysis mainly relies on external measurements of the body motion. While a variety of features are captured, the level of detail in these measurements might contribute to the limited comprehension of how scoliosis affects spinal movement. The analysis remains superficial and is not providing the underlying internal spinal kinematics. As shown in this chapter, subject-specific biomechanical models can address this gap. These models, based on X-ray medical images allow the reconstruction of the spinal trajectories from external marker positions.

In section 3.4, we proposed a new approach that facilitates the marker placement and allows the analysis of the back and spine motion at the vertebra level. For this purpose, we use a subject-specific kinematic model of the patients created from different sources: the spine obtained using a 3D low-dose imaging system (EOS) and the skin shape captured with an optical 3D sensor. Our method leverage radio-opaque markers that allows the registration of an articulated anatomical model on these different modalities. As a result, we can reconstruct a kinematic digital twin capturing his external and internal characteristics. In a preliminary study we evaluated the ability of our model to reconstruct spine dynamics from the superficial marker positions. This validation, based on a small number of patients (2), shows promising results in predicting these 3D vertebra trajectories in translation and rotation.

# Conclusion and perspectives

## 1 Summary

### 1.1 3D static characterization of scoliosis with non-ionizing methods

Adolescent Idiopathic Scoliosis (AIS) is a progressive disease of the spine that needs to be detected rapidly for prompt and effective treatment. This detection relies on measurements of internal spinal deformities and their evolution between medical visits. However, the characterization process needs the use of ionizing imaging techniques which carry a potential risk of cancer development, particularly for patients who need regular monitoring.

Safe and non-ionizing approaches, based on 2D or 3D acquisitions of the back surface, are showing promising results in detecting and characterizing spinal deformities [135]. These methods, in particular those coupled with machine-learning algorithms, allow for the inference of deformation parameters that could previously only be obtained from X-ray images [80, 146]. However, these techniques have limitations when it comes to characterize deformations. They are essentially based on local, 2D measurement of the main Cobb angle, whereas scoliosis is by nature a three-dimensional deformation affecting the entire spine [25, 130].

In a first contribution, we propose to go further and to push the characterization in 3D in the full thoracolumbar spine while proposing an accessible, non-ionizing examination method. For this purpose, our approach is based on depth maps of the back that can be obtained from cheap and easy-to-use 3D sensors and deep-learning algorithms. We also leveraged a public database, the New Mexico Decedent Image Database [44], to include additional examples to our hospital dataset. The resulting dataset provides 121 representations of the torso and their corresponding 3D spine reconstructions that can be used to train our regression model. To ease spine predictions, we use a low dimensional representation of the spine based on Principal Component Analysis. Our approach extends the spine examination, usually in the coronal plane (scoliosis), to the sagittal plane (kyphosis and lordosis). In addition to the 3D characterization of the spinal alignments, we show that our method can also be considered into the detection of early scoliosis disorders.

### 1.2 Towards a 4D analysis of the spine with AIS

Beyond the static aspects in the description of the spinal deformities, recent advancements in motion capture enable the dynamic analysis of the human body. Studies dedicated to idiopathic scoliosis rely on the analysis of superficial markers that are not describing the actual internal motion. For this purpose, novel approaches propose to use biomechanical models, built from 3D imaging techniques, to reconstruct the internal spine dynamics. These methods have been developed and

validated primarily on Adult Spinal Deformity patients and, however, can be challenging to apply to young patients with idiopathic scoliosis.

In this manuscript, we propose a new approach that leverage a digital twin of the patient with AIS allowing the analysis of spine motion. This model is created from different sources: the spine obtained from a 3D low-dose imaging system (EOS) and the skin captured with an optical 3D sensor. Our method leverages radio-opaque markers that enable the registration of an articulated anatomical model on these different modalities. The resulting digital twin can be then driven from outer measurements, like motion capture, to reproduce realistic internal motion. In a preliminary study, we validated our kinematic model on two voluntary patients with AIS who underwent lateral flexion radiographs. Driven by the 3D radio-opaque marker positions, the model show promising results in the prediction of the 3D displacement of the vertebra in translation and rotation.

## 2 Discussions and near future research directions

In this section, we provide a discussion on several points of our methodology. Our works present various uncertainties and limitations that could be assessed and resolved in near research directions.

### 2.1 Contribution 1: 3D inference of the scoliotic spine from depth maps

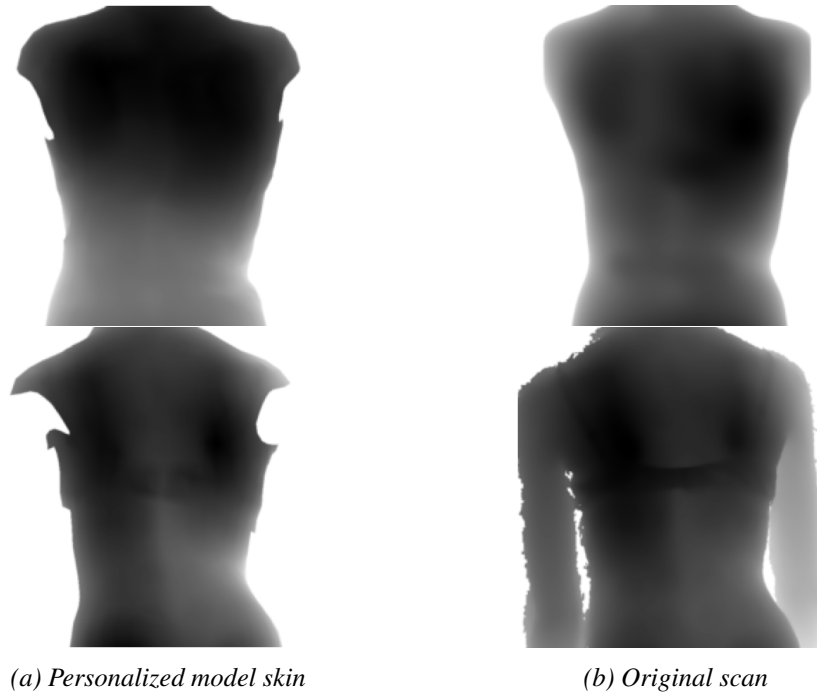


*Figure 3.9: Difference between model skin representation and original scans for patients with full (first row) and partial (second row) back acquisition.*

In the first contribution, the inference models are trained and tested with data samples that encompassed real back views (NMDID segmentations) and skin reconstructions derived from anatomical models (GH patients).

As we can note, we were not able to use the original surface scans because they were acquired in a pose that may differ from the one obtained for the spine (fig. 3.9). In future studies, we could annotate and incorporate these scans into the analysis, thereby validating the inference models with more realistic image captures of backs with AIS.

We could consider the kinematic model developed in section 3.4 that can potentially be integrated into the data processing pipeline. Ultimately, this integration could facilitate the reconstruction of vertebral positions within the original scans.

Consequently, we could enhance the training process by incorporating data from various sources and poses, aiming to improve model performance and enhance its generalization capabilities across different 3D acquisition sources.

## 2.2 Contribution 2: Multi-Modal Data Correspondence for the 4D Analysis of the Spine with Adolescent Idiopathic Scoliosis

### 2.2.1 The localization of the radio-opaque markers in biplanar X-rays

#### 2.2.1.1 Facilitate marker identification

Our second contribution, presented in chapter 3, is based on a primary manual task of localization of the radio-opaque markers on the biplanar X-rays. This task can be complicated in specific conditions, particularly when the markers are aligned in the same axis as presented fig. 3.10. In this situation, precise visual inspection of the marker shape and 3D surface acquisition of the back are needed to associate the markers in the two views. Alternatively, this issue can be limited in future acquisitions by avoiding markers alignment.

In addition, we can facilitate this task by making it fully automatic. As markers are easily localized in images, we could easily train a Convolutional Neural Network to detect and identify these markers in the images. This requires, however, collecting a sufficient number of images to train the network.

#### 2.2.1.2 Quantify precision noise

In future experiments, it would be of interest to assess the effect of errors in marker localization. For this purpose, we can design an experiment by introducing random noise in their 2D coordinates and thus, evaluating the resulting alterations in the model's dynamic predictions. This experiment has the potential to offer a quantitative understanding of the influence of the marker localization task in our results.

### 2.2.2 Increase the classification of the numerical twins to the patients characteristics

As presented in chapter 3 section 3.4, our subject-specific kinematic model construction allows a fine capture of the patients spine geometries. However, the kinematic constraints in the 6D intervertebral joints, are defined from healthy adult subjects while the aim of the model is to represent young patients with spine deformities. Thus, our model is not reproducing the behaviour of an unhealthy spine with altered biomechanics. The use of more specific stiffness matrices, derived from patient acquisitions, like X-rays in bending or motion capture, with inverse kinematics experi-

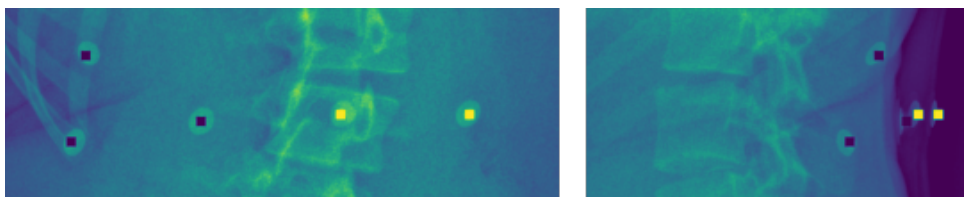


Figure 3.10: Ambiguity with the manual identification and matching of markers on the X-ray images. The difficulty is to correlate the two markers located in yellow on the profile view (on the right) with their corresponding positions on the frontal view (on the left).

ments, can increase the accuracy of the model's dynamic predictions. Furthermore, compare these specific intervertebral joints properties to those obtained from healthy patients can significantly enhance our understanding of the influence of scoliosis on the spine dynamics.

### **2.2.3 Limitations with dynamic validations**

A limitation in the evaluation of dynamic predictions is linked the challenge to obtain true *in vivo* spinal kinematic measurements. The current state-of-the-art [101] and our approach, compare predictions against different poses of patients during low-dose X-rays with the EOS imaging system. These evaluations are semi-static and are not taking in account the entire body motion. For this purpose, dynamic radiography can be investigated to collect such measurements but the risk of radiation exposure should be considered, particularly for young patients followed for adolescent idiopathic scoliosis [78].

In addition, to the best of our knowledge, there is no standard defining the accuracy of motion prediction for clinical use. Results can be compared with similar studies, in our case Overbergh et al. 2020 [101], to evaluate the magnitude of our errors.

## **2.3 On both contributions**

### **2.3.1 Need of additional acquisition of patients with scoliosis**

Our contributions show promising results towards the 3D characterization of the spine with AIS from external acquisitions of the back, whether static or in motion. However, we can point out some improvements that can be mainly leveraged by the inclusion of additional subjects in the near future, particularly with patients with moderate to severe scoliosis.

As shown in chapter 2 section 3, our model tends to underestimate these scoliosis curvatures in the inference from depth maps. In fig. 2.22 page 46, we can see that patients below  $25^\circ$  of scoliosis tend to be underestimated by our method. This issue can be explained by a scarce representation of these deformities in our dataset, mainly constituted of asymptomatic and mild scoliosis subjects.

We can also point out the limited number of patients recruited for our study chapter 3 section 3: we validated our model with two voluntary patients while the use of a high variety of scoliotic curvatures and movements would provide a better overview of our model performances. In its current form, our analysis is limited to a preliminary analysis in the reconstruction of the vertebra trajectories.

### **2.3.2 Facilitate validation and comparisons between studies**

The current state-of-the-art is usually reporting results without sharing any dataset or source code. In future, the creation of a public, freely accessible database, like the New Mexico Decedent Image Database, would greatly facilitate the creation and validation of data-driven methods. It could also allow clear results comparisons between studies which are currently difficult to interpret due to the variations in datasets, made on different populations (scoliosis prevalence, severity, etc.).

Another aspect is the availability of the code, frequently not easily accessible, which would facilitate the reproducibility of the experiments and tests. For this reason, we make our code available, with the trained models, for research purposes.

### 3 Long term directions

Our works are opening several possible research directions towards the assessment of scoliosis with non-ionizing methods and motion capture.

#### 3.1 3D inference of the spine alignments from depth maps

##### 3.1.1 Creation of an accessible mobile screening tool

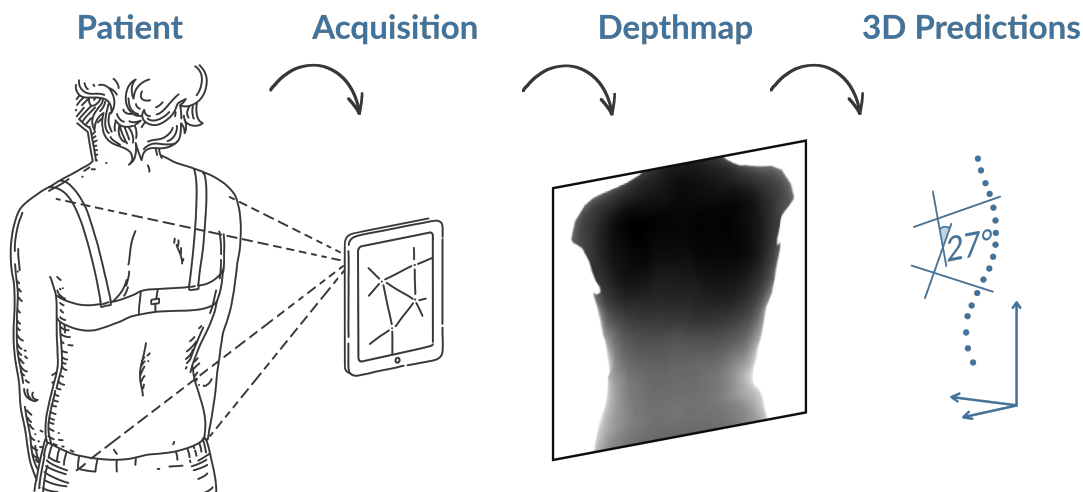


Figure 3.11: Summary of our method. A depth map is rendered from a 3D capture of the back. Then, a Convolutional Neural Network is trained to infer the 3D vertebrae positions inside the image. Scoliosis, lordosis and kyphosis can be estimated from the predicted spinal alignments.

In chapter 2 page 34, our work demonstrates the capability of deducing 3D spinal alignments from a single depth map of the back. With the widespread availability of 3D sensors in common mobile devices like smartphones and accessories, these tools become easy-to-use and cost-effective for data acquisition. By integrating specialized software, such as ours, into these devices, we have the potential to simplify the detection and the monitoring of idiopathic scoliosis (fig. 3.11). This could be facilitated by medical personnel during school screenings but also by the general public.

However, there are still additions to be made to this software. Our results are given according to depth maps in inputs that are already cropped on the spine. As [151], we can include an automated task of cropping to propose a fully automated method of inference. Faster-RCNN, for instance, shows accurate results in the localization of the spine from RGB images of the back [151]. This method can be implemented to propose a complete automated solution for screening and monitoring scoliosis disorders.

Furthermore, we identify scoliosis curvatures from vertebra centroids defined by the gravity centers of the full vertebra geometries. We employ the approach established by Choi et al. in 2017 [20] to locate and estimate the Cobb angles. A comprehensive examination of this measurement method is furnished in Appendix B, and is showing similar results with the traditional



method of measurement as reported in [20]. However, this method has some constraints that may arise in particular subjects leading to false negative cases.

### **3.1.2 Additional features**

We can also push the characterization further by investigating the ability of our approach to infer the Vertebral Axial Rotation (VAR), presented in chapter 2 page 24, that is also an important descriptor of the scoliosis deformities at a given vertebra level. Several studies highlight their importance in the estimation of the risk of progression of scoliosis [25, 129]. This step needs an accurate measurement of the vertebra rotations that can be made from EOS images and 3D reconstructions [64]. Choi et al [19], and then Watanabe et al 2019 [146], show in their study, the possibility to retrieve such measurements from Moiré images. However, their method is based on the location of the spinous process that can be deformed in scoliosis condition. By choosing an appropriate method (like those using vertebra pedicles [130]), we could train our model to infer the axial rotations in addition of the vertebra positions. As a result, our model will be able to give more advanced descriptors of 3D scoliosis deformations, such as the Torsion index, based on intervertebral rotations [39].

Therefore, by having a detailed analysis of the spine alignments provided by our inference method, we would also explore the possibility of reconstructing the vertebra geometries and thus, provide a full 3D representation of the spine. In this direction, we can use the current knowledge in statistical shape modeling used in semi-automated reconstructions methods of the spine [62] that can even work with partial information [93]. This direction has recently been investigated by Liang et al 2023 [87]. They were able to infer the vertebra alignments and geometries of a given person from an RGB-D image, with unclothed back surface in standing position. Unfortunately, due to a lack of annotated ground-truth data, they could only evaluate the accuracy of their predictions in the coronal alignments.

## **3.2 Towards a facilitated comprehensive 4D analysis of the spine**

### **3.2.1 The use of marker-less motion capture methods**

As discussed in chapter 3 page 58, our protocol requires a short preparation by placing the markers on the back. Even if our method is simplifying the protocol of placement of the markers, recent acquisition systems of motion capture are eliminating this preliminary task: the marker-less systems. These methods rely on depth or RGB cameras and computer vision techniques to track and analyze the motion [137]. By correlating images captured from different points of view and identifying common points in each frame, the system can effectively reconstruct the body surface in 3D. For this purpose, deformable kinematic models like SMPL [88] are commonly employed to accurately represent the human body and its motion.

Methods like Keller et al. 2022 [73] can also be considered. In their study, the authors trained a statistical model to learn the correlation between the full body surface and the skeleton allowing

a reconstruction of the bony elements from surface reconstructions in different poses with better results compared to *Anatomy transfer* [33]. However, their work was not focused on accurate 3D spinal reconstruction. Additional research can be made by integrating patients with scoliosis, biplanar X-ray images in their method with the inclusion of models capable of capturing asymmetrical trunk affected with scoliosis, as discussed in section 2.2.3 page 32.

In our approaches, the external surface is also included and associated with spinal elements, and thus can be integrated into these techniques. This can be achieved by registering the personalized kinematic model onto the 3D surface reconstructions obtained from the marker-less methods as we registered this one on mocap markers positions.

This change in motion capture technique, combined with subject-specific models has the potential to significantly enhance and simplify the dynamic analysis of the spine motion in future clinical routines.

### **3.2.2 Towards a comprehensive analysis of the spine to investigate new biomarkers**

In chapter 3 section 3.4, our contribution opened the possibility to combine the current low-dose 3D characterization techniques of the spine with motion capture. Our method provides a detailed description of the motion of the spine at each vertebra level. This advancement allows us to combine dynamic descriptors, such as the Range of Motion, at each anatomical plane, with the detailed static characterization of the spine and torso, as established in previous works [85, 129].

This integration of static and dynamic data is invaluable in the context of scoliosis research and treatment. Integrating these multi-modal data into a statistical analysis would lead to identify specific patterns and correlations between static structural irregularities and the individual dynamic motion characteristics.

### **3.3 Incorporation of our models into longitudinal studies**

Our subject-specific model offers an opportunity to facilitate the investigation of novel 4D biomarkers for predicting scoliosis progression into a comprehensive longitudinal analysis. For this purpose, we can create multiple instances, or digital twins, of a given patient at specific time intervals, allowing the examination of their scoliosis development over time. Beside the current static 3D descriptors collected from radiographs, our model can also provide kinematic descriptors (e.g. Range of Motions) of the spine, correlated with surface measurements.

In term, by collecting and analyzing this data across a sufficient cohort of AIS patients, we can significantly enhance our understanding of scoliosis and its progression during adolescence. The identification of biomarkers, taking into account both spatial, motion and aging dimensions, becomes feasible through this approach and will lead to the development of predictive models, improving the detection and the management of patients at an early stage of the disease.



# Bibliography

- [1] Anatoscope. <https://www.anatoscope.com/>. Accessed: 2023-09-12.
- [2] CMBBE 2023 symposium, 18th international symposium on computer methods in biomechanics and biomedical engineering. <https://www.cmbbe-symposium.com/2023/>. Accessed: 2023-09-12.
- [3] Dynamic Digital Radiography — healthcare.konicaminolta.us. <https://healthcare.konicaminolta.us/radiography/dynamic-digital-radiography>. [Accessed 19-Jul-2023].
- [4] IABM 2023, colloque français d’intelligence artificielle en imagerie biomédicale. <https://iabm2023.sciencesconf.org/>. Accessed: 2023-09-12.
- [5] IABM 2023, colloque français d’intelligence artificielle en imagerie biomédicale, best posters. <https://iabm2023.sciencesconf.org/resource/page/id/12>. Accessed: 2023-09-12.
- [6] Occipital Structure Sensor. <https://structure.io/>, 2021. [Online; accessed 09-April-2021].
- [7] M. M. Adankon, J. Dansereau, H. Labelle, and F. Cheriet. Non invasive classification system of scoliosis curve types using least-squares support vector machines. Artificial Intelligence in Medicine, 56:99–107, 10 2012.
- [8] A. Alfraihat, A. F. Samdani, and S. Balasubramanian. Predicting curve progression for adolescent idiopathic scoliosis using random forest model. PLOS ONE, 17(8):e0273002, Aug. 2022.
- [9] V. L. Alves and O. Avanzi. Objective assessment of the cardiorespiratory function of adolescents with idiopathic scoliosis through the six-minute walk test. Spine (Phila Pa 1976), 34(25):E926–929, Dec 2009.
- [10] C.-É. Aubin, N. Cobetto, J. Clin, F. Desbiens-Blais, H. Labelle, S. L. May, and S. Parent. Improved brace design combining CAD/CAM and finite element simulation for the conservative treatment of adolescent idiopathic scoliosis (AIS): preliminary results of a randomized control trial. Scoliosis, 10(S1), Jan. 2015.

- [11] P. Bernstein, J. Metzler, M. Weinzierl, C. Seifert, W. Kisel, and M. Wacker. Radiographic scoliosis angle estimation: spline-based measurement reveals superior reliability compared to traditional COBB method. European Spine Journal, 30(3):676–685, Aug. 2020.
- [12] E. Berthonnaud and J. Dimnet. Analysis of structural features of deformed spines in frontal and sagittal projections. Computerized Medical Imaging and Graphics, 31(1):9–16, Jan. 2007.
- [13] P. Besl and N. D. McKay. A method for registration of 3-d shapes. IEEE Transactions on Pattern Analysis and Machine Intelligence, 14(2):239–256, 1992.
- [14] B. Biot, E. Clément, and M. Lejeune. Le mouvement de la colonne scoliothique à l’âge adulte. Annales de Readaptation et de Medecine Physique, 47(2):64–71, mar 2004.
- [15] M. Bolzinger, I. Bernardini, C. T. Lemoine, A. Gallini, F. Accadbled, and J. S. de Gauzy. Monitoring adolescent idiopathic scoliosis by measuring ribs prominence using surface topography device. Spine Deformity, 9(5):1349–1354, Mar. 2021.
- [16] A. Breen, E. Claerbout, R. Hemming, R. Ayer, and A. Breen. Comparison of intra subject repeatability of quantitative fluoroscopy and static radiography in the measurement of lumbar intervertebral flexion translation. Scientific Reports, 9(1), Dec. 2019.
- [17] A. G. Bruno, M. L. Bouxsein, and D. E. Anderson. Development and validation of a musculoskeletal model of the fully articulated thoracolumbar spine and rib cage. Journal of Biomechanical Engineering, 137(8):1–10, aug 2015.
- [18] S. Caturano, M. Kaiser, M. Bertsch, T. Bassani, W. R. Taylor, and S. Cukovic. Prediction of the 3d spinal alignment from external shape of the back in AIS patients using regression model. In 2022 IEEE 21st Mediterranean Electrotechnical Conference (MELECON). IEEE, June 2022.
- [19] R. Choi, K. Watanabe, N. Fujita, Y. Ogura, M. Matsumoto, and S. Demura. Measurement of Vertebral Rotation from Moire Image for Screening of Adolescent Idiopathic Scoliosis. IEEE Transactions on Image Electronics and Visual Computing, 6(2):56–64, 2018.
- [20] R. Choi, K. Watanabe, H. Jinguji, N. Fujita, Y. Ogura, S. Demura, T. Kotani, K. Wada, M. Miyazaki, H. Shigematsu, and Others. CNN-based Spine and Cobb Angle Estimator Using Moire Images. IEEE transactions on image electronics and visual computing, 5(2):135–144, 2017.
- [21] M. Christophy, N. A. F. Senan, J. C. Lotz, and O. M. O’Reilly. A musculoskeletal model for the lumbar spine. Biomechanics and Modeling in Mechanobiology, 11:19–34, 2012.
- [22] N. Comte, S. Pujades, A. Courvoisier, O. Daniel, J.-S. Franco, F. Faure, and E. Boyer. Multi-modal data correspondence for the 4d analysis of the spine with adolescent idiopathic scoliosis. Bioengineering, 10(7), 2023.

- [23] J. S. Coogan, W. L. Francis, T. D. Eliason, T. L. Bredbenner, B. D. Stemper, N. Yoganandan, F. A. Pintar, and D. P. Nicoletta. Finite element study of a lumbar intervertebral disc nucleus replacement device. Frontiers in Bioengineering and Biotechnology, 4, Dec. 2016.
- [24] A. Courvoisier. Recherche d'indicateurs cliniques tridimensionnels d'aggravation et de correction par orthèse des scolioses idiopathiques modérées l'École Nationale Supérieure d'Arts et Métiers, 2012.
- [25] A. Courvoisier, X. Drevelle, J. Dubousset, and W. Skalli. Transverse plane 3D analysis of mild scoliosis. European Spine Journal, 22(11):2427–2432, 2013.
- [26] A. Courvoisier, M. Nesme, J. Gerbelot, A. Moreau-Gaudry, and F. Faure. Prediction of brace effect in scoliotic patients: blinded evaluation of a novel brace simulator—an observational cross-sectional study. European Spine Journal, 28(6):1277–1285, Mar. 2019.
- [27] R. J. Cummings, E. A. Loveless, J. Campbell, S. Samelson, and J. M. Mazur. Interobserver reliability and intraobserver reproducibility of the system of King et al. for the classification of adolescent idiopathic scoliosis. J Bone Joint Surg Am, 80(8):1107–1111, Aug 1998.
- [28] A. Daryabor, M. Arazpour, G. Sharifi, M. A. Bani, A. Aboutorabi, and N. Golchin. Gait and energy consumption in adolescent idiopathic scoliosis: A literature review, apr 2017.
- [29] J. C. de Mauroy, P. Fender, B. Tato, P. Lusenti, and G. Ferracane. Lyon brace. Stud Health Technol Inform, 135:327–340, 2008.
- [30] M. de Sèze and E. Cugy. Pathogenesis of idiopathic scoliosis: A review. Annals of Physical and Rehabilitation Medicine, 55(2):128–138, 2012.
- [31] M. de Zee, L. Hansen, C. Wong, J. Rasmussen, and E. B. Simonsen. A generic detailed rigid-body lumbar spine model. Journal of Biomechanics, 40:1219–1227, 2007.
- [32] G. Desroches, C. E. Aubin, D. J. Sucato, and C. H. Rivard. Simulation of an anterior spine instrumentation in adolescent idiopathic scoliosis using a flexible multi-body model. Medical and Biological Engineering and Computing, 45(8):759–768, 2007.
- [33] A.-H. Dicko, T. Liu, B. Gilles, L. Kavan, F. Faure, O. Palombi, and M.-P. Cani. Anatomy transfer. ACM Transactions on Graphics (proceedings of ACM SIGGRAPH ASIA), 32(6), 2013.
- [34] S. Donzelli, S. Poma, L. Balzarini, A. Borboni, S. Respizzi, J. H. Villafane, F. Zaina, and S. Negrini. State of the art of current 3-d scoliosis classifications: a systematic review from a clinical perspective. Journal of NeuroEngineering and Rehabilitation, 12:1–11, 2015.
- [35] M. Dreischarf, A. Rohlmann, G. Bergmann, and T. Zander. Optimised loads for the simulation of axial rotation in the lumbar spine. Journal of Biomechanics, 44(12):2323–2327, aug 2011.

- [36] M. Dreischarf, A. Shirazi-Adl, N. Arjmand, A. Rohlmann, and H. Schmidt. Estimation of loads on human lumbar spine: A review of in vivo and computational model studies. *Journal of Biomechanics*, 49(6):833–845, 2016.
- [37] M. Dreischarf, T. Zander, A. Shirazi-Adl, C. M. Puttlitz, C. J. Adam, C. S. Chen, V. K. Goel, A. Kiapour, Y. H. Kim, K. M. Labus, J. P. Little, W. M. Park, Y. H. Wang, H. J. Wilke, A. Rohlmann, and H. Schmidt. Comparison of eight published static finite element models of the intact lumbar spine: Predictive power of models improves when combined together. *Journal of Biomechanics*, 47(8):1757–1766, 2014.
- [38] B. Drerup. Rasterstereographic measurement of scoliotic deformity. *Scoliosis*, 9(1), Dec. 2014.
- [39] X. Drevelle. Analyse biomécanique des mécanismes d’aggravation de la scoliose idiopathique de l’adolescent à l’aide de la modélisation géométrique et mécanique personnalisée. biomécanique [physics.med-ph]. Arts et Métiers ParisTech, 2011.
- [40] A. du Bois d’Aische, M. de Craene, B. Macq, and S. Warfield. An articulated registration method. In *IEEE International Conference on Image Processing 2005*, volume 1, pages I–21, 2005.
- [41] J. Dubousset, G. Charpak, I. Dorion, W. Skalli, F. Lavaste, J. Deguise, G. Kalifa, and S. Ferey. [A new 2D and 3D imaging approach to musculoskeletal physiology and pathology with low-dose radiation and the standing position: the EOS system]. *Bull Acad Natl Med*, 189(2):287–297, Feb 2005.
- [42] L. Duong, F. Cheriet, and H. Labelle. Towards an automatic classification of spinal curves from x-ray images. *Studies in Health Technology and Informatics*, 123:419–424, 2006.
- [43] G. Duval-Beaupere. Threshold values for supine and standing cobb angles and rib hump measurements: Prognostic factors for scoliosis. *European Spine Journal*, 5:79–84, 1996.
- [44] H. Edgar, S. Daneshvari Berry, E. Moes, N. Adolphi, P. Bridges, and K. Nolte. New Mexico Decedent Image Database, Office of the Medical Investigator, University of New Mexico. <http://doi.org/10.25827/5s8c-n515>, 2020. [Online; accessed 15-July-2022].
- [45] F. Faure, C. Duriez, H. Delingette, J. Allard, B. Gilles, S. Marchesseau, H. Talbot, H. Courtecuisse, G. Bousquet, I. Peterlik, and S. Cotin. SOFA: A Multi-Model Framework for Interactive Physical Simulation. In Y. Payan, editor, *Soft Tissue Biomechanical Modeling for Computer Assisted Surgery*, volume 11 of *Studies in Mechanobiology, Tissue Engineering and Biomaterials*, pages 283–321. Springer, June 2012.
- [46] M. A. Fischler and R. C. Bolles. Random sample consensus: A paradigm for model fitting with applications to image analysis and automated cartography. *Commun. ACM*, 24(6):381–395, June 1981.

- [47] K. P. F.R.S. Liii. on lines and planes of closest fit to systems of points in space. The London, Edinburgh, and Dublin Philosophical Magazine and Journal of Science, 2(11):559–572, 1901. PCA beginnings.
- [48] R. Fujii, H. Sakaura, Y. Mukai, N. Hosono, T. Ishii, M. Iwasaki, H. Yoshikawa, and K. Sugamoto. Kinematics of the lumbar spine in trunk rotation: in vivo three-dimensional analysis using magnetic resonance imaging. European Spine Journal, 16(11):1867–1874, June 2007.
- [49] L. Gajny, S. Ebrahimi, C. Vergari, E. Angelini, and W. Skalli. Quasi-automatic 3d reconstruction of the full spine from low-dose biplanar x-rays based on statistical inferences and image analysis. European Spine Journal, 28:658–664, 4 2019.
- [50] S. Galvis, D. Burton, B. Barnds, J. Anderson, R. Schwend, N. Price, S. Wilson, and E. Friis. The effect of scoliotic deformity on spine kinematics in adolescents. Scoliosis Spinal Disord, 11:42, 2016.
- [51] E. García-Cano, F. A. Cosío, L. Duong, C. Bellefleur, M. Roy-Beaudry, J. Joncas, S. Parent, and H. Labelle. Prediction of spinal curve progression in adolescent idiopathic scoliosis using random forest regression. Computers in Biology and Medicine, 103:34–43, 2018.
- [52] B. Garg, N. Mehta, T. Bansal, and R. Malhotra. Eos® imaging: Concept and current applications in spinal disorders. Journal of Clinical Orthopaedics and Trauma, 11(5):786–793, Sept. 2020.
- [53] S. Gill, P. Mousavi, G. Fichtinger, E. Chen, J. Boisvert, D. Pichora, and P. Abolmaesumi. Biomechanically constrained groupwise us to ct registration of the lumbar spine. Lecture Notes in Computer Science (including subseries Lecture Notes in Artificial Intelligence and Lecture Notes in Bioinformatics), 5761 LNCS:803–810, 2009.
- [54] D. A. Glaser, J. Doan, and P. O. Newton. Comparison of 3-dimensional spinal reconstruction accuracy: Biplanar radiographs with eos versus computed tomography. Spine, 37(16):1391–1397, July 2012.
- [55] B. Groisser. Geometry of the eos(r) radiographic scanner, 2019.
- [56] B. Groisser, R. Kimmel, G. Feldman, N. Rozen, and A. Wolf. 3d reconstruction of scoliotic spines from stereoradiography and depth imaging. Annals of Biomedical Engineering, 46(8):1206–1215, apr 2018.
- [57] M. Gstoettner, K. Sekyra, N. Walochnik, P. Winter, R. Wachter, and C. M. Bach. Inter- and intraobserver reliability assessment of the cobb angle: manual versus digital measurement tools. European Spine Journal, 16(10):1587–1592, June 2007.
- [58] K. He, X. Zhang, S. Ren, and J. Sun. Deep residual learning for image recognition. CVPR, pages 770–778, 12 2015.



- [59] J. E. Herzenberg, N. A. Waanders, R. F. Closkey, A. B. Schultz, and R. N. Hensinger. Cobb angle versus spinous process angle in adolescent idiopathic scoliosis the relationship of the anterior and posterior deformities. Spine, 15(9):874–879, Sept. 1990.
- [60] D. A. Hoffman, J. E. Lonstein, M. M. Morin, W. Visscher, I. Harris, Benjamin S. H., and J. Boice, John D. Breast Cancer in Women With Scoliosis Exposed to Multiple Diagnostic X Rays. JNCI: Journal of the National Cancer Institute, 81(17):1307–1312, 09 1989.
- [61] A. Hong, N. Jaswal, L. Westover, E. C. Parent, M. Moreau, D. Hedden, and S. Adeeb. Surface topography classification trees for assessing severity and monitoring progression in adolescent idiopathic scoliosis. Spine, 42(13):E781–E787, July 2017.
- [62] L. Humbert, J. D. Guise, B. Aubert, B. Godbout, and W. Skalli. 3d reconstruction of the spine from biplanar x-rays using parametric models based on transversal and longitudinal inferences. Medical Engineering & Physics, 31(6):681–687, July 2009.
- [63] D. Ignasiak, S. Dendorfer, and S. J. Ferguson. Thoracolumbar spine model with articulated ribcage for the prediction of dynamic spinal loading. Journal of Biomechanics, 49(6):959–966, 2016.
- [64] T. Illes, F. Lavaste, J.-F. Dubousset, T. S. Illés, F. Lavaste, and J. F. Dubousset. The third dimension of scoliosis: The forgotten axial plane. Orthopaedics & Traumatology: Surgery & Research, 105(2):351–359, 2019.
- [65] Y. Ishikawa, T. Kokabu, K. Yamada, Y. Abe, H. Tachi, H. Suzuki, T. Ohnishi, T. Endo, D. Ukeba, K. Ura, M. Takahata, N. Iwasaki, and H. Sudo. Prediction of cobb angle using deep learning algorithm with three-dimensional depth sensor considering the influence of garment in idiopathic scoliosis. Journal of Clinical Medicine, 12(2):499, Jan. 2023.
- [66] J. L. Jaremko, P. Poncet, J. Ronsky, J. Harder, J. Dansereau, H. Labelle, and R. F. Zernicke. Estimation of spinal deformity in scoliosis from torso surface cross sections. Spine, 26(14):1583–1591, jul 2001.
- [67] J. L. Jaremko, P. Poncet, J. Ronsky, J. Harder, J. Dansereau, H. Labelle, and R. F. Zernicke. Genetic Algorithm–Neural Network Estimation of Cobb Angle from Torso Asymmetry in Scoliosis . Journal of Biomechanical Engineering, 124(5):496–503, 09 2002.
- [68] B. F. Jeffries, M. Tarlton, A. A. D. Smet, S. J. Dwyer, and A. C. Brower. Computerized measurement and analysis of scoliosis: a more accurate representation of the shape of the curve. Radiology, 134(2):381–385, Feb. 1980.
- [69] S. Kadoury and H. Labelle. Classification of three-dimensional thoracic deformities in adolescent idiopathic scoliosis from a multivariate analysis. European Spine Journal, 21(1):40–49, 2012.

- [70] Z. Kamal, G. Rouhi, N. Arjmand, and S. Adeeb. A stability-based model of a growing spine with adolescent idiopathic scoliosis: A combination of musculoskeletal and finite element approaches. Medical Engineering and Physics, 64:46–55, 2019.
- [71] I. Kapandji. Physiologie Articulaire 5e Edition. Maloine, 27, rue de l'école-de-médecine - 75006 PARIS, 2004.
- [72] T. Karachalios, J. Sofianos, N. Roidis, G. Sapkas, D. Korres, and K. Nikolopoulos. Ten-year follow-up evaluation of a school screening program for scoliosis. Spine, 24(22):2318, Nov. 1999.
- [73] M. Keller, S. Zuffi, M. J. Black, and S. Pujades. OSSO: Obtaining skeletal shape from outside. In Proceedings IEEE/CVF Conf. on Computer Vision and Pattern Recognition (CVPR), pages 20492–20501, June 2022.
- [74] C. Kelly and I. Delakis. Technical evaluation of a clinical, bi-planar, digital and upright x-ray imaging unit. Journal of Medical Radiation Sciences, 68(4):475–481, June 2021.
- [75] H. Kim, H. S. Kim, E. S. Moon, C. S. Yoon, T. S. Chung, H. T. Song, J. S. Suh, Y. H. Lee, and S. Kim. Scoliosis imaging: What Radiologists should know. Radiographics, 30(7):1823–1842, 2010.
- [76] H. A. King, J. H. Moe, D. S. Bradford, and R. B. Winter. J Bone Joint Surg Am The selection of fusion levels in thoracic idiopathic scoliosis. J Bone Joint Surg Am, 65(9):1302–1313, Dec 1983.
- [77] M. D. R. Klarqvist, S. Agrawal, N. Diamant, P. T. Ellinor, A. Philippakis, K. Ng, P. Batra, and A. V. Khera. Estimating body fat distribution – a driver of cardiometabolic health – from silhouette images. medRxiv, 2022.
- [78] P. Knott, E. Pappo, M. Cameron, J. deMauroy, C. Rivard, T. Kotwicki, F. Zaina, J. Wynne, L. Stikeleather, J. Bettany-Saltikov, T. B. Grivas, J. Durmala, T. Maruyama, S. Negrini, J. P. O'Brien, and M. Rigo. SOSORT 2012 consensus paper: reducing x-ray exposure in pediatric patients with scoliosis. Scoliosis, 9(1), Apr. 2014.
- [79] P. Knott, P. Sturm, B. Lonner, P. Cahill, M. Betsch, R. McCarthy, M. Kelly, L. Lenke, and R. Betz. Multicenter comparison of 3d spinal measurements using surface topography with those from conventional radiography. Spine Deformity, 4(2):98–103, 2016.
- [80] T. Kokabu, S. Kanai, N. Kawakami, K. Uno, T. Kotani, T. Suzuki, H. Tachi, Y. Abe, N. Iwasaki, and H. Sudo. An algorithm for using deep learning convolutional neural networks with three dimensional depth sensor imaging in scoliosis detection. Spine Journal, 21:980–987, 6 2021.
- [81] T. Kokabu, N. Kawakami, K. Uno, T. Kotani, T. Suzuki, Y. Abe, K. Maeda, F. Inage, Y. M. Ito, N. Iwasaki, and H. Sudo. Three-dimensional depth sensor imaging to identify

- adolescent idiopathic scoliosis: a prospective multicenter cohort study. Scientific Reports, 9:1–8, 2019.
- [82] C. Koutras, J. Pérez, K. Kardash, and M. A. Otaduy. A study of the sensitivity of biomechanical models of the spine for scoliosis brace design. Computer Methods and Programs in Biomedicine, 207:106125, 2021.
- [83] J. W. M. Kouwenhoven and R. M. Castelein. The pathogenesis of adolescent idiopathic scoliosis: review of the literature. Spine, 33:2898–2908, 2008.
- [84] H. Labelle, C. E. Aubin, R. Jackson, L. Lenke, P. Newton, and S. Parent. Seeing the spine in 3D: How will it change what we do? Journal of Pediatric Orthopaedics, 31(1 SUPPL.):37–45, 2011.
- [85] T. Langlais, C. Vergari, G. Rougereau, L. Gajny, A. Assi, I. Ghanem, J. Dubousset, R. Vialle, R. Pietton, and W. Skalli. Balance, barycentremetry and external shape analysis in idiopathic scoliosis: What can the physician expect from it? Medical Engineering & Physics, 94:33–40, Aug. 2021.
- [86] L. G. Lenke, R. R. Betz, J. Harms, K. H. Bridwell, D. H. Clements, T. G. Lowe, and K. Blanke. Adolescent idiopathic scoliosis: a new classification to determine extent of spinal arthrodesis. J Bone Joint Surg Am, 83(8):1169–1181, Aug 2001.
- [87] Y. Liang, C. Wang, Y. Yu, Y. Zhou, Y. Zheng, Y. Luo, D. Wang, L. Qian, H. Yang, and S. Du. 3d spine model reconstruction based on rgbd images of unclothed back surface. IEEE Transactions on Biomedical Engineering, pages 1–12, 2023.
- [88] M. Loper, N. Mahmood, J. Romero, G. Pons-Moll, and M. J. Black. Smpl: A skinned multi-person linear model. ACM Trans. Graph., 34(6), nov 2015.
- [89] W. E. Lorensen and H. E. Cline. Marching cubes: A high resolution 3d surface construction algorithm. In Proceedings of the 14th Annual Conference on Computer Graphics and Interactive Techniques, SIGGRAPH '87, page 163–169, New York, NY, USA, 1987. Association for Computing Machinery.
- [90] B. A. MacWilliams, A. Rozumalski, A. N. Swanson, R. A. Wervey, D. C. Dykes, T. F. Novacheck, and M. H. Schwartz. Assessment of three-dimensional lumbar spine vertebral motion during gait with use of indwelling bone pins. The Journal of Bone & Joint Surgery, 95(23):e184, Dec. 2013.
- [91] J. D. Mathews, A. V. Forsythe, Z. Brady, M. W. Butler, S. K. Goergen, G. B. Byrnes, G. G. Giles, A. B. Wallace, P. R. Anderson, T. A. Guiver, P. McGale, T. M. Cain, J. G. Dowty, A. C. Bickerstaffe, and S. C. Darby. Cancer risk in 680,000 people exposed to computed tomography scans in childhood or adolescence: data linkage study of 11 million australians. BMJ, 346(may21 1):f2360, May 2013.

- [92] D. Meng, E. Boyer, and S. Pujades. Vertebrae localization, segmentation and identification using a graph optimization and an anatomic consistency cycle. Computerized Medical Imaging and Graphics, 107:102235, 2023.
- [93] D. Meng, M. Keller, E. Boyer, M. J. Black, and S. Pujades. Learning a statistical full spine model from partial observations. In ShapeMI@MICCAI, 2020.
- [94] K. Menon. Classification systems in adolescent idiopathic scoliosis revisited: Is a three-dimensional classification needed? Indian Spine Journal, 3(2):143, 2020.
- [95] C. L. Nash and J. Moe. A study of vertebral rotation. The Journal of bone and joint surgery. American volume, 51 2:223–9, 1969.
- [96] A. Nerot, W. Skalli, and X. Wang. A principal component analysis of the relationship between the external body shape and internal skeleton for the upper body. Journal of Biomechanics, page 49, 2016.
- [97] A. Nerot, W. Skalli, and X. Wang. Estimation of spinal joint centers from external back profile and anatomical landmarks. Journal of Biomechanics, 70:96–101, 3 2018.
- [98] F. Netter. Atlas of human anatomy. Elsevier, Philadelphia, PA, 2018.
- [99] S.-Y. Ng and J. Bettany-Saltikov. Imaging in the diagnosis and monitoring of children with idiopathic scoliosis. The Open Orthopaedics Journal, 11(1):1500–1520, Dec. 2017.
- [100] A. Nérot, J. Choisne, C. Amabile, C. Travert, H. Pillet, X. Wang, and W. Skalli. A 3d reconstruction method of the body envelope from biplanar x-rays: Evaluation of its accuracy and reliability. Journal of Biomechanics, 48(16):4322–4326, 2015.
- [101] T. Overbergh, P. Severijns, E. Beaucage-Gauvreau, I. Jonkers, L. Moke, and L. Scheys. Development and validation of a modeling workflow for the generation of image-based, subject-specific thoracolumbar models of spinal deformity. Journal of Biomechanics, 110:109946, 2020.
- [102] T. R. Oxland. Fundamental biomechanics of the spine-What we have learned in the past 25 years and future directions. Journal of Biomechanics, 49(6):817–832, 2016.
- [103] A. Panjabi and M. White. The basic kinematics of the human spine. A review of past and current knowledge., 1978.
- [104] B.-K. Park, J. C. Lumeng, C. N. Lumeng, S. M. Ebert, and M. P. Reed. Child body shape measurement using depth cameras and a statistical body shape model. Ergonomics, 58(2):301–309, 2015. PMID: 25323820.
- [105] Y. S. Park, B. Woo, J. Kim, W. sik Chae, D. S. Kim, J.-H. Jung, C.-H. Lee, and Y. tae Lim. Comparison of gait analysis between adolescent idiopathic scoliosis patients and age matched controls. 2012.

- [106] A. Paszke, S. Gross, F. Massa, A. Lerer, J. Bradbury, G. Chanan, T. Killeen, Z. Lin, N. Gimelshein, L. Antiga, A. Desmaison, A. Kopf, E. Yang, Z. DeVito, M. Raison, A. Tejani, S. Chilamkurthy, B. Steiner, L. Fang, J. Bai, and S. Chintala. Pytorch: An imperative style, high-performance deep learning library. In H. Wallach, H. Larochelle, A. Beygelzimer, F. d'Alché-Buc, E. Fox, and R. Garnett, editors, Advances in Neural Information Processing Systems 32, pages 8024–8035. Curran Associates, Inc., 2019.
- [107] M. J. Pearcy and N. Bogduk. Instantaneous Axes of Rotation of the Lumbar Intervertebral Joints, 1988.
- [108] R. Perdrille and J. Vidal. [A study of scoliotic curve. The importance of extension and vertebral rotation (author's transl)]. Rev Chir Orthop Reparatrice Appar Mot, 67(1):25–34, 1981.
- [109] C. Perret, S. Poiraudou, J. Fermanian, and M. Revel. Validité et reproductibilité du rachimètre pour l'étude de la mobilité spino-pelvi-fémorale dans le plan sagittal. Annales de Réadaptation et de Médecine Physique, 43:116–124, 03 2000.
- [110] P. Poncet, J. Dansereau, and H. Labelle. Geometric torsion in idiopathic scoliosis: A first 3d analysis and a proposal to a new classification. Studies in Health Technology and Informatics, 59(20):122–125, 1999.
- [111] P. Poncet, J. Dansereau, and H. Labelle. Geometric torsion in idiopathic scoliosis. Spine, 26(20):2235–2243, Oct. 2001.
- [112] I. V. Ponseti and B. Friedman. Prognosis in idiopathic scoliosis. Journal of Bone and Joint Surgery, 2(32):381–395, 1950.
- [113] L. Ramirez, N. G. Durdle, V. J. Raso, and D. L. Hill. A support vector machines classifier to assess the severity of idiopathic scoliosis from surface topography. IEEE Transactions on Information Technology in Biomedicine, 10:84–91, 1 2006.
- [114] M. D. Rigo, M. Villagrasa, and D. Gallo. A specific scoliosis classification correlating with brace treatment: Description and reliability. Scoliosis, 5:1–11, 2010.
- [115] C. M. Ronckers, M. M. Doody, J. E. Lonstein, M. Stovall, and C. E. Land. Multiple Diagnostic X-rays for Spine Deformities and Risk of Breast Cancer. Cancer Epidemiology, Biomarkers & Prevention, 17(3):605–613, 03 2008.
- [116] A. Rozumalski, M. H. Schwartz, R. Wervej, A. Swanson, D. C. Dykes, and T. Novacheck. The in vivo three-dimensional motion of the human lumbar spine during gait. Gait & Posture, 28(3):378–384, 2008.
- [117] A. P. Sangole, C. E. Aubin, H. Labelle, I. A. Stokes, L. G. Lenke, R. Jackson, and P. Newton. Three-dimensional classification of thoracic scoliotic curves. Spine, 34(1):91–99, 2009.

- [118] A. Sattout, J. Clin, N. Cobetto, H. Labelle, and C. E. Aubin. Biomechanical assessment of providence nighttime brace for the treatment of adolescent idiopathic scoliosis. Spine Deformity, 4:253–260, 2016.
- [119] C. G. Schizas, I. A. Kramers-de Quervain, E. Stüssi, and D. Grob. Gait asymmetries in patients with idiopathic scoliosis using vertical forces measurement only. Eur Spine J, 7(2):95–98, 1998.
- [120] S. Schmid, K. A. Burkhart, B. T. Allaire, D. Grindle, and D. E. Anderson. Musculoskeletal full-body models including a detailed thoracolumbar spine for children and adolescents aged 6–18 years. Journal of Biomechanics, 102:109305, 2020.
- [121] S. Schmid, D. Studer, C.-C. Hasler, J. Romkes, W. R. Taylor, R. Brunner, and S. Lorenzetti. Using skin markers for spinal curvature quantification in main thoracic adolescent idiopathic scoliosis: An explorative radiographic study. PLOS ONE, 10(8):e0135689, Aug. 2015.
- [122] S. Schmid, D. Studer, C. C. Hasler, J. Romkes, W. R. Taylor, S. Lorenzetti, and R. Brunner. Quantifying spinal gait kinematics using an enhanced optical motion capture approach in adolescent idiopathic scoliosis. Gait and Posture, 44:231–237, feb 2016.
- [123] H. Schmidt, F. Heuer, L. Claes, and H.-J. Wilke. The relation between the instantaneous center of rotation and facet joint forces – a finite element analysis. Clinical Biomechanics, 23(3):270–278, 2008.
- [124] P. Severijns, T. Overbergh, S. Schmid, L. Moke, and L. Scheys. Spinal palpation error and its impact on skin marker-based spinal alignment measurement in adult spinal deformity. Frontiers in Bioengineering and Biotechnology, 9, 6 2021.
- [125] P. Severijns, T. Overbergh, A. Thauvoye, J. Baudewijns, D. Monari, L. Moke, K. Desloovere, and L. Scheys. A subject-specific method to measure dynamic spinal alignment in adult spinal deformity. Spine Journal, 20:934–946, 6 2020.
- [126] J. Shen, S. Parent, J. Wu, C. É. Aubin, J. M. Mac-Thiong, S. Kadoury, P. Newton, L. G. Lenke, V. Lafage, S. Barchi, and H. Labelle. Towards a new 3D classification for adolescent idiopathic scoliosis. Spine Deformity, 8(3):387–396, 2020.
- [127] D. S. Shin, K. Lee, and D. Kim. Biomechanical study of lumbar spine with dynamic stabilization device using finite element method. CAD Computer Aided Design, 39(7):559–567, 2007.
- [128] C. Simonidis, M. Scharmacher, and W. Seemann. Reduced kinematic model of the human spine. Pamm, 7(1):4020025–4020026, 2007.
- [129] W. Skalli, C. Vergari, E. Ebermeyer, I. Courtois, X. Drevelle, R. Kohler, K. Abelin-Genevois, and J. Dubousset. Early detection of progressive adolescent idiopathic scoliosis: A severity index. Spine, 42:823–830, 2017.

- [130] I. A. Stokes. Three-dimensional terminology of spinal deformity. A report presented to the Scoliosis Research Society by the Scoliosis Research Society Working Group on 3-D terminology of spinal deformity. Spine (Phila Pa 1976), 19(2):236–248, Jan 1994.
- [131] I. A. Stokes and J. P. Laible. Three-dimensional osseo-ligamentous model of the thorax representing initiation of scoliosis by asymmetric growth. Journal of Biomechanics, 23(6):589–595, 1990.
- [132] I. A. F. Stokes, L. C. Bigalow, and M. S. Moreland. Three-dimensional spinal curvature in idiopathic scoliosis. Journal of Orthopaedic Research, 5(1):102–113, 1987.
- [133] L. Struber, A. Courvoisier, J. Griffet, O. Daniel, P. Cinquin, and V. Nougier. Analyse cinématique des mouvements du tronc chez les adolescentes scoliotiques modérées. Revue de Chirurgie Orthopédique et Traumatologique, 102(4):391, 2016.
- [134] L. Struber, V. Nougier, J. Griffet, O. Daniel, A. Moreau-Gaudry, P. Cinquin, and A. Courvoisier. Comparison of trunk motion between moderate ais and healthy children. Children, 9(5), 2022.
- [135] X. Su, R. Dong, Z. Wen, and Y. Liu. Reliability and validity of scoliosis measurements obtained with surface topography techniques: A systematic review. Journal of Clinical Medicine, 11(23), 2022.
- [136] R. Szeliski. Computer vision algorithms and applications, 2011.
- [137] S. Vafadar, W. Skalli, A. Bonnet-Lebrun, M. Khalifé, M. Renaudin, A. Hamza, and L. Gajny. A novel dataset and deep learning-based approach for marker-less motion capture during gait. Gait & Posture, 86:70–76, may 2021.
- [138] L. Vavruch and H. Tropp. A comparison of cobb angle: Standing versus supine images of late-onset idiopathic scoliosis. Polish Journal of Radiology, 81:270–276, 2016.
- [139] C. Vergari, I. Courtois, E. Ebermeyer, H. Bouloussa, R. Vialle, and W. Skalli. Experimental validation of a patient-specific model of orthotic action in adolescent idiopathic scoliosis. European Spine Journal, 25:3049–3055, 2016.
- [140] C. Vergari, G. Ribes, B. A. MEnga, C. Adam, L. Miladi, B. Ilharreborde, K. Abelin-Genevois, P. Rouch, and W. Skalli. Evaluation of a patient-specific finite-element model to simulate conservative treatment in adolescent idiopathic scoliosis. Spine Deformity, 3:4–11, 2015.
- [141] T. Vrtovec, F. Pernuš, and B. Likar. A review of methods for quantitative evaluation of spinal curvature. European Spine Journal, 18(5):593–607, Feb. 2009.
- [142] T. Vrtovec, F. Pernuš, and B. Likar. A review of methods for quantitative evaluation of axial vertebral rotation. European Spine Journal, 18:1079–1090, 8 2009.

- [143] W. Wang, G. R. Baran, R. R. Betz, A. F. Samdani, J. M. Pahys, and P. J. Cahill. The Use of finite element models to assist understanding and treatment for scoliosis: A review paper. Spine Deformity, 2(1):10–27, Jan 2014.
- [144] W. Wang, D. Wang, A. Falisse, P. Severijns, T. Overbergh, L. Moke, L. Scheys, F. De Groote, and I. Jonkers. A dynamic optimization approach for solving spine kinematics while calibrating subject-specific mechanical properties. Annals of Biomedical Engineering, 49(9):2311–2322, Apr. 2021.
- [145] J. M. Warren, A. P. Mazzoleni, and L. A. Hey. Development and validation of a computationally efficient finite element model of the human lumbar spine: Application to disc degeneration. International Journal of Spine Surgery, 14(4):502–510, 2020.
- [146] K. Watanabe, Y. Aoki, and M. Matsumoto. An application of artificial intelligence to diagnostic imaging of spine disease: Estimating spinal alignment from moiré images. Neurospine, 16(4):697–702, Dec. 2019.
- [147] S. L. Weinstein, L. A. Dolan, J. C. Cheng, A. Danielsson, and J. A. Morcuende. Adolescent idiopathic scoliosis. The Lancet, 371(9623):1527–1537, May 2008.
- [148] S. Willner. Moiré topography – a method for school screening of scoliosis. Archives of Orthopaedic and Traumatic Surgery, 95(3):181–185, Nov. 1979.
- [149] G. Wu, S. Siegler, P. Allard, C. Kirtley, A. Leardini, D. Rosenbaum, M. Whittle, D. D. D’Lima, L. Cristofolini, H. Witte, O. Schmid, and I. Stokes. Isb recommendation on definitions of joint coordinate system of various joints for the reporting of human joint motion—part i: ankle, hip, and spine. Journal of Biomechanics, 35(4):543–548, 2002.
- [150] I. Yamamoto, M. Panjabi, T. Crisco, and T. Oxland. Three-dimensional movements of the whole lumbar spine, 1989.
- [151] J. Yang, K. Zhang, H. Fan, Z. Huang, Y. Xiang, J. Yang, L. He, L. Zhang, Y. Yang, R. Li, Y. Zhu, C. Chen, F. Liu, H. Yang, Y. Deng, W. Tan, N. Deng, X. Yu, X. Xuan, X. Xie, X. Liu, and H. Lin. Development and validation of deep learning algorithms for scoliosis screening using back images. Communications Biology, 2:1–8, 2019.







# Glossary

AI	Artificial Intelligence
AIS	Adolescent Idiopathic Scoliosis
ALL	Anterior longitudinal ligament
ASD	Adult Spinal Deformity
ASIS	Anterior superior iliac spine
AUC	Area Under the Curve
BFP	Best fit plane
BMI	Body Mass Index
CX	Xth Cervical vertebra
CA	Cobb Angle
CHUGA	Centre Hospitalier Universitaire Grenoble-Alpes
CI	Confidence Interval
CNN	Convolutional Neural Network
CSVL	Central Sacral Vertebra Line
CT	Computed Tomography
DICOM	Digital imaging and communications in medicine
DL	Deep Learning
DLA	Deep Learning Algorithms
DOF	Degree of freedom
EMG	Electromyography
FE	Finite element

FEM	Finite Element Model
FJ	Facet Joint
FSU	Functional Spine Unit
GH	Grenoble Hospitals
GRF	Ground Reaction Force
IAR	Inter-vertebral Axial Rotation
ICP	Iterative Closest Point
ICR	Instantaneous Center of Rotation
ISB	International Society of Biomechanics
ISL	Inter-spinous ligament
IVD	Intervertebral disc
LX	Xth Lumbar vertebra
LBS	Linear Blend Skinning
LF	Ligamentum flavum
MAE	Mean Absolute Error
MBM	Multi-body model
ML	Machine Learning
mocap	motion capture
MRI	Magnetic Resonance Imaging
MSE	Mean Squared Error
NMDID	New Mexico Decedent Image Database
NN	Neural Network
PCA	Principal Component Analysis
PLL	Posterior longitudinal ligament
PMC	Plane of maximum curvature
PSIS	Posterior superior iliac spine

RANSAC	RANdom SAmpLe Consensus
RBM	Rigid-body model
ROC	Receiver Operating Characteristic
ROI	Region of Interest
ROM	Range of Motion
SX	Xth Sacral vertebra
SL	Spinous ligament
SRS	Scoliosis Research Society
SVM	Support Vector Machines
TX	Xth Thoracic vertebra
TL	Transverse ligament
TOF	Time of Flight
VAR	Vertebral Axial Rotation

## List of Figures

1.1	The three anatomical planes of reference . . . . .	7
1.2	Natural curves along the spine . . . . .	8
1.3	Differences in shape of the vertebrae along the spine. Geometries obtained from anatomical models provided by the company Anatoscope [1]. . . . .	9
1.4	Structure of a vertebra . . . . .	9
1.5	Anatomy of the thoracic skeleton . . . . .	10
1.6	Anatomy of the pelvis. Left: face view of the pelvis ; Right: lateral view of the left hip bone. Created by Nicolas Comte. . . . .	11
1.7	Global movements of the spine . . . . .	12
1.8	Example of measurements for a flexion at the FSU . . . . .	13
1.9	X-ray on scoliotic patient showing its thoracic and thoracolumbar scoliotic curvatures on the frontal plane . . . . .	15
1.10	Scoliosis evolution law of Duval-Beaupere (1988) . . . . .	16
1.11	The Adam’s forward bend test . . . . .	17
2.1	Structure of a scoliotic curvature and measurement of the Cobb angle from X-rays (left). N: neutral vertebra; E: end vertebra; A: apical vertebra . . . . .	21
2.2	Grading of vertebral axial rotation with the Nash-Moe method . . . . .	22
2.3	Lenke et al. 2001 classification . . . . .	23
2.4	Geometry of the EOS imaging system. Figure from Kelly and Delakis 2021 [74].	25
2.5	The da Vinci view . . . . .	27
2.6	Different approaches of the 3D nature of the spine for 3D classification . . . . .	28
2.7	The Adam’s forward bend test with a scoliometer. Created by Nicolas Comte. . .	30
2.8	Different works allowing scoliosis monitoring from outer images of the back and CNN approaches . . . . .	31
2.9	Example of the issue of back flattening . . . . .	35
2.10	Segmentation on a trunc slice . . . . .	36
2.11	The use of the visual hull . . . . .	38
2.12	Superimposition of the skin according to the silhouettes . . . . .	39
2.13	Resulting avatar of the patient with the spine coming from 3D reconstruction of the SterEOS software and the skin from our anatomical registration workflow. . .	39
2.14	Dataset examples. For each subject we have a depth map, the 3D vertebrae locations and the measured angles. Coronal (left) and sagittal (right) views. . . . .	40
2.15	Distribution of the main Cobb angle (scoliosis severity in °) in our dataset. . . . .	40
2.16	Effects of the PCA in the prediction of the vertebra positions with our CNN model	41
2.17	Cumulative explained variance by the PCA according to the number of components.	42
2.18	Effects of the first components on the PCA average of the spine positions. . . . .	42
2.19	Reconstruction error by the PCA on the training dataset according to the number of components. . . . .	43

2.20	Global architecture of our network: Resnet18 is making a regression on the depth image in order to find a reduced representation of the coordinates . . . . .	44
2.21	Selection of results. White: ground-truth; blue: predictions. Top row: coronal view for each case, bottom row: sagittal view. GH: institution; NMDID: New Mexico Decedent Image Database; L: Left; R: Right; P: Posterior; A: Anterior. . . . .	45
2.22	Comparison between predicted scoliosis severity and ground-truth measurements. . . . .	46
3.1	Different types of models of the spine and purposes . . . . .	55
3.2	Model involved in the study of Overbergh et al. 2020, figure from [101]. . . . .	57
3.3	Summary of our workflow with the annotated data . . . . .	58
3.4	Types of data collected for a single patient at Grenoble Hospitals. . . . .	59
3.5	Positioning of the joints relatively to the two connected vertebrae. . . . .	60
3.6	Biplanar X-rays of the same patient in standing (a) and lateral bending (b) . . . . .	63
3.7	Distance error per marker from the resulting model to the radiograph positions . . . . .	64
3.8	Predictions (blue) against the ground-truth (black) on the coronal and sagittal planes (scale in mm) . . . . .	67
3.9	Difference between model skin representation and original scans for patients with full (first row) and partial (second row) back acquisition. . . . .	73
3.10	Ambiguity with the manual identification and matching of markers on the X-ray images . . . . .	74
3.11	Summary of our method . . . . .	77
A.1	Full torso version of our model. . . . .	105
A.2	Light version of our model. . . . .	105
A.3	Overview of the registration of the model surfaces onto the patient data. . . . .	106
A.4	Overview of the registration of the model skin onto the X-rays informations . . . . .	107
A.5	Registration of the shapes of the anatomical model onto the input data. Blue: model (source) surface; Red: target . . . . .	108
A.6	Correction of the model surface on the X-ray pose. Blue: model surface (source); Red: target (X-ray informations) . . . . .	108
B.1	Overview of their method of measurement (from [146]) . . . . .	110
B.2	Estimation of the Cobb angle with the Choi et al. method compared to the ground-truth measurements (usual method). . . . .	111
B.3	Coronal views of cases where Choi et al. 2017 fails to evaluate the Cobb angle . . . . .	112
B.4	Estimation of the Cobb angle according to our method and Choi et al. 2017 against the classic X-rays measurement. . . . .	113
B.5	Bland-Altman diagrams of the two Cobb angle estimation methods . . . . .	115
B.6	Coronal views of cases where Choi et al. 2017 fails to evaluate the Cobb angle; Results with our method . . . . .	115

## List of Tables

2.1	Definitions of the local axis system orientations in the literature. The SRS and ISB systems are based on the location of anatomical landmarks: the middle of the endplates (red) and the pedicles (blue). Figures by Nicolas Comte. . . . .	26
2.2	Spine prediction accuracy . . . . .	46
2.3	Comparison with binarized depth information, i.e. silhouette (silh) . . . . .	47
2.4	MAE in locations in mm and standard deviations comparing results according to subjects included in training and testing processes. . . . .	47
3.1	Stiffness values at each joint of the model. Shear and compression are expressed in $kN/m$ , flexion-extension, axial-rotation and lateral bending in $N.m/rad$ . . . . .	61
3.2	Accuracy (Mean Absolute Error, MAE) of the avatar vertebrae in shape, positions and orientations . . . . .	65
3.3	Accuracy of the predictions (MAE) of the vertebra positions and orientations according to the marker positions in lateral bending. . . . .	66
B.1	Paired-sample T-Tests of the two methods against the Ground-truth measurement	116





# A

## Appendix A: Anatomical model registration workflow for creation of patients digital twins including their internal and external anatomy

---

*In this appendix, we provide a comprehensive overview of our anatomical models with details about the rigid and elastic registration methods involved in our work.*

---

## 1 Overview of the anatomical models

Two anatomical models, developed with Anatoscope [1], are involved in our studies depending on the surface scan of the patient that can include the full surface of the trunk (fig. A.1) or the back only (fig. A.2).

The first model is a full trunk anatomical representation including the rib cage, the spine (C01-Coccyx) with the pelvis. Each bone surface is associated with a rigid body (6 DOFs, 3 in translation and 3 in rotation). This model has been used to create avatars from patient data including a full scan of their torso.

The second version of the model is a lighter one, from which we removed bony structures that have not been reconstructed during the EOS acquisitions (ribs, costal cartilage, sternum and cervical vertebrae). The front part of the model has also been removed to fit the back acquisitions of patients.

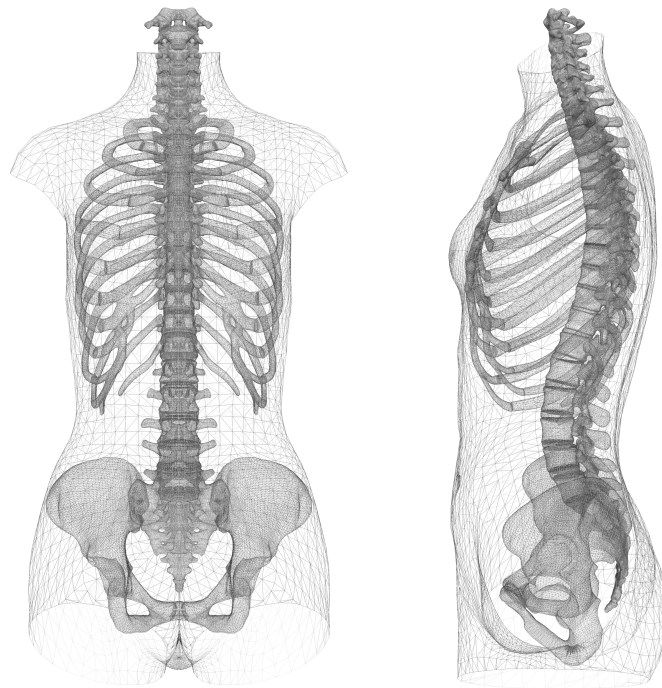
In the two models, each bone  $i$  is represented by a mesh associated with a rigid-body defined in positions  $t_i \in \mathbb{R}^3$  and rotations  $R_i \in \mathbb{R}^{3 \times 3}$ . Each body  $x_i$  is then connected to the others with an elastic joint of 6 DOFs defined by translational and rotational stiffnesses. In addition each bone is associated with a set of shape parameters  $\mathbf{s}$  that modify the scales of the model geometries. The bones are connected to the adjacent element by  $K$  joints of 6 degrees-of-freedom (DOFs). The model also has a skin surface which is rigged by the articulated rigid bodies. The "light" version of the model is associated with a set of barycentric landmarks  $\mathbf{l}^A$  that represent superficial markers used in marker-based motion capture.

## 2 Model registration workflow

In the following steps, we call "source" the model elements that are going to the registration processes. We call "target" the collected data, the vertebra geometries of the patients, obtained from the X-rays, and the skin obtained from surface scans. The registrations are implemented and run in Sofa [45].

**Initial model positioning and scaling** For each version of the model, we start with a first global registration in position and scale of the vertebra source geometries onto the targets obtained from the X-rays reconstructions.

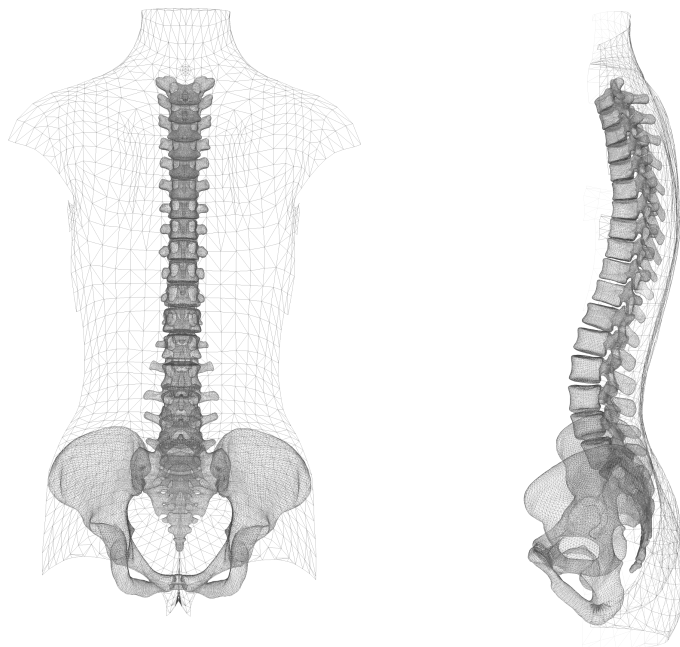
**Pose and scale registration.** The first step of the registration process is to change the 3D pose  $\mathbf{x}$  and the scales  $\mathbf{s}$  of the model, so that the models' spine fits the 3D target spine. The association between the source and the target is managed by an implementation of the Iterative Closest Point (ICP) algorithm in Sofa finding the closest target surface of a given source vertex by minimizing the euclidean distance. To avoid unnatural poses, we use a regularization term  $E_A$  that is defined



*(a) Face*

*(b) Profile*

*Figure A.1: Full torso version of our model.*



*(a) Face*

*(b) Profile*

*Figure A.2: Light version of our model.*

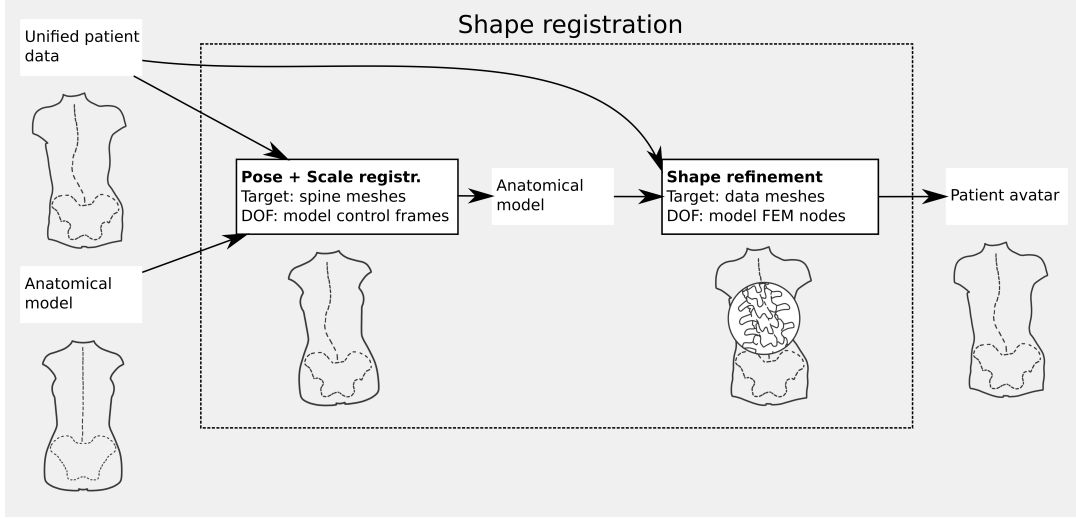


Figure A.3: Overview of the registration of the model surfaces onto the patient data.

by the joint constraints inside the kinematic rig. The final optimization is thus

$$(\hat{\mathbf{x}}, \hat{\mathbf{s}}) = \arg \min_{\mathbf{x}, \mathbf{s}} (d_{ps}(S_A(\mathbf{x}, \mathbf{s}), S_X) + E_A(\mathbf{x}, \mathbf{s})), \quad (\text{A.1})$$

where  $d_{ps}$  is the point-to-surface distances defined by the ICP,  $S_A$  are surfaces of the source, determined by the pose and shape vectors and  $S_X$  the target meshes obtained from the EOS reconstructions. These steps are resumed fig. A.3 with screenshots fig. A.5.

**Shape refinement.** As the shape parameters  $\mathbf{s}$  only capture scales of the model, the obtained geometries do not precisely match the patient specific geometries. Thus, we refine the geometries of the source vertebrae and skin to match the patient's observations with a non-linear deformation.

The rigid frames of the rig  $\mathbf{x}$  are fixed as the scale parameters  $\mathbf{s}$ . The model surfaces (skin and bones) are subdivided into FEM sub-volumes. Each element is parameterized by control frames  $\boldsymbol{\phi}$  optimized in order to match model surfaces  $S_A$  onto the target meshes (EOS  $S_X$  and skin scan  $S_S$ ). This step is constrained by  $E_{FEM}$  regularization term with a constant young modulus property constant during the process that avoid unrealistic folds during the elastic deformation.

$$\hat{\boldsymbol{\phi}} = \arg \min_{\boldsymbol{\phi}} (d_{ps}(S_A^{FEM}(\boldsymbol{\phi}), (S_X, S_S)) + E_{FEM}(\boldsymbol{\phi})), \quad (\text{A.2})$$

Once the patient surfaces have been captured by the model, the shape parameters are fixed.

**Pose correction.** Let us note that the patients pose during the surface scan is slightly different than the pose in the radiography. We can retrieve informations about the radiographic skin pose in different ways.

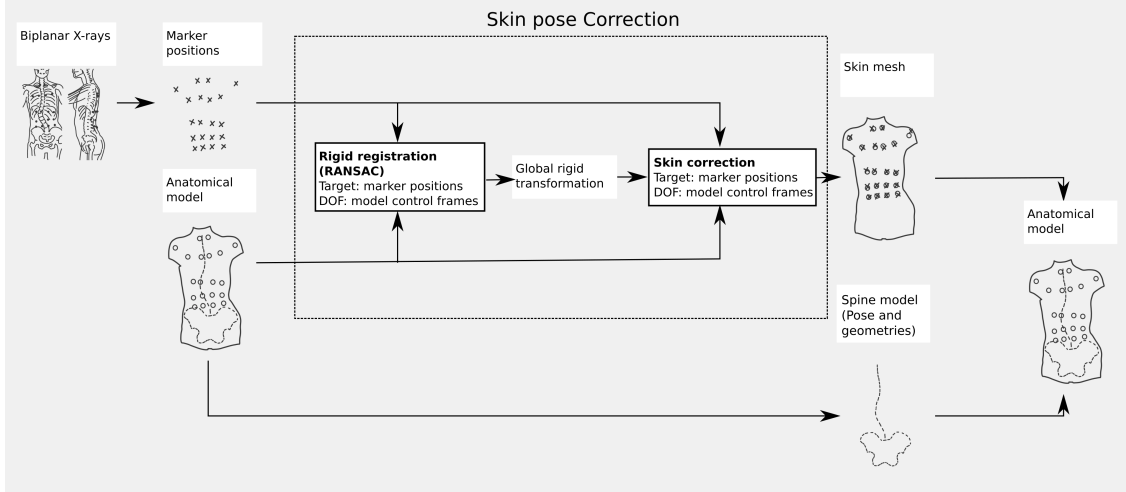


Figure A.4: Overview of the registration of the model skin onto the X-rays informations. In the case of the patients without markers, the silhouette (visual hull) is inferred from the biplanar X-rays and used as target in the pose registration step.

For the patients from which we acquired a full torso acquisition, we used the 3D silhouette (visual hull, fig. A.6a) obtained from their biplanar radiographs. However that is not possible for patient with partial acquisitions (back only, fig. A.6b). For these patients, we leverage a set of  $M$  radio-opaque markers that can be located in 3D from the X-rays and surface scans.

The association between the source and target features is straightforward for cases with the markers that can easily be identified. For full-torso acquisition, we can associate these features with an ICP at each iteration of the registration process.

Then we use a temporary set of pose parameters  $\mathbf{x}'$  that will be optimized so that the external model landmarks (markers or skin vertices)  $\mathbf{l}^A(\mathbf{x}')$  match the ones in the X-rays  $\mathbf{l}^X$  (radio-opaque markers or closest-points in the visual hull). This will effectively change the model skin surface to match the pose of the patient in the EOS device. The marker-based optimization is computed as

$$\hat{\mathbf{x}}' = \arg \min_{\mathbf{x}'} \left( \sum_{i=1}^{i=M} \|\mathbf{l}_i^A(\mathbf{x}') - \mathbf{l}_i^X\|^2 + E_A(\mathbf{x}') \right), \quad (\text{A.3})$$

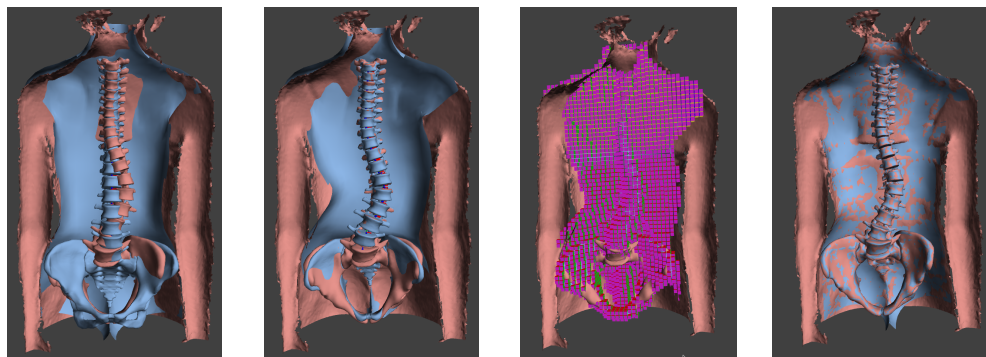
where the energy  $E_A$  is a regularization term enforcing anatomic constraints on the joints of the model.

The resulting model skin surface matches the pose of the back surface during the X-ray acquisitions. Thus, we create a synced skin and spine model, by disregarding the temporal parameters  $\mathbf{x}'$  and associating the current optimized skin to the original model parameters  $\mathbf{x}$  obtained during the first registration process.

The full workflow for this step is summarized fig. A.4.

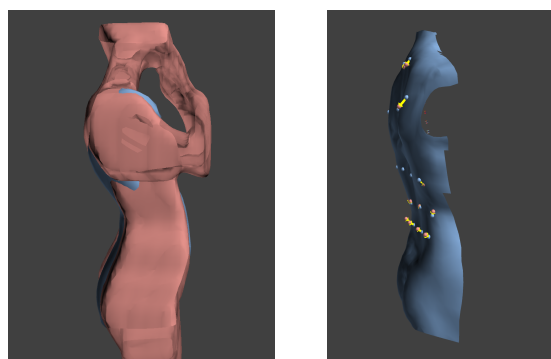
As a result, the anatomical model is a numerical twin of the patient, including the skeleton and

the skin rigged with common model parameters. The association of the skin and spine is done on the pose observed during the X-ray acquisitions with the help of the radio-opaque markers or the visual hull.



(a) Initial step: global rigid registration of the model onto the input data (b) Spine scale+pose (c) Initial step of the refinement by subdividing the model meshes into subvolumes (d) Results

Figure A.5: Registration of the shapes of the anatomical model onto the input data. Blue: model (source) surface; Red: target



(a) Registration on the visual hull for patients with full torso scan (b) Registration on the radio-opaque markers (balls) for patients with partial scan

Figure A.6: Correction of the model surface on the X-ray pose. Blue: model surface (source); Red: target (X-ray informations)

# B

## Appendix B: Detection and quantification of scoliosis from splines

---

*In this appendix, we will provide a detailed analysis of the Choi-Watanabe method [20, 146], used section 2.3, allowing the estimation of the Cobb angle from vertebra positions. According to the limitations highlighted by this analysis we propose an alternative approach.*

---



### 3 The Choi - Watanabe method

#### 3.1 Introduction

In chapter 2, we estimate the Cobb angle (scoliosis severity) from vertebra positions. For this purpose, we use the method developed by Choi et al. 2017 [20], and re-published in Watanabe et al. 2019 [146]. This method enables the localization and estimation of the intensity of scoliotic curvatures from the positions of vertebra centroids along the coronal plane (Fig. B.1). Their method is similar to Jeffries et al. 1980 [68], Stokes et al. 1987 [132] and Berthonnaud and Dimnet 2007 [12] estimating the Cobb angle from curves and by the location of inflexion points (using polynomials or B-Splines). Alternative approaches, such as the one presented in [8], locate the Cobb angle by pinpointing the apical vertebra. This involves the identification of the maxima and minima points along the spinal curve. Subsequently, the Cobb angle is derived by locating the most-tilted vertebrae above and below the apical level.

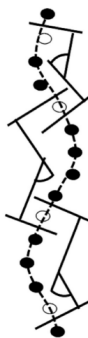


*Figure B.1: Overview of their method of measurement (from [146]). The first steps are dedicated to the location of inflexion points along a spline draw from the vertebra positions. Then, these points were selected according to their location from the others and designated as end-vertebrae. Finally, the Cobb angle is measured at the intervertebral levels.*

In their study, Choi et al. 2017 [20], and then Watanabe et al. 2019 [146], the authors compare the estimated maximum angles with those measured by a specialist using the traditional radiographic method (i.e. based on endplates, see section 2.1.1.1). According to their results [20, 146], evaluation metrics over all scoliotic curvatures (below and above the 10 deg. threshold) gives a remarkable accuracy of  $3.42^\circ$  (std:  $2.64^\circ$ ) with a mean error that decreases with scoliosis magnitude. Jeffries et al. [68] and Stokes et al. 1987 [132] provided the correlation coefficient between their method and the traditional measurement, both evaluated to 0.97. Unfortunately, these approaches lack any measurement of their capability to differentiate scoliotic and asymptomatic spines.

The aim of this section is to evaluate the Choi et al. 2017 method in our dataset and provide a detailed analysis of the accuracy of this approach in the assessment of scoliosis from vertebra positions.

## 3.2 Methods

### 3.2.1 Our dataset

To evaluate the Choi et al. 2017 method we created a dataset of 51 3D spines reconstructions of Grenoble Hospital patients with Adolescent Idiopathic Scoliosis (simple or double curve, Cobb angle between 10 and 68 °). Spine alignments and geometries are obtained with the SterEOS software (EOS Imaging, Paris, France) from biplanar X-rays. From each spine, we extract the gravity center of each vertebra geometries and project their positions on the frontal plane. We will consider as ground-truth the maximum Cobb angle measured from the traditional method (chapter 2, section 3.4.1.4).

### 3.2.2 Metrics

We compared the ground-truth measurements with those obtained using Choi et al. 2017 by computing the linear correlation and providing the Pearson coefficient of correlation (R). In addition, we compute the Mean Absolute Error (MAE) as provided in their paper [20] and conduct a paired-sample T-test to evaluate the similarity of the obtained angles with the traditional method.

## 3.3 Results and discussion

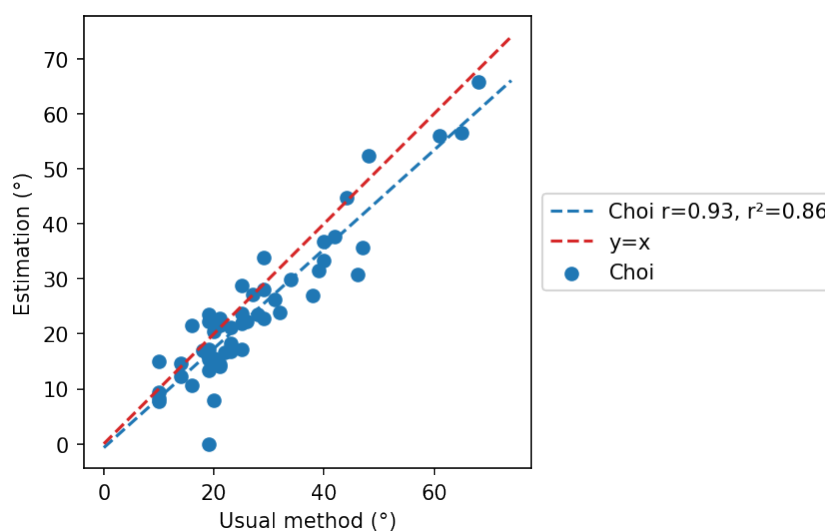


Figure B.2: Estimation of the Cobb angle with the Choi et al. method compared to the ground-truth measurements (usual method).

From our dataset, we observe a MAE of  $4.82^\circ$  (std:  $3.77^\circ$ ). The correlation between the two methods of measurement is high with a correlation coefficient of 0.93 (fig. B.2). We can notice a slight underestimation of the Cobb angle we measure at  $3.42^\circ$  (std:  $5.07^\circ$ ) in average.

The paired-sample t-test can be conducted with the Shapiro-Wilk statistic, test of normality, of the differences that can not be rejected (p-value = 0.18). The t-test shows a significant (p-value =  $1.67e-05$ ) difference between the two measurement methods in our dataset.

Five patients (10% of the dataset) were estimated as asymptomatic according to the Choi et al. 2017 method while their "true" Cobb angle is higher than  $10^\circ$  (fig. B.3, left). No Cobb angle has been detected for one of them while his scoliosis has been evaluated at  $19^\circ$  from the traditional method. This can be explained by the fact that only one inflexion point has been detected due to the "S" shape of his spine. In other cases scoliosis is not accurately located (fig. B.3, right), resulting in a wrong estimation of the scoliosis severity.

### 3.4 Conclusion

The Choi et al. 2017 method performs well in the localization and quantification of scoliosis along vertebra centroids. However it fails in particular cases where the number of inflexion points is too low or too high. Thus, we can conclude that methods based on inflexion points can fail in particular cases.

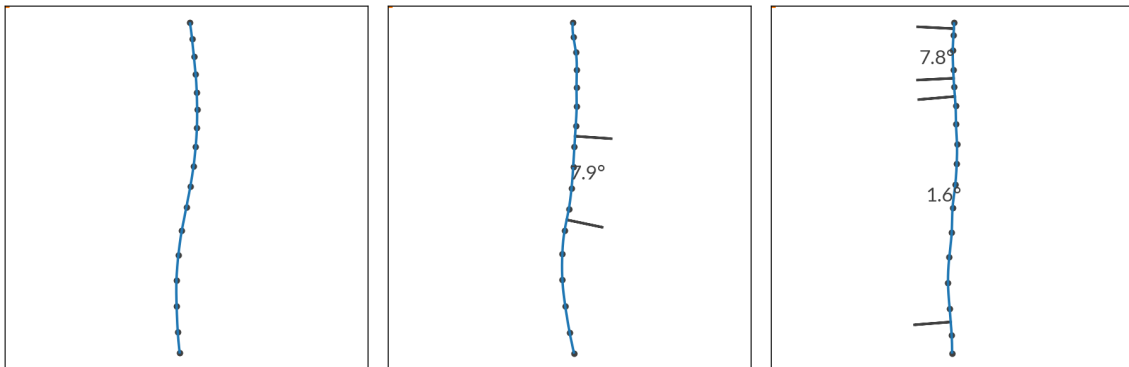


*Figure B.3: Coronal views of cases where Choi et al. 2017 fails to evaluate the Cobb angle. The actual values (obtained from X-rays) are from left to right:  $19^\circ$ ,  $20^\circ$  and  $10^\circ$ . The errors are mainly due to the mis-localization of the end vertebrae. On the left, only one inflexion point has been identified. On the right too many of them were detected (6), leading to the deletion of the relevant end-vertebrae during the selection of inflexion points in the Choi et al. 2017 algorithm.*

## 4 Our proposal

As highlighted by the subjects where the algorithm fails, the analysis of curvatures from inflexion points can miss scoliosis cases. In this section, we propose another method to evaluate the Cobb angle that extends the analysis on the entire spine shape. We evaluate our method against the Choi et al. method, with regard to ground-truth measurements by computing the MAE and the linear correlation between the measurement methods. A paired sample T-Test will be conducted to test the similarity of the estimations between the different methods.

### 4.1 Algorithm

Our method starts as Choi et al. 2017 with a Cubic B-Spline drawn from the 2D vertebra positions. Perpendicular lines from the spline are computed at each vertebra level. The following steps are then detailed in the pseudo-code 1. Our algorithm traverses through all potential curvatures from top to bottom and retains those that maximize the magnitude (given by the Cobb angle). The detection and localization of the curvature is based on the sign and the value of the angle between the upper line (level  $i$ ) and lower one (level  $j$ ). In absolute value, this angle correspond to the Cobb angle between end vertebrae as used in [11].

### 4.2 Results and discussion

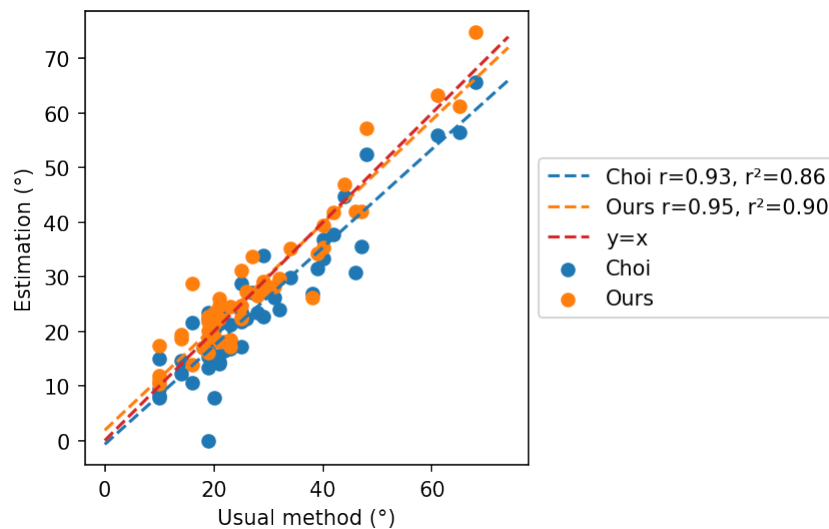


Figure B.4: Estimation of the Cobb angle according to our method and Choi et al. 2017 against the classic X-rays measurement.

Fig. B.4 we compare the our predictions with ground-truth measurements. It appears in these results that our method is better to retrieve the actual Cobb angle values with a MAE of  $3.28^\circ$  (std:  $2.78^\circ$ ). The Pearson correlation coefficient is higher ( $R=0.95$ ,  $p\text{-value} < 0.05$ ) without False Negative spines with scoliosis. in fig. B.6 we can notice that the cases where Choi et al. 2017 fails are correctly annotated by our method.

---

**Algorithm 1** Pseudo-code of our method

---

**Require:**  $\mathbf{t}$  ▷ List of perpendicular lines to the spline at each vertebra level  
 $n_v \leftarrow 17$  ▷ Number of vertebrae  
 $n_s \leftarrow 3$  ▷ Minimum number of vertebrae -1 along a scoliotic curvature  
 $\boldsymbol{\kappa} \leftarrow []$  ▷ List of Cobb angles  
 $i \leftarrow 0$   
**while**  $i < n_v - n_s$  **do** ▷ For each vertebra from T01 to L05  
   $t_i \leftarrow \mathbf{t}[i]$   
   $j \leftarrow i + 1$   
   $\alpha_i \leftarrow \text{None}$   
  **while**  $j < n_v$  **do** ▷ For each vertebra below  
     $t_j \leftarrow \mathbf{t}[j]$   
     $\alpha_j \leftarrow \text{SIGNED\_ANGLE}(t_i, t_j)$  ▷ Compute the signed angle between lines  
    **if**  $\alpha_i \neq \text{None}$  AND  $(\text{SIGN}(\alpha_i) \neq \text{SIGN}(\alpha_j)$  OR  $|\alpha_j| < |\alpha_i|)$  **then**  
      **break** ▷ End of the curvature, leave  
    **end if**  
     $\alpha_i = \alpha_j$  ▷ Update maximum angle in the current curvature  
  **end while**  
  **if**  $(j - i) > n_s$  **then**  
    **if**  $\text{LENGTH}(\boldsymbol{\kappa}) == 0$  **then**  
      Append  $\alpha_i$  in  $\boldsymbol{\kappa}$   
    **else**  
      **if**  $\text{SIGN}(\boldsymbol{\kappa}[i - 1]) == \text{SIGN}(\alpha_i)$  **then** ▷ If the current angle is in the same curvature  
        as before, update with the maximum value  
        **if**  $|\text{SIGN}(\boldsymbol{\kappa}[i - 1])| < |\alpha_i|$  **then**  
           $\boldsymbol{\kappa}[i - 1] \leftarrow \alpha_i$   
        **end if**  
      **else if**  $\text{SIGN}(\boldsymbol{\kappa}[i - 1]) \neq \text{SIGN}(\alpha_i)$  **then** ▷ Change of curvature  
        Append  $\alpha_i$  in  $\boldsymbol{\kappa}$   
      **end if**  
    **end if**  
  **end if**  
**end while**

---

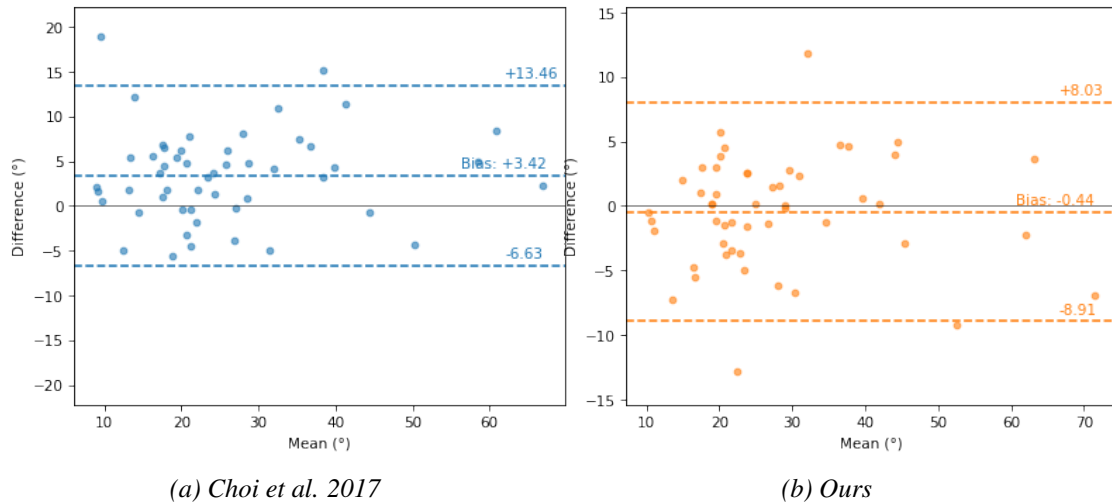


Figure B.5: Bland-Altman diagrams of the two Cobb angle estimation methods. The ground-truth is measured with the classic method from X-rays. A positive value on the ordinate indicates an underestimation, and a positive value an overestimation. Dashed-lines=1.96-fold standard deviation with mean deviation (bias).

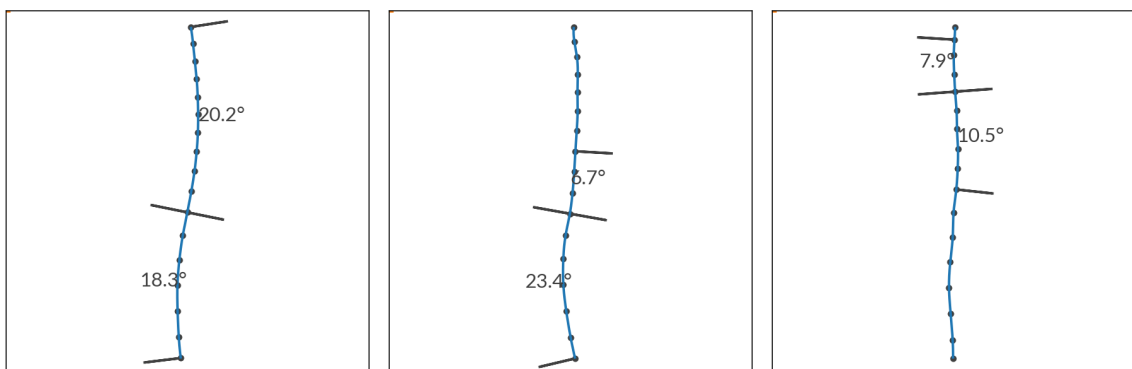


Figure B.6: Coronal views of cases where Choi et al. 2017 fails to evaluate the Cobb angle; Results with our method. The actual values (obtained from X-rays) are from left to right:  $19^\circ$ ,  $20^\circ$  and  $10^\circ$ .

*Tableau B.1: Paired-sample T-Tests of the two methods against the Ground-truth measurement. The normality of the differences (method-ground-truth) is evaluated with a Shapiro-Wilk test. The p-value is given in parenthesis.*

Method	Choi et al. 2017	Ours
Shapiro-Wilk	0.97 (0.18)	0.98 (0.50)
T-test	-4.76 (1.67e-05)	0.73 (0.47)

In fig. B.5 we present Bland-Altman diagrams of the Choi et al. 2017 results and ours allowing the analysis of measurement bias and heteroscedasticity. We can notice that there is no underestimation of scoliosis in average with a bias close to zero which is confirmed by the paired-Sample T-test provided table B.1.

These superior results can be attributed to the inclusion of T01 and L05 levels in our algorithm. In addition, our algorithm seeks the highest Cobb angle within a specific curvature, effectively addressing the challenge of multiple inflection points present in noisy zig-zag shaped curvatures.

### 4.3 Conclusion

The Choi et al. 2017 method of Cobb angle measurement is showing comparative results in the estimation of scoliosis with the traditional method using endplates from X-rays. This method has the advantage to identify the end-vertebrae compared to other methods [68, 132]. Unfortunately, it fails in a few cases, leading to an underestimation of scoliosis severity, and thus, an increased number of False-Positive.

We thus proposed a new method to solve the problems encountered by Choi et al. 2017 in these particular cases. Our results are superior and could even replace the traditional measurement method. Indeed, the "traditional" method requires interpretation of X-ray images to locate the end-vertebrae and estimate their slope from their endplates conducting to a lack of reliability [11, 141] in the estimation of the scoliosis severity.

In future work, methods of measurement should be evaluated with metrics that inform about the precision of the Cobb angle (with the MAE for instance), in correlation with the manual method, and the location of the detected apical and end-vertebrae (that were not available in our dataset). Furthermore, it is possible to contrast these techniques with variations of spinal poses with individuals with and without symptoms. Conducting such investigations would offer a reliable assessment of these approaches while pinpointing their specific practical boundaries.

